Using stable copper isotopes to trace contamination from two historical mining sites in Norway

Master thesis in Earth Sciences

Ingvild Aarrestad

Department of Earth Science

University of Bergen, June 2020

Blank page

Abstract

During the last few decades, the stable copper isotope system (δ^{65}Cu) has gained attention because of its potential as a method to indicate the source of copper in contaminated surface waters. The δ^{65}Cu of dissolved copper is a result of the isotopic composition of source rocks as well as fractionation that may occur during weathering, biological processes, organic complexation and inorganic adsorption. The most significant copper isotope fractionation occurs from oxidative weathering of sulfides exposed to atmospheric O_2 and water, which is the key process responsible for acid mine drainage and the release of heavy metals into the environment. This thesis tests the stable copper isotope system as a tracer for copper in contaminated surface water around two historical sulfide mines in Trøndelag, Norway. The two study areas are Storwartz mining field in Røros and the copper mines in Løkken Verk. The closed mines are still considered an environmental risk and are responsible for heavy metal release and acidity into local surface waters. We collected samples of surface waters and potential sources of copper (ores, background rocks, mining waste) and analyzed samples for major and trace element concentrations by ICP-OES, and copper isotope ratios (δ^{65}Cu) by multi-collector-ICP-MS. Sampled surface water show copper concentrations above 8 ppm and pH ranges from neutral to below pH 4. The contamination appears to be higher in Røros compared to Løkken, which indicates that the remediation measures at Løkken has successfully reduced the release of copper into the environment and also neutralized acid mine drainage to near-neutral pH. In Røros, the most contaminated samples show a relatively small range of δ^{65}Cu (avg. +1.35 ± 0.27‰, n=6). Less contaminated samples generally show higher δ^{65}Cu, besides two samples displaying background copper isotope signature. In all sampled surface water, δ^{65}Cu ranges from +0.10‰ to +6.89‰. The variation in surface water δ^{65}Cu is higher in Røros, and solid samples δ^{65}Cu are consistently lower. Copper isotope signatures of contaminated natural surface waters represents a complex biogeochemical system. Results show that most copper found in the surface waters are likely derived from weathering of exposed mine waste, and thus highlighting the method's potential as an environmental tracer.

Acknowledgements

First, I would like to express my gratitude to my supervisor Dr. Desiree Roerdink for making this thesis possible and helping with every aspect leading up to the finished thesis, from field sampling, lab work, data processing, thesis writing and also for always being positive, helpful and motivating. Also, thanks to my co-supervisor Dr. Eoghan Reeves for teaching me valuable aspects of aquatic geochemistry. I would also like to thank Siv Hjorth Dundas, Hildegunn Almelid and Yuval Ronen for various lab-work assistance, geochemical analyses and sample preparation, even during the COVID-19 lockdown.

A big thanks is also owed to everyone at K.G. Jebsen Center for Deep-Sea Research. In particular the morning-coffee crew and the students at the “Black Smoker” office. My final years at the department would not have been the same without you.

Thank you to everyone I have met at GEO during my five years here. I will remember all the good times we have had and wish you all the best in the future. Special thanks to Dina Elisabeth Moter Hauge, Oda Rostøl Haga and Thea Aske Haugen for all the support, fun times, coffee breaks and great friendship.

Finally, thanks to my non-GEO friends and family for support, encouragement and for at least pretending to understand when I have talked about what I have worked on for the last two years. Special thanks to my mom Elisabeth for supporting me no matter what.

Table of contents

Glossary

- Acid mine drainage – *Acidic water draining from a mining site*
- Black smoker – *Oceanic hydrothermal vent/chimney releasing sulfide- and metal-rich fluids*
- Contamination – *Presence of undesirable elements*
- Epigenetic – *Used about minerals formed after the surrounding rock*
- Flotation – *Process used for concentrating metal sulfides by separation*
- Fractionation – *Here: Isotope fractionation. The relative partitioning of the heavy and light isotope between to natural systems. Kinetic or equilibrium type.*
- Gangue – *Minerals closely associated with ore but economically worthless and disposed of*
- Heavy metals – *Metallic elements with relatively high density and are toxic*
- Hypogene – *Used about a high temperature, unaltered mineral*
- ICP-OES – *Inductively coupled plasma optical emission spectrometer*
- Leachate – *Liquid that extracts a component from the material it passes through*
- Leaching – *Loss or extraction of a certain material usually from solid to liquid*
- Mass bias – *Deviation from "true value" because of the different transmission of isotopes from one element in a mass spectrometer*
- MC-ICP-MS – *Multi-collector inductively coupled plasma mass spectrometer*
- Pollution – *Presence of harmful contaminants*
- Porphyry copper deposit – *Ore deposit with porphyric texture. Usually low-angle subduction related*
- Ppb – *parts per billion, ng/ml*
- Ppm – *parts per million, μg/ml*
- Remediation – *The action of reversing or preventing environmental damage*
- Slags – *Residual material after metal extraction by smelting*
- Smelters – *A factory smelting metal from ore*
- Syngenetic – *Used about minerals formed at the same time as the surrounding rock*
- Tailings – *Fine-grained residual material after flotation. Mainly iron sulfides*
- Tailings pond – *A pond (often artificial) used for under water tailings disposal*
- Vasskis – *A fine grained, syngenetic pyrite mineral from the Løkken deposit*
- VMS deposit – *Volcanogenic massive sulfide deposit*
- Waste material – *Collective term used for waste material from mining (tailings, gangue, slags)*

Chapter 1: Introduction

Historical mining sites are of environmental concern because of their potential to release heavy metal contamination and acidity into streams, rivers and lakes. Local biodiversity and land cover may be irreversibly damaged even years after mines have closed. Elevated levels of heavy metals like copper, are toxic to fish and other living organisms. Extreme concentrations also affect human health and life. There is an abundancy of reports where copper mining has negatively affected surrounding nature and communities. In Zambia, locals have claimed their homes were becoming uninhabitable due to health effects and lower crop yields and eventually sued a mining company because of the damage to their health and livelihood (Voller and Andersen 2016). Also, pollution of a drinking water source led to more than 1000 incidents of abdominal pain, diarrhoea and vomiting reported in local clinics (Voller and Andersen 2016). Potential release from closed sulfide mines is also considered an environmental issue. The Holden mine in Washington state, USA, is an underground copper mine that closed in 1957 (Rio Tinto n.d.). The closed mine, together with the tailings and waste piles left exposed were considered such an environmental risk that the responsible mining companies were ordered to pursue remediation of the site in 2012, 55 years after the mine closed (Rio Tinto n.d.). Hundreds of millions of dollars and several years were spent on implementing various remediation measures to isolate the exposed wastes and treat mine drainage.

Geochemical field studies are key to assess the extent and origin of contamination from mining sites and provide crucial information for targeted remediation strategies. Most commonly, this involves the analysis of trace metals and environmental variables such as pH and conductivity. However, advances in mass spectrometry (MC-ICP-MS) since the early 1990s have enabled the use of metal stable isotopes (Fe, Cu, Zn) for fingerprinting sources of contamination with promising results. For example, Song et al. (2016) used stable copper isotopes to fingerprint contaminant sources of copper from the active Dexing porphyry copper mine in China. The results showed that the isotopic composition of copper in the aqueous environment could be used to indicate the source of the copper in surface waters surrounding the highly contaminated mining site. Song et al. (2016) were able to divide the copper into three distinct groups of isotope ratios: off-deposit, on-deposit and near tailings.

However, other studies have found the method to be insufficient at explaining copper isotope variations in the environment (i.e. Sillerová et al. 2017).

The application of copper isotopes to study environmental pollution from mining is still a relatively new area of research and remains to be tested in mining areas with different geological settings and degrees of contamination. Here, we investigate the use and limitations of the stable copper isotope system in determining the source of the copper in natural surface water surrounding closed, underground copper mines in eastern Norway. The areas of study in this master thesis are the closed mines in the Storwartz mining field in Røros, and the mines in Løkken Verk (from here: 'Løkken'). Storwartz is located just outside of Røros, and Løkken is located southwest of Trondheim, both in Trøndelag county, Norway. Both areas were subject to copper sulfide mining for several hundred years, from the mid 1600s to mid-late 1900s. In 2015, Storwartz was declared a protected area by the Norwegian Ministry of Climate and Environment due to its historical and cultural importance, and Storwartz is therefore protected, by law, from any invasive remediation measures. This means that acid mine drainage and all surface runoff is introduced directly into the environment. At Løkken, the waste piles have been covered and practically all surface runoff is directed back into the mines to limit contamination. The area has been monitored for environmental contamination for many years, and it is clear that the mining has affected the environment by heavy metal release and acidity. However, previous geochemical work by the Norwegian Environment Agency indicates that Cu concentrations in surrounding natural waters are much lower than at the active Dexing mine in China (Iversen 2010; Song et al. 2016), thus enabling us to assess the copper isotope tool at less strongly contaminated mining sites. In addition, the two study locations are great for comparing if and how the remediation at Løkken has affected the release from the two historical mining sites, both in regard to contamination and the copper isotopic composition.

This thesis strengthens the copper isotope tool for assessing the source of harmful concentrations of heavy metals, and the effectiveness of remediation strategies in contaminated areas and actions to limit further pollution. This type of environmental research plays an important role in today's focus on building a more sustainable planet, and the theme of this thesis can be directly related to several of the United Nation's Sustainable Development Goals (SDGs), in particular #14 "Life below water". Understanding metal

contaminant behavior is essential to preserve and protect the environment, as well as ensuring a responsible development of future and current mining activities. Increased mining activity is to be expected in the future to reach the demands of a growing, modern world that simultaneously efforts to transition into a low-carbon economy. To strive for a sustainable development of the mining industry's future, understanding metal pollutants and how to trace them is critical from an environmental perspective.

Chapter 2: Copper isotope geochemistry

Copper (from here: Cu) is a native element and transition metal with atomic number 29. It is a siderophile, highly chalcophile and moderately volatile element with two naturally occurring stable isotopes - ^{63}Cu and ^{65}Cu (Moynier et al. 2017). Their abundance in nature is 69.15% and 30.85% respectively, and their masses 62.929 u and 64.927 u (De Laeter et al. 2003). Furthermore, Cu has three oxidation states: Cu^0 ($[Ar]3d^{10}4s^1$; r = 128 pm), Cu^+ ($[Ar]3d^{10}$; r = 77 pm) and Cu^{2+} ($[Ar]3d^9$; r = 73 pm) (Moynier et al. 2017). The Cu^+ ion is unstable and will disproportionate to Cu^0 or Cu^{2+}, form cuprous oxide (Cu_2O) or organic complexes with carbon; Cu^{2+} occurs freely or as aqua complexes in aqueous solution (Drever 1997 p. 189, Moynier et al. 2017). Cu^{2+} has an ionic radius of 73 pm, which makes it similar in size to Fe^{2+} (r = 70 pm), Cu^{2+} and Fe^{2+} can therefore substitute for each other and Cu can be found in trace amounts in iron minerals like hematite (Fe_2O_3) and pyrite (FeS_2), as well as in silicate rocks (Albarède 2004). The solubility of Cu is strongly affected by acidity, being drastically more soluble at acidic pH (i.e. Maher et al. 2011). In the lithosphere, Cu is mostly hosted in sulfides, and is commonly mined from chalcopyrite ($CuFeS_2$) as well as chalcocite (Cu_2S), cuprite (Cu_2O) and malachite ($Cu_2CO_3(OH)_2$) (Albarède 2004). In the absence of organic ligands, free Cu^{2+} ions dominate in freshwater; carbonate complexes $CuCO_3$ and $[Cu(CO_3)_2]^{2-}$ dominate in seawater (Albarède 2004). However, inorganic dissolved Cu represents a small fraction of Cu in solution compared to Cu organically complexed or sorbed onto oxyhydroxides (Moynier et al. 2017). Cu is also an important biologically active element and a critical nutrient for all organisms; In the ocean Cu is utilized by phytoplankton at the surface, which results in an observable increase in Cu-concentration with depth in seawater (Albarède 2004).

Copper isotope signatures are given as a delta (δ) value in permille (‰). The delta value expresses the variation of the isotope ratio ($^{65}Cu/^{63}Cu$) of a sample relative to a known standard:

$$\delta^{65}Cu = \left(\frac{\frac{^{65}Cu}{^{63}Cu}_{sample}}{\frac{^{65}Cu}{^{63}Cu}_{standard}} - 1 \right) \times 1000 \quad (1)$$

Originally, the standard reference material used for Cu-isotope work was *National Institute of Standards and Technology's* Standard Reference Material 976 (NIST SRM976), however, this material is no longer produced nor commercially available. The reference material used as a standard reference during analysis in this thesis is *European Reference Material* (ERM) AE647 produced by the *Institute for Reference Materials and Measurements* (IRMM) in Geel, Belgium. Moeller et al. (2012) was the first to link ERM AE647 to the original NIST SRM976; The Cu-isotope ratio was determined to give $\delta^{65}Cu = -0.21 \pm 0.05‰$ relative to NIST SRM976 (Moeller et al. 2012). To adjust results obtained using the ERM AE647 standard to literature and data using NIST SRM976 as a reference, +0.21‰ is added to the $\delta^{65}Cu_{AE647}$ results. Throughout this thesis, δ^{65}Cu-values are primarily reported and referred to relative to the original NIST SRM976. Only in Chapter 5: Results, values are sometimes reported relative to ERM AE647 as well as NIST SRM976. If not stated otherwise, NIST SRM976 is the reference standard material when presenting δ^{65}Cu data in this thesis.

2.1 Behavior of copper in natural waters

The behavior heavy metals in natural waters is explained in detail in Drever's (1997) *"The geochemistry of natural waters"* and this subchapter is a short description of the most important properties of Cu as described in Drever (1997). Cu is usually present only in low concentrations in uncontaminated, neutral-pH natural waters; The typical concentration in uncontaminated streams is 7 ppb (Drever 1997 p. 176). The dominant species of Cu in solution is the divalent cation (Cu^{2+}), either free or complexed. Under oxidizing, acidic conditions, Cu is soluble and mobile; Under reducing conditions with sulfides present, relatively insoluble Cu-sulfides form (fig. 2.1). Under reducing conditions without sulfides present, insoluble native Cu is stable. Further, Cu forms anionic species at high pH, but pH is rarely high enough in nature to make these species relevant in natural systems (Drever 1997 p.189). In addition, Cu has a strong affinity to form complexes with natural organic matter, and also adsorbs to Fe- and Mn-oxyhydroxides. The adsorption to Fe- and Mn-oxyhydroxides is pH dependent; Adsorption of Cu^{2+} is essentially zero at and below pH 4, and essentially complete at and above pH 6 (fig. 2.2; Drever 1997 p. 99). With rising pH,

adsorption by Fe- and Mn-oxyhydroxides increases and thus dissolved Cu concentration decreases. In natural surface waters, redox reactions are central chemical reactions. Redox conditions are determined by the balance between the supply of oxygen and the oxygen consumption by organic matter decomposition (Drever 1997 p. 174). Organic matter acts as a reducing agent in natural waters. In this thesis we are exclusively dealing with surface waters in an open natural system, where conditions are generally oxidizing. Redox conditions can be expressed as pe (or pE), an unitless measure of electron activity. A pe-pH diagram displays the solubility information of a system in equilibrium. Figure 2.1 displays a simplified pe-pH diagram of the Cu-S-O-H_2O system at standard conditions (1 atm, 25°C).

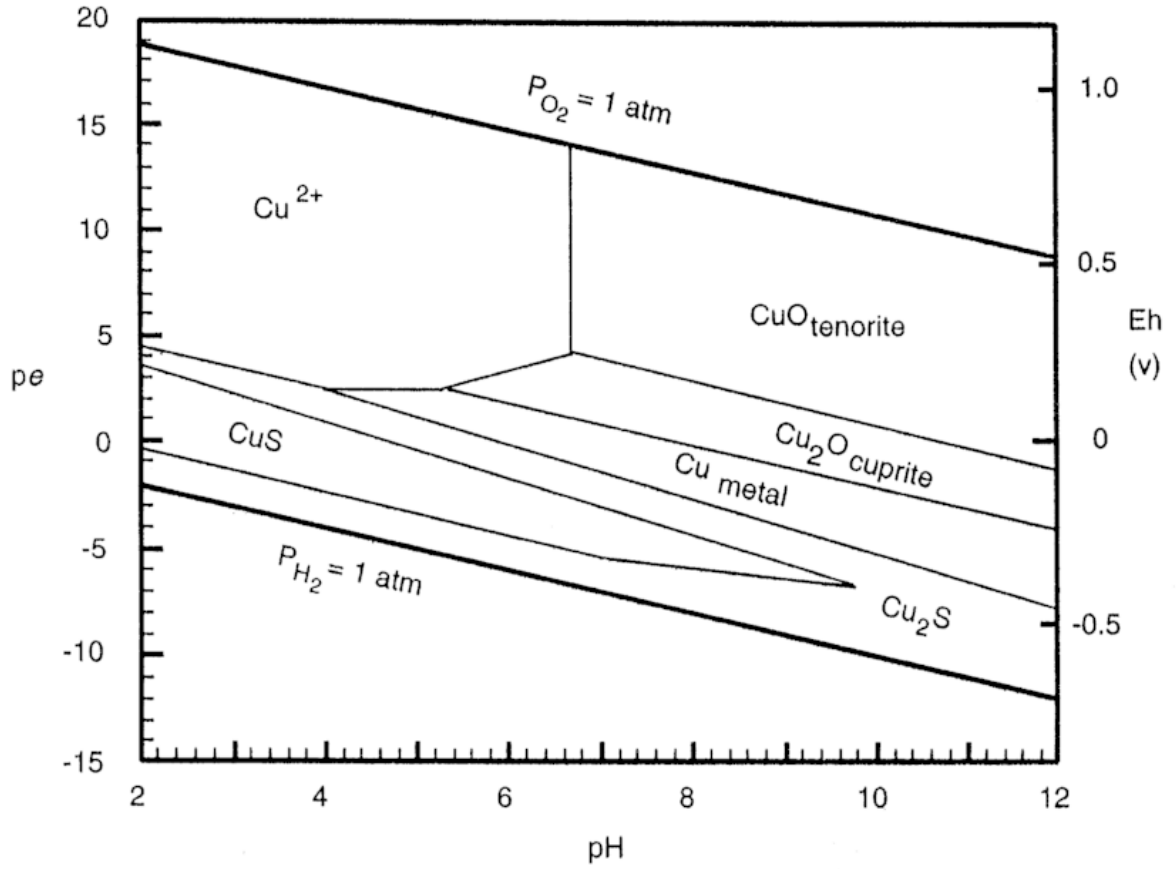

Figure 2.1: Simplified pe-pH diagram for the Cu-S-O-H_2O system at standard conditions (1 atm, 25°C) (Drever 1997 p.190).

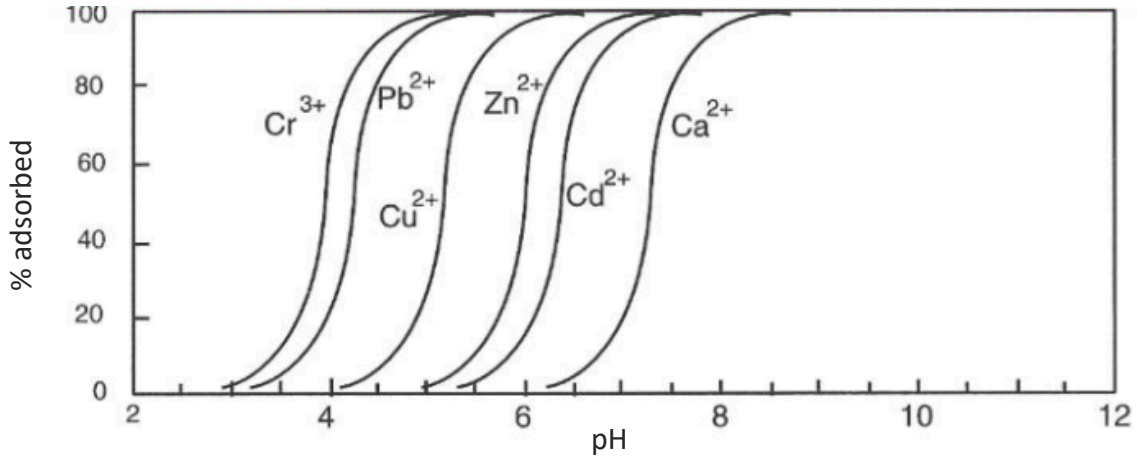

Figure 2.2: Adsorption of metal cations on hydrous ferric oxide as a function of pH (Drever 1997 p.99).

2.2 Natural isotopic variations

In natural samples, Cu is the transition metal that displays the largest isotopic variation found in the environment (Larson et al. 2003; Song et al. 2016). This subchapter aims to give an overview of the natural isotopic variations in some natural reservoirs, before the next subchapter (*2.3 Fractionation of stable copper isotopes*) presents the most important processes that control the fractionation of Cu in nature. Figure 2.5 summarizes the isotopic signatures of some Earth reservoirs.

2.2.1 Igneous rocks

Igneous rocks are mantle derived and formed by the crystallization of molten rock (mantle). Bulk Silicate Earth (BSE) is a term used for the hypothetical reservoir of the Earth's primitive mantle before the first crust formed. BSE can be used as a reference point for δ^{65}Cu-values in other igneous rocks, as it represents the "original" isotopic composition of the mantle after the core was partitioned. Using various ultramafic rocks together with δ^{65}Cu-values of mid-ocean ridge and ocean island basalts (MORB and OIB) from literature, Savage et al. (2015) defined BSE δ^{65}Cu= +0.07 $\pm$ 0.10‰. Liu et al. (2015) also used data on a variety of igneous rocks to constrain BSE δ^{65}Cu. Results from metasomatized and non-metasomatized peridotites show δ^{65}Cu= -0.64‰ to +1.82‰ and δ^{65}Cu= -0.15‰ to +0.18‰, respectively; MORB and OIB: δ^{65}Cu= +0.09 $\pm$ 0.13‰ and; arc and continental basalts δ^{65}Cu= -0.19‰ to +0.47‰. Liu et al. (2015) propose the isotopic composition of Bulk Silicate Earth

to be δ^{65}Cu= +0.06 $\pm$ 0.20‰. Collectively, Cu isotope data from a wide range of studied igneous rocks makes it apparent that they generally show a limited range of δ^{65}Cu-values, that clusters tightly around zero when unaltered (i.e. Albarède 2004; Li et al. 2014; Liu et al. 2015; fig. 2.5).

2.2.2 Ore deposits

Cu is mainly concentrated in sulfide ore deposits in the lithosphere. There are two important types of Cu sulfide deposits: porphyry copper and volcanogenic massive sulfide (VMS) deposits. Both deposit types are magmatic hydrothermal deposits, meaning Cu is concentrated from a metal- and sulfide-rich hydrothermal fluid precipitating the metals. Porphyry deposits are related to hydrothermal activity in island-arc, low angle subduction zones, where magma first cools slowly at depth, precipitating larger crystals (porphyry texture) before quickly rising to the surface (Blundy et al. 2015; Sun et al. 2016). The Cu-rich ore is formed from hydrothermal fluids rising from a magma chamber and precipitates in cracks and veins (disseminated ore) (Blundy et al. 2015). VMS deposits are formed on the ocean floor in hydrothermal sulfide chimney systems called black smokers. Here, seawater penetrates and circulates in the oceanic crust, is heated by a magma source, dissolves metals and sulfides and finally rises to the surface of the ocean floor where metal sulfides precipitate when encountering the cool seawater. The most common mineral for economical Cu-extraction is chalcopyrite ($CuFeS_2$).

In terrestrial porphyry copper deposits, three distinct reservoirs based on isotopic composition has been established: leached, supergene and hypogene (Mathur et al. 2009; Mirnejad et al. 2010). Leach minerals, like hematite (Fe_2O_3), goethite (α-FeOOH) and jarosite ($KFe^{3+}_3(OH)_6(SO_4)_2$), are found above the water table (fig. 2.3). These are residual minerals formed by oxidation and leaching (weathering) of the original ore (Mathur et al. 2009). Supergene minerals are secondary minerals that precipitate beneath the leached zone (fig. 2.3). These minerals are formed by precipitation from leachant which contains the metals derived from the primary ore in the overlying zone. The Cu removed from the leached zone can precipitate as secondary minerals like chalcocite (CuS_2) and covellite (CuS) below the water table where conditions change from oxidizing to reducing (Mirnejad et al. 2010). Hypogene minerals, like chalcopyrite, are unaltered and were formed at high temperatures

(Mirnejad et al. 2010). Primary, unaltered (hypogene) minerals display a narrow δ^{65}Cu signature around zero (approximately -1‰ to +1‰) (Mathur et al. 2009); Leached minerals have an isotopically light δ^{65}Cu signature (δ^{65}Cu= -6.16‰ to -1.00‰); Supergene enrichment minerals show a significantly heavier signal (δ^{65}Cu= +2.52‰ to +4.82‰) (Mathur et al. 2009; Mirnejad et al. 2010). VMS deposits often have complex formation histories with multiple stages of precipitation, heating, cooling and mixing (Rouxel et al. 2004). Chalcopyrite samples from a variety of oceanic hydrothermal deposits show a wider δ^{65}Cu range (-1.30‰ to 2.91‰) compared to hypogene porphyry chalcopyrite (Rouxel et al. 2004). VMS deposits varies in mineralogy within the same deposit, with Cu-rich minerals like chalcopyrite precipitating closer to the high temperature vent compared to Zn- and Pb-rich minerals like sphalerite and galena (fig. 2.4).

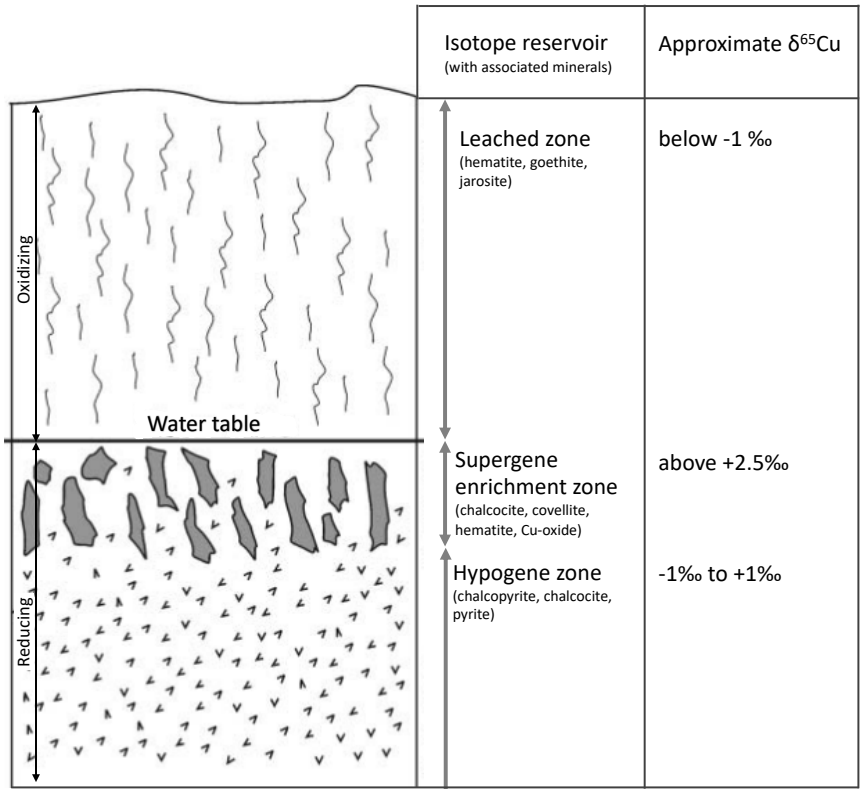

Figure 2.3: Schematic figure of the three separate isotope reservoirs in a typical porphyry copper ore deposit, together with some associated minerals and their expected approximate δ^{65}Cu-values (Mathur et al. 2009). Figure modified from Mirnejad et al. (2010).

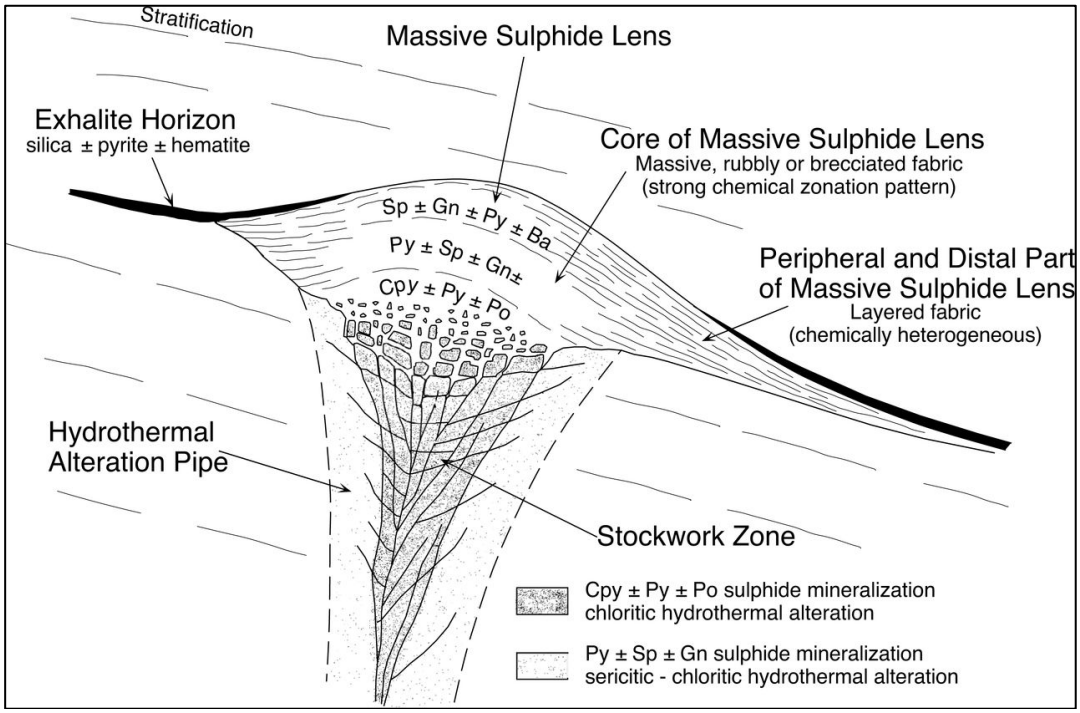

Figure 2.4: Idealized cross-section through a VMS-deposit with the typical characteristic features. Ba – barite, cpy – chalcopyrite, gn – galena, po – pyrrhotite, py – pyrite, sp – sphalerite (McClenaghan and Peter 2016; modified from Lydon 1984).

2.2.3 Soils, sediments and lithosphere

Fekiacova et al. (2015) has collected and compiled isotopic compositions of soils from various literature as well as supplied additional data on δ^{65}Cu in soils. Unpolluted soils show δ^{65}Cu= -0.95‰ to +0.44‰ whereas polluted soils range -0.48‰ to +0.36‰ (Fekiacova et al. 2015). The distribution is centred at δ^{65}Cu = 0‰ for unpolluted soils and +0.2‰ for polluted soils, indicating that polluted soils are slightly enriched in the heavy ^{65}Cu isotope (Fekiacova et al. 2015). El Azzi et al. (2013) found riverbed sediments to have approximately the same isotopic signature as the local bedrock, and thus varies dependent on local geology. Marine sediments appear to have a remarkably homogeneous composition around +0.3‰; Sediment samples from a broad spectrum of marine settings (oxic, euxinic, continental margin) only ranging between δ^{65}Cu= +0.04‰ to +0.32‰ are presented in Little et al.'s (2017) work. For other lithospheric Cu, Little et al. (2014) found ferromanganese (Fe-Mn) crusts on the ocean floor to be δ^{65}Cu= +0.12‰ to +0.58‰. Cu bound to silicates does not show any significant isotope variations, δ^{65}Cu = 0 ± 1‰ (i.e. Chapman et al. 2006; Pokrovsky et al. 2008; Li et al. 2009; Bigalke et al. 2010; Song et al. 2016).

2.2.4 Hydrosphere

Wang et al. (2017) has reviewed a handful of literature data on Cu isotopic composition in aquatic surface environments. For rivers in general, suspended particulate matter (SPM) show a similar δ^{65}Cu-value to the surrounding bedrock, whereas dissolved Cu displays a slightly heavier signature (Wang et al. 2017). The review established that dissolved Cu in uncontaminated rivers span an isotopic range of -0.69‰ < δ^{65}Cu < +1.55‰, with an average of δ^{65}Cu = +0.53‰. SPM in the same environment shows a complementary light pool of δ^{65}Cu between -1.02‰ to +0.09‰, with an average composition of -0.31‰ (Wang et al. 2017). In general, dissolved δ^{65}Cu in uncontaminated aquatic environments are slightly above the local bedrock's isotopic signature. However, isotopic composition of rivers and streams can be heavily influenced by anthropogenic sources disturbing the general trend. For example, studies from vineyard rivers in southern France show a lighter dissolved δ^{65}Cu signature than expected due to the use of $CuSO_4$ fungicide, which has a light isotopic signature disturbing the expected higher dissolved δ^{65}Cu (El Azzi et al. 2013; Petit et al. 2013). Mining of Cu-sulfides is another source of anthropogenic disturbance of the copper isotope composition of natural surface waters that will be discussed in detail later. For seawater, Wang et al. (2017) reports δ^{65}Cu values varying between +0.38‰ and +1.44‰ (averaging +0.70‰). Seawater thus represents a heavier average isotopic signature than average riverine input (+0.70‰ versus +0.53‰). In addition, Takano et al. (2014) found a general trend in the North and South Atlantic, South Indian and North Pacific oceans of δ^{65}Cu at approximately +0.5‰ in the surface ocean, increasing with depth. Reported δ^{65}Cu values of seawater is also higher than the average isotopic composition of the Earth (~0‰) (Takano et al. 2014).

2.2.5 Biosphere

Bacterial cells contain negatively charged organic acid groups like carboxyl (-COOH), phosphoryl ($-PO_3^{2-}$) and hydroxyl (-OH) that form complexes with aqueous metal cations like Cu^+ and Cu^{2+} (Navarrete et al. 2011). In general, bacterial cells preferentially incorporates the light ^{63}Cu. However, Mathur et al. (2005) performed a bacterial uptake experiment with the acidophilic *T.Ferrooxidans* bacteria where the results showed that after the 30 day experiment the bacteria pellets had a significantly higher $\delta^{65}Cu$ compared to the initial Cu-rich medium that they were grown in. The $\delta^{65}Cu$ of the bacteria pellet centrifuged in a $\delta^{65}Cu$ = +2.55‰ medium for 30 days had an average $\delta^{65}Cu$ value of +5.59‰ (Mathur et al. 2005). Cu isotope work has also been carried out on various plants. Wang et al. (2017) for instance, found that plants appear to be systematically enriched in the light isotope compared to the soil in which the plant grew in. Isotopic variation is also found within the plant itself (Wang et al. 2017).

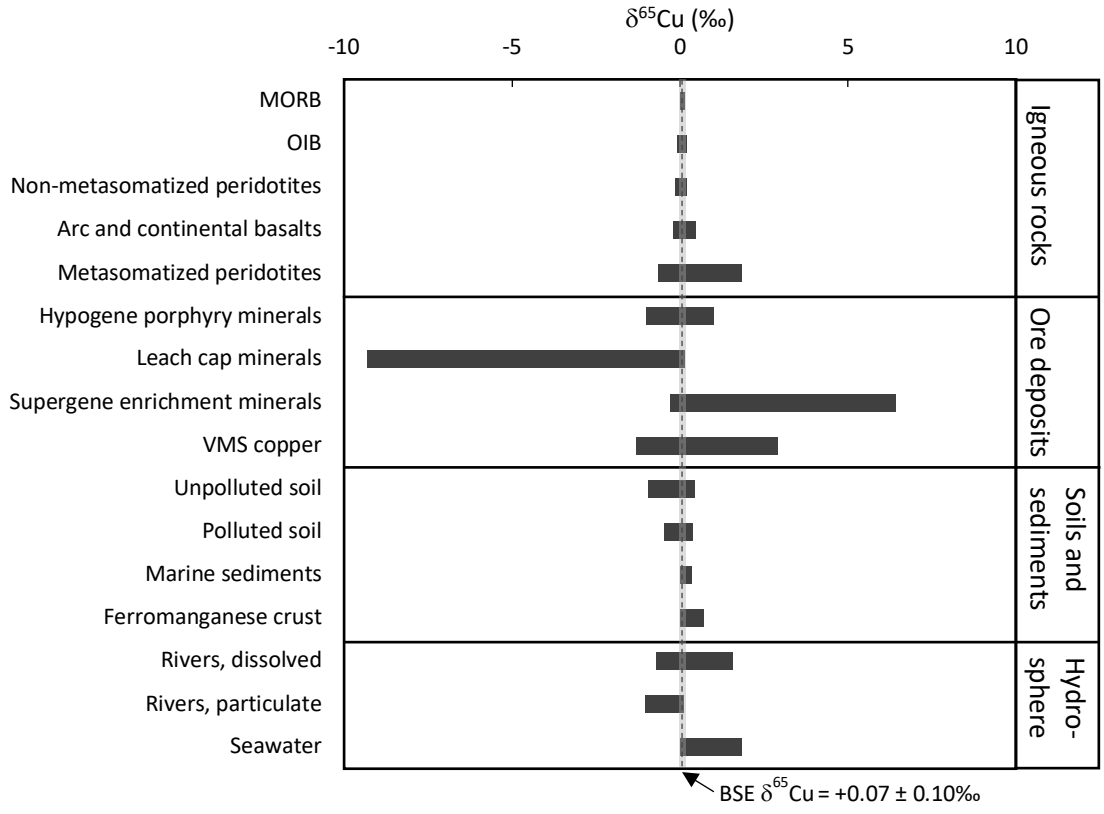

Figure 2.5: Natural isotopic composition range ($\delta^{65}Cu$) from literature review of various igneous rocks (Liu et al. 2015; Savage et al. 2015), ore deposits (Rouxel et al. 2004; Mathur et al. 2009), sediments and soils (Little et al. 2014, 2017; Fekiacova et al. 2015), the hydrosphere (Wang et al. 2017) and Bulk Silicate Earth (Savage et al. 2015).

2.3 Fractionation of stable copper isotopes

Isotope fractionation is the relative partitioning of the heavy and light isotope between two compounds or phases. Fractionation can be divided into equilibrium fractionation and kinetic fractionation. Equilibrium fractionations are reversible and only occurs under chemical equilibrium, whereas kinetic fractionations are irreversible, unidirectional reactions where forward and backward rates are not identical. Fractionation is expressed by a fractionation factor (α), also known as an enrichment factor. The fractionation factor is defined by the relative abundances of the light (l) and heavy (h) isotopes in the original ($R_A = A_h/A_l$) and new sample ($R_B = B_h/B_l$):

$$\alpha_{A-B} = \frac{R_A}{R_B} \tag{2}$$

The relationship between a fractionation factor and the delta notation is:

$$\alpha_{A-B} = \frac{1000 + \delta_A}{1000 + \delta_B} \tag{3}$$

Fractionation can also be displayed as a separation factor (Δ), which is defined as:

$$\Delta^{65}Cu_{x-y} = \delta^{65}Cu_x - \delta^{65}Cu_y \tag{4}$$

Δ^{65}Cu is a measurement of the isotopic difference between two substances, i.e. solution-solid. Constraining fractionation and separation factors from natural samples is complicated as isotopic compositions typically result from several fractionation processes. The processes can in many cases only be partly constrained and can be difficult to isolate for experimental purposes (Maher et al. 2011). A general observation for Cu-isotopes is that literature data

from various reservoirs of the Earth indicate a relative isotopic homogeneity of samples characterized by high temperature processes, whereas samples formed and equilibrated at low temperatures shows a much higher variability (Moynier et al. 2017). The following subchapters address some of the most important processes of Cu isotope fractionation in nature.

2.3.1 High-temperature processes

As stated previously, **high-temperature processes** appear to not result in large fractionation of Cu, as most studies of isotopic variation within high temperature hypogene mineral deposits and igneous rocks generally show limited variation (i.e. Zhu et al. 2000; Maher et al. 2011; Moynier et al. 2017). However, some studies have found naturally produced variations of up to +4‰ in hypogene Cu-deposits (Graham et al. 2004; Li et al. 2010). Various hypotheses explaining these exceptions have been proposed, one of them is that the fractionation is caused by a vapor phase coexisting with the aqueous phase, and results in a lighter leached phase compared to the residual mineral phase (Maher et al. 2011). Another explanation lies in a possible heterogeneity of the source in regards to pH, oxidation condition and temperature (Gregory and Mathur 2017). Temperature appears to be an important factor in the fractionation of Cu, as also seen in hydrothermal low temperature deposits that display large δ^{65}Cu differences even within the same deposit, whereas igneous hosted, high temperature, chalcopyrites show a similar δ^{65}Cu worldwide (Zhu et al. 2000). Klein and Rose (2020) also found no significant fractionation between ore rock and slag rock after experimental testing of Cu-sulfide smelting under ideal conditions. Under uncontrolled, oxidizing conditions fractionation is expected (Klein and Rose 2020). Conclusively, there appears to be a common agreement that high temperature conditions and processes generally show an insignificant amount of fractionation of Cu, and large fractionations are mainly a result of low temperature processes and secondary reaction mechanisms.

2.3.2 Low-temperature abiotic processes

For Cu as well as for most other metals, **redox reactions** are the most important cause of large isotopic fractionation. Reduced Cu minerals (Cu(I)) are enriched in the light isotope up to $\Delta^{65}Cu_{min.-sol.}$ = -4‰, and oxidized minerals (Cu(II)) are enriched in the heavy isotope up to $\Delta^{65}Cu_{min.-sol.}$ = +5.3‰ (Ryan et al. 2014). Cumulative fractionations of up to 20‰ have been observed in environmental samples that have undergone one or more redox cycles (Moynier et al. 2017). In the supergene environment, Cu is found in both reduced and oxidized form, and the transition between Cu^{+} and Cu^{2+} occurs at surface conditions (Moynier et al. 2017). Zhu et al. (2000) was the first to experimentally confirm that the fractionation following a redox transition is large: ~4‰ separation between aqueous Cu^{2+} and Cu-iodide (CuI) precipitate. Furthermore, Ehrlich et al. (2004) demonstrated that the change in isotopic signature is almost certainly caused by a change in oxidation state, not a phase change. This is proven by the pair of separation factors, $\Delta^{65}Cu$, which show the difference in $\delta^{65}Cu$ for the two phases. $\Delta^{65}Cu$ for the precipitation of covellite (Cu(I)S) from aqueous Cu^{2+} is constrained by the phase change reaction between $Cu(OH)_2$ precipitate and aqueous Cu^{2+} (fig. 2.6). The separation factors strongly indicate that a change in oxidation state will influence the fractionation significantly more than the phase change between solid and aqueous Cu of the same oxidation state.

a) $\Delta^{65}Cu_{Cu(II)\ aq–Cu(I)S\ s} = +3.5 \pm 0.02‰$

b) $\Delta^{65}Cu_{Cu(II)\ aq–Cu(II)(OH)2\ s} = +0.27 \pm 0.02‰$

Figure 2.6: Cu isotope separation factors ($\Delta^{65}Cu$) for **a)** the reduction of aqueous Cu(II) to solid Cu(I)S at T=25°C; **b)** a phase change reaction between aqueous Cu(II) to $Cu(II)(OH)_2$ solid (Ehrlich et al. 2004).

Fernandez and Borrok (2009) executed an experiment of oxidative leaching of Cu-sulfides in order to quantify the fractionation during weathering release of Cu from chalcopyrite. The experiment determined that Cu released from a chalcopyrite-rich rock was up to 2‰ heavier than the primary mineral. Mathur et al. (2005) and Kimball et al. (2009) found chalcopyrite weathering to result in 1.2‰ and 1.4‰ heavier signatures respectively. Song et al. (2016) presents a similar result, where fractionation of Cu from Cu-sulfides

results in a dissolved phase that is +1‰ to +3.5‰ heavier than various primary Cu sulfides. Fernandez and Borrok (2009) also proved that the fractionation of Cu during oxidative weathering of chalcopyrite is a function of the amount of Cu leached – ultimately related to the pH of the solution. Fernandez and Borrok's (2009) experiments showed that the separation factor between solution and rock, $\Delta^{65}Cu_{sol\text{-}rock}$, decreased and converged toward $\Delta^{65}Cu_{sol\text{-}rock} = 0‰$, as the percent of leached Cu increased. This means that the $\delta^{65}Cu$ composition of Cu leached from chalcopyrite will converge toward the same $\delta^{65}Cu$ value as the primary source chalcopyrite with extensive leaching.

Secondary mineralization may follow oxidative weathering by precipitation from the Cu-rich fluid leachate. Secondary minerals like covellite (CuS) and chalcocite (Cu_2S) precipitate in the supergene enrichment zone (fig. 2.3). The minerals precipitate below the water table where conditions are reducing. Consequently, the observed $\delta^{65}Cu$ in the minerals reflects the (relatively high) dissolved $\delta^{65}Cu$ in the leachate from oxidative weathering, and therefore secondary minerals are enriched in the heavy isotope relative to hypogene minerals (Mathur et al. 2018). However, the aqueous phase is further enriched in ^{65}Cu compared to the source. Further, the secondary minerals can be exposed to oxidative dissolution following uplift and erosion, and multiple leaching-precipitation events cause supergene minerals to become progressively enriched in the heavy isotope (Mathur et al. 2005).

Isotopic fractionation is also caused by **inorganic adsorption** of Cu onto various substrates. Balistrieri et al. (2008) found a preferential adsorption of heavy ^{65}Cu onto ferric oxyhydroxide surfaces of $\Delta^{65}Cu_{sol.\text{-}solid} = -0.73‰ \pm 0.08‰$; and for goethite $\Delta^{65}Cu_{sol.\text{-}solid} = -0.35‰ \pm 0.11‰$. Enrichment of ^{65}Cu has been also been observed in organo-Cu complexes. Ryan et al. (2014) and Wang et al. (2017) reports **organic complexation** to significantly prefer ^{65}Cu with $\Delta^{65}Cu_{free\text{-}complex} = -0.84‰$ to $-0.14‰$.

2.3.3 Biological processes

Isotopic fractionation of Cu can also be triggered by biological processes. Biological fractionation is complex and has been researched and attempted constrained in a number of studies (i.e. Mathur et al. 2005; Wang et al. 2017). Microorganisms require Cu for the

functioning of important enzymes and can incorporate Cu by two processes: **biotic surface adsorption** and **intracellular incorporation** (Navarrete et al. 2011). Both of these processes show a preferential uptake of the light ^{63}Cu isotope in the *Bacillus subtilis* and *Escherichia coli* bacteria (Navarrete et al. 2011). The results gave separation factors of $\Delta^{65}Cu_{sol.\text{-}bacteria}$ = +0.20‰ to +2.60‰ for adsorption and +1.0‰ to +4.4‰ for intracellular incorporation (Navarrete et al. 2011). Conclusively, regardless of experimental conditions living bacteria prefer the light isotope, leaving the solution enriched in the heavy isotope. This is reflected in marine sediments which show a lighter isotopic signature than the ocean (fig. 2.5), most likely due to the preferential scavenging of the light ^{63}Cu by planktonic biomass. When the plankton dies it "rains" down on the seafloor and is incorporated into the ocean floor sediment which consequently gains a lower isotopic signature (Chi Fru et al. 2016). In addition, more fractionation occurs under However, other studies (i.e. Kimball et al. 2009; Mathur et al. 2005) have found the *T.Ferrooxidans* bacteria to preferentially adsorb the heavy ^{65}Cu isotopes, with a separation up to $\Delta^{65}Cu_{sol.\text{-}T.Ferrooxidans}$ = -3‰. This effect is most likely from the layer of Cu-Fe oxide minerals surrounding the bacterial cells, resulting in overlapping signals from any bacterial uptake and the adsorption onto the mineral coating (Navarrete et al. 2011; Mathur et al. 2005).

2.3.4 Summary of fractionation processes

(1) High temperature processes cause insignificant fractionation for the most part.
(2) Redox reactions cause the most significant fractionation of Cu. Reduced Cu is enriched in the light isotope (^{63}Cu); oxidized Cu enriched in the heavy ^{65}Cu. Oxidative weathering of sulfide minerals leads to an enriched aqueous phase.
(3) Secondary mineralization of Cu is enriched in the heavy isotope. Progressively heavier signature with several events of oxidative dissolution - mineralization.
(4) Inorganic adsorption preferentially adsorbs heavy Cu.
(5) Organic complexation causes heavy isotope to be enriched in the complex
(6) For biotic adsorption/incorporation, living organisms preferentially adsorb/incorporate the light isotope.

Chapter 3: Study location

This thesis is focused on copper isotopic compositions of natural surface waters around historical copper mines in Norway. The two locations chosen for the purpose of this thesis are the Storwartz mining field in Røros and the copper mines in Løkken (fig. 3.1). Cu-mining is a historically important industry in Norway. The oldest Cu mining in the country dates back to the medieval period, large-scale mining followed in Selje, Telemark in 1524 (Nissen 1976, p. 9). Mining activity was especially high from the mid 1600s and throughout the 1700s. In 1660 there were 23 active mines in Norway; However, only the mines in Røros and Løkken were significant for a long period of time (Nissen 1976, p. 11). At their time, the mines in Røros and Løkken were the biggest and most important in Norway, both actively mining for over 300 years from the mid 1600s to the late 1990s. In total, the mines in Røros and at Løkken mined approximately 28 Mt (4 + 24) of ore rock, yielding about 0.67 Mt of Cu (Bjerkgård 2015).

Figure 3.1: Location of the two study areas, south of Trondheim in Trøndelag county, Norway. Made with ArcGIS Online (Map layers by Esri, HERE, Garmin, INCREMENT P, METI/NASA, USGS).

3.1 Røros, Storwartz copper mines

3.1.1 Historical background

In 1644, farmer Hans Olsen Aasen stumbled upon the copper rich ore rock while reindeer hunting (Geithe 2014; Nissen 1976, p. 20). The name Storwartz comes from the Germanified version of Storvola, one of the mountain peaks in the area. The mining started in *Gamle Storwartz mine* the year after, in 1645. The high-grade ore, up to 4% Cu (Bjerkgård 2015), tempted the miners to further explore the region for even more exploitable deposits. In total, the Storwartz mining field comprises nine mines that were active throughout the 333 years of production. Røros was an important mining town, and several other mines are found in the area in addition to Storwartz. The infrastructure in the Røros area was expanded through the long history of mining, and many traces of the old industry are still left to this day. At lower Storwartz, a flotation plant for processing the ore was built and residual waste from the flotation process (tailings) was dumped into an artificial tailings pond called Slamdammen as well as surrounding surface waste deposits (fig. 3.2). Water from the tailings pond drains southward through Prestbekken, running into Djupsjøen in Hitterdalsvassdraget. The concentrated ore was transported by a cable system to Røros, were it was processed in the smelters. Still today, large piles of slag material lie next to the smeltery (fig. 3.3). The slag heaps are waste material from the smelting process and is a mixture of oxides, silicates and other residues.

Table 3.1: The Storwartz mines and their active period (Geithe 2013b)

Mine	Active period
Gamle Storwartz	1645-1946
Nyberget	1650-1713 1859-1890
Heskletten	1659-1756
Gamle Solskinn	1673-1730 1870-1890
Christian Quintus	1691-1775
Myrgruva	1694-1770
Nye Storwartz	1708-1946
Nye Solskinn	1854 1861-1890
Olavsgruva	1937-1972

Table 3.1 lists the nine mines in the Storwartz area together with their active years of mining. *Heskletten*, *Christian Quintus* and *Myrgruva* are connected underground – the same applies for *Nye Solskinn* and *Nyberget* (Geithe 2013a). *Nye Storwartz* is considered the main mine in the field, continuously producing for almost 250 years. *Nye Storwartz* was closed in 1946 whereas *Olavsgruva* was the final mine to close in 1972, marking the end of the mining at the Storwartz mining field (Rygg n.d.). In total, 4 Mt of material was extracted, yielding 0.25 Mt of resources, mainly Cu, Zn and Pb (Bjerkgård 2015).

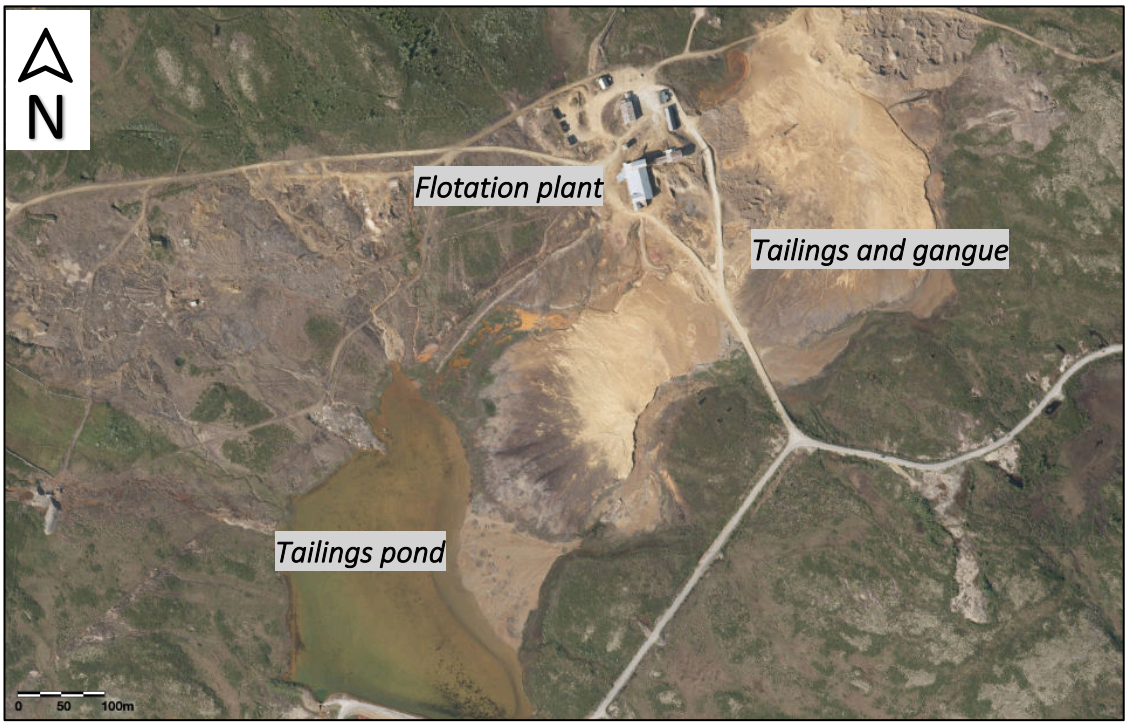

Figure 3.2: Lower Storwartz where the flotation plant was built. The tailings pond, Slamdammen, used for under water disposal of tailings. Large exposed waste piles of tailings and gangue also clearly visible in the area. Made with Norge i bilder (2020).

Figure 3.3.: The slag heaps next to the smelter in Røros town centre. Hyttelva runs between the smelter and the slag heaps, from Hitterdalsvassdraget in the northeast. Made with Norge i bilder (2020).

3.1.2 Geological setting

The Storwartz mining field is located approximately 10 kilometres northeast of Røros town in Trøndelag county, Norway. The lithology is mainly dominated by clastic metasedimentary rocks such as calcareous phyllite and meta greywacke as well as subordinate mafic intrusives, mainly medium to coarse-grained deformed gabbros (Bjerkgård 2015; Rui 1981). The lithology belongs to the Aursund Sequence, an underlying group of the Trondheim Nappe Complex. The Trondheim Nappe Complex is an allochton of Cambro-Silurian age, overthrust onto the Baltic shield during the Caledonian orogeny (Rui 1981). The entire succession is metamorphosed at lower greenschist to lower amphibolite facies condition, with an increasing grade of metamorphism towards northeast (Barrie et al. 2010). In addition, the bedrock is complexly folded and characterized by a series of low-angle thrusts gently dipping to the west (Rosholt and Wilberg 2001 p.2).

The ore-deposit in the Storwartz mining field is a volcanogenic massive sulfide (VMS) deposit, classified by most as a Besshi-type VMS because it occurs in a mixed sedimentary-volcanic environment and is pyrrhotite-rich (Taylor et al. 1995; Barrie et al. 2010). It is believed that the deposit formed in an oceanic marginal sedimentary basin near the Baltic shield approximately 440 Ma (Rosholt and Wilberg 2001 p.2; Bjerkgård 2015). The ore varies in chemical composition but is particularly rich in Cu (1-4%) and Zn (3-12%) (Bjerkgård 2015). The most important minerals in the Storwartz field are pyrite (FeS), pyrrhotite ($Fe_{1-x}S$), chalcopyrite ($CuFeS_2$), sphalerite (ZnS) and galena (PbS). Cu precipitates at a higher temperature than Pb and Zn, displaying relative distance from the high temperature vent (fig. 2.4) and results in a zonation of predominantly Zn-rich ore toward west, and more Cu-rich ore in the east. Several ore bodies were found in the area; However, it is believed that they all are from the same original deposit that was deformed and fragmented during the intense deformation of the Caledonian orogeny (Bjerkgård 2015). Nine separate mines exist in the Storwartz mine field, seven of which mined in Cu-rich chalcopyrite-pyrrhotite (cpy-po) ore bodies in the eastern part, while the two westernmost mines, Gamle and Nye Storwartz, mined Zn-rich pyrrhotite-pyrite-sphalerite (po-py-sp) deposits (Bjerkgård 2015).

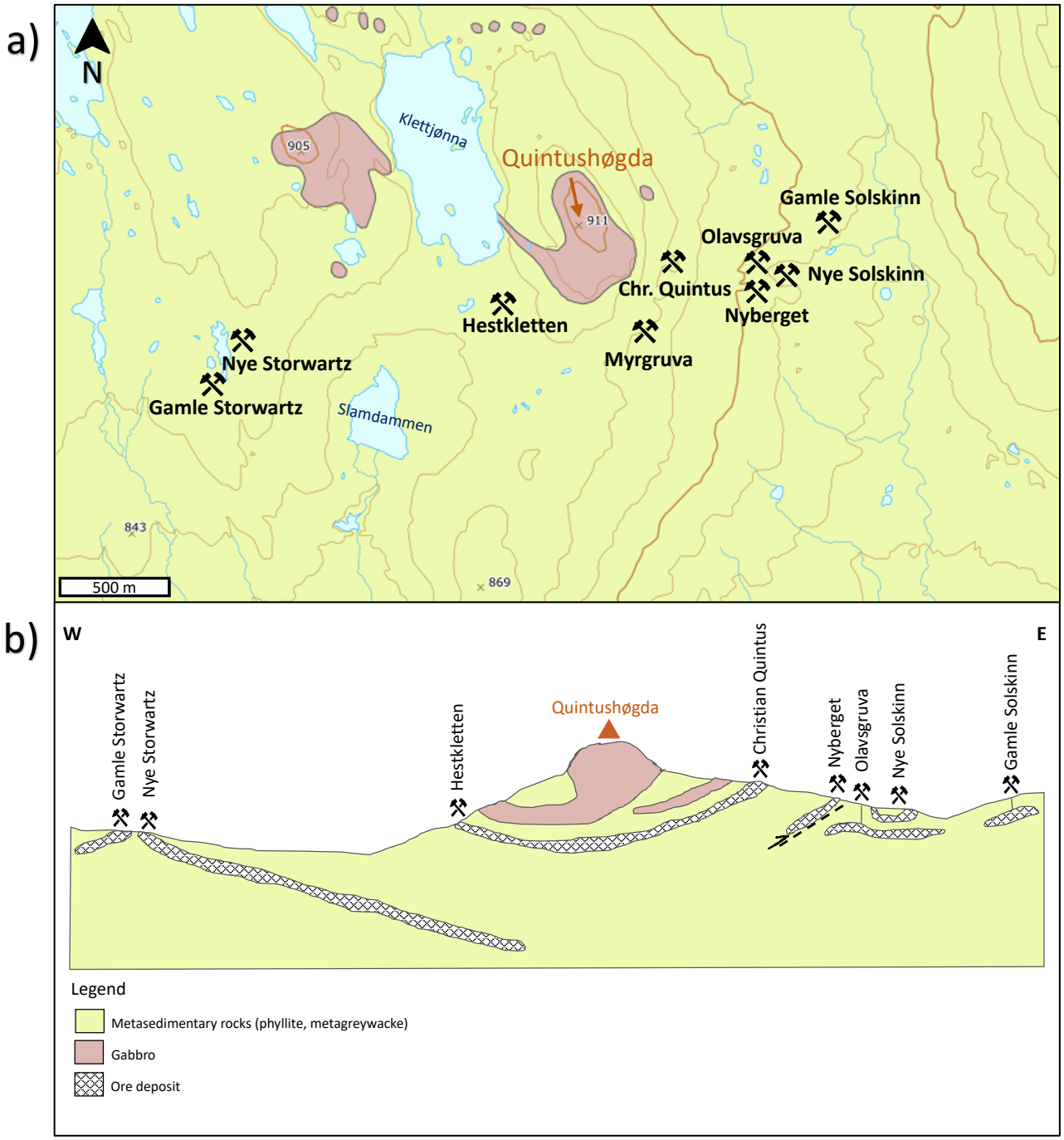

Figure 3.4: (a) Geological map of the Storwartz mining field and overview of the mines and **(b)** Schematic profile of the Storwartz mining field. Modified from (a) NGU (2020) and (b) Bjerkgård (2015).

3.2 Løkken copper mines

3.2.1 Historical background

The mining history at Løkken begins in 1654, 10 years after the ore was accidentally discovered by Swedish tailor Lars Olufson (Orkla Industrimuseum n.d). The Løkken mines were active for 333 years and 4 different mine shafts were used to extract ore from the deposit. For the first 250 years, the mine was operated as an open pit mine at the surface of the deposit, where the entrance of Gammelgruva lies (fig. 3.5). However, during the 1900s, more advanced techniques and equipment made it possible to discover and explore the deeper parts of the deposit. Four shafts were used to transport the ore from the depths of the mine to the surface. The deepest shaft is Astrup – it reaches 1000 meters beneath the surface. The local infrastructure also had to be expanded to streamline the production with multiple smelters, flotation plants, a railway and a power plant. According to the Norwegian Environment Agency, Løkken is responsible for the largest disposal of sulfidic waste rocks and processing waste in Norway (Skei et al. 2019). Pyrite tailings were during the last years of production deposited under water in Bjørndalstjørna (Skei et al. 2019; fig. 3.5). During the period of mining, a total of 25 million tonnes of ore were mined – yielding 6 Mt of resources (Bjerkgård 2015). The mines closed in 1987, after 333 years of operation in the area.

3.2.2 Geological setting

Løkken is located in Meldal municipality in Sør Trøndelag county, southwest of Trondheim in Norway. The geology of the area is dominated by a 487 Myr old ophiolite complex commonly referred to as the Løkken ophiolite (Bjerkgård 2015) and is a part of the Trondheim Nappe Complex. The Trondheim Nappe Complex consists of three nappes (Støren, Meråker and Gula) that were overthrust onto the Baltic shield during the Caledonian orogeny. Løkken lies within the Støren Nappe – the westernmost and least metamorphosed nappe of the complex (Grammeltvedt 2004). The Støren Nappe is low-metamorphic (low to upper greenschist facies) and subdivided into three groups: Upper Hovin group, Lower Hovin group and Støren group. The sampling area is focused within lithologies from the Støren group, where volcanic rocks such as greenstone, pillow basalts and pyroclastic lava lithologies dominate, as well as some plutonic rocks like gabbro and

trondhjemite, of Ordovician to Silurian age (Grammeltvedt 2004). Evidence such as frequent pillow structured basalts with associated bedded jaspers indicate a submarine “black smoker” environment.

The ore rock at Løkken is a volcanogenic massive sulphide (VMS) deposit (fig. 2.4), that originates from hydrothermal activity at the seafloor prior to the obduction onto land. Such deposits are created when seawater permeates the bedrock, is heated by a magma source and enriches the water in various elements before it rises to the seafloor where metal sulfides precipitate in contact with cool seawater. The deposit is classified as a Cyprus type VMS, approximately 480 Myr old and was displaced onto land during the Caledonian orogeny (Bjerkgård 2015). Cyprus type deposits typically have a lens-shaped main orebody, that is underlain by a Cu-rich stringer zone in extensively chloritized basalts (Taylor et al. 1995). The ore was first discovered at the surface but extends 4 km west and 1 km down from the place of discovery, and is lenticular shaped, up to 250 m wide and 50-60 m thick (Orkla industrimuseum 2019a). Two smaller deposits named Indien and Bakindien lie above the main deposit, near Wallenberg shaft (fig. 3.4). The main deposit at Løkken is believed to be one of the largest Cyprus-type VMS deposits in the world (Orkla Industrimuseum 2019a). The minerals are separated into two types: (1) a vein mineral deposit and (2) an iron-sulfide mineral called “vasskis” (*Løkken Verk: En norsk grube gjennom 300 år* 1954 s.484-490). The vein mineral composition averages 70-75% pyrite, 6% chalcopyrite and 2.6% sphalerite as well as 14% quartz and small amounts of chlorite and calcite (*Løkken Verk: En norsk grube gjennom 300 år* 1954 s. 486), and is an epigenetic ore, meaning it was formed after the surrounding bedrock. The “vasskis” contains mainly pyrite, pyrrhotite and quartz and is a syngenetic ore type, meaning it formed at the same time as the surrounding greenschist (*Løkken Verk: En norsk grube gjennom 300 år* 1954 s.488-489). The average composition of the mined ore rock is 41.4% sulfur, 37.5% iron, 13.7% quartz, 2.1% copper and 1.9% zinc, as well as small amounts of several other trace elements (Orkla industrimuseum 2019b).

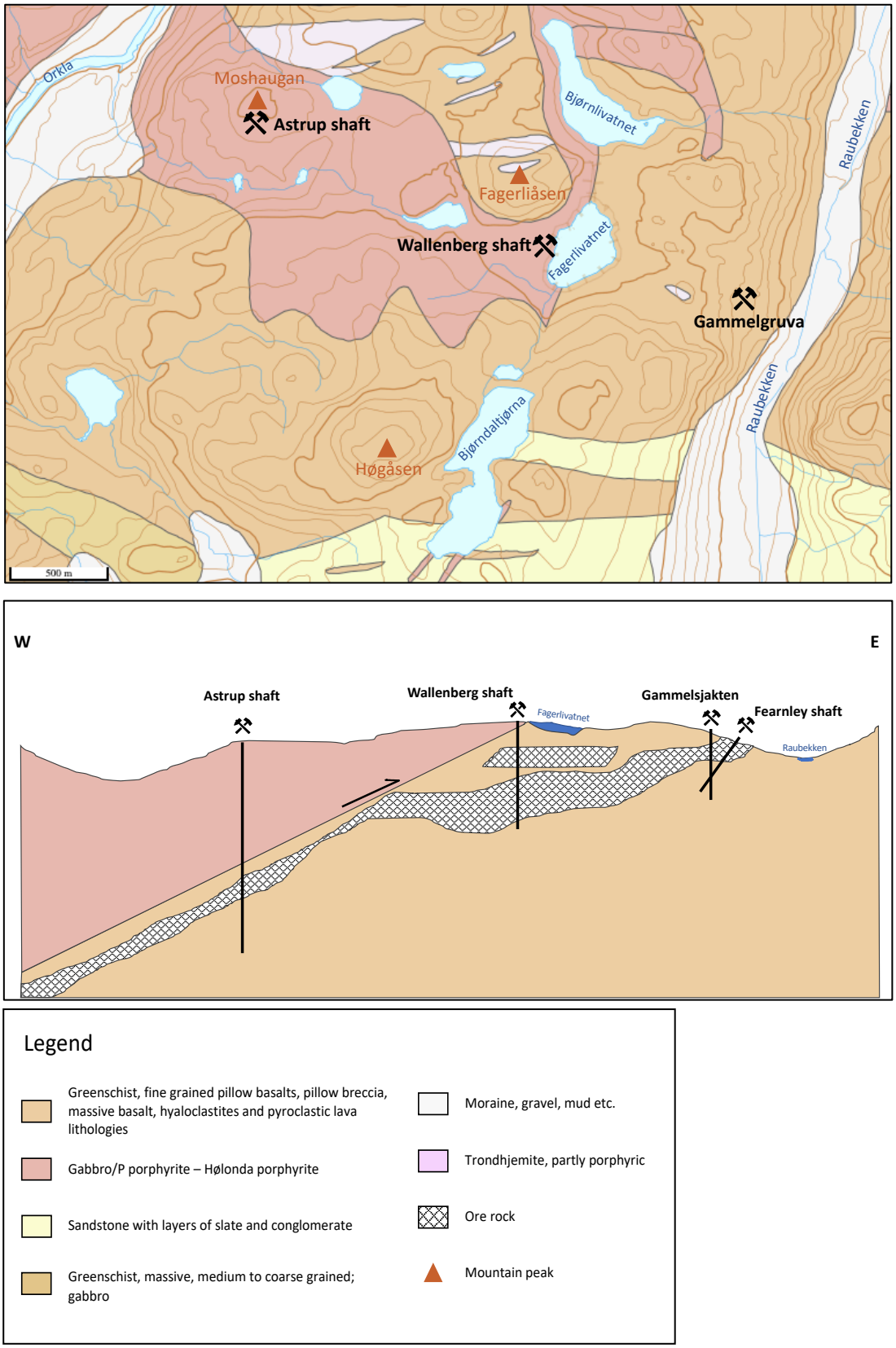

Figure 3.5: **(a)** Geological map of Løkken (modified from NGU (2020)) and **(b)** Schematic profile of the Løkken deposit (modified from Orkla industrimuseum (2019a)) .

3.3 Environmental impact of copper sulfide mining

3.3.1 Acid mine drainage and heavy metals

Copper mining impacts nature first by the extensive use of land. In addition, mining anthropogenically exposes toxic heavy metals and acidity to the environment by disposing metal sulfides to oxidative weathering. At elevated concentrations Cu is one of the most widespread inorganic toxic contaminants found in the environment (Wang et al. 2017). The behavior of metal contaminants and their environmental fate is a complex system of many variables; A combination of physical, chemical and biological processes affect the dispersion and severity of contamination. In general, weathering of mine tailings release acidity, metals and sulfate into the environment (Balistrieri et al. 2007). The composition and extent of mining-related drainage is a function of the unique mineralogy and geochemistry of the area, as well as the climatic and hydrologic processes the system is exposed to (Balistrieri et al. 2007). Closed mines are not exempt of environmental issues; mine waste material left exposed at the surface can still pollute water and surrounding areas with leached metals and acidic pH. Mine waste includes tailings, which are the residual fine-grained material left after concentrating the ore by flotation. Tailings from sulfide mines are mainly pyrite (FeS_2) and are often disposed under water in tailings ponds. Waste material is a term used for the fractions of rock that is rejected from further extraction due to relatively low Cu content. Waste rocks disposed at surface conditions are readily oxidized and releases dissolved heavy metals as well as acidity.

Ecosystems suffer from released metals and unnatural pH levels. High concentrations of Cu are toxic to all living organisms – humans included. The acute toxicity varies significantly both within one species and between species. The lethal dose for an adult human lies between 4-400 mg of Cu(II)-ions per kg of bodyweight, but lower doses can cause health effects similar to food poisoning (nausea, vomiting, headaches, diarrhoea) (World Health Organization 2004). Studies have shown long-term exposure of 1-3 mg/litre Cu in drinking water to have gastrointestinal effects on humans (World Health Organization 2004). Both the World Health Organization (World Health Organization) and the European Union (EU) defines the health-based highest acceptable limit for Cu-concentration in drinking water to be 2.0 mg/l (Lenntech *WHO EU water standards*).

3.3.2 Storwartz remediation

At Storwartz, no remediation strategies have been implemented. Røros is a historically important mining town and is considered a UNESCO World Heritage site. In 2015 Storwartz was declared a protected area by the Norwegian Ministry of Climate and Environment (Forskrift om fredning av statens kulturhistoriske eiendommer 2015 § 15). Invasive measures are thus not permitted by law because of the cultural importance of the mining town. Waste from flotation, waste material from unmined rocks as well as slag material, lies completely exposed and mine drainage runs directly into the environment. From the tailings dam at lower Storwartz (Slamdammen), water drains through Prestbekken and into Djupsjøen. Djupsjøen is a part of Hitterdalsvassdraget, upstream from Glåma – Norway's longest river. The last lake in the watercourse is Hittersjøen, which is used for drinking water in Røros.

3.3.3 Løkken remediation

Due to the impact of acidic, metal-rich input to the environment, several remediation measures have been made at Løkken. Today, practically all acid mine drainage and surface runoff are re-directed into the mines and chemically treated. Waste piles are covered with material to reduce weathering and metal leaching into the drainage water. During the first years of production, the mine drainage was released directly into Raubekken without any treatment. From 1952 the mine drainage was transported through a 26 km long wood pipe along the railroad to Thamshavn, where a further 200-300 tons of Cu was extracted from the water. The rest was released into the deep waters of Orkdalsfjorden. Between 1984 and 1992 all mine drainage was directed into and stored in Gammelgruva and Wallenberg mine while natural surface drainage still went into Raubekken. From 1992 onward, practically all drainage is led into Gammelgruva, where the heavy metals over time precipitate and settle at the bottom. The surface water is pumped out through Wallenberg shaft and into Fagerlivatnet where it is treated with chalk to neutralize the acidity before it runs into Orkla (Orkla industrimuseum 2019c). The exposed waste piles around the mines has been covered with moraine material and swamp soil to prevent weathering and erosion, and some waste piles have been partially vegetated naturally after being covered. An artificial dam, Bjørndalstjørna, is used to store fine-grained iron pyrite waste below water, due to its high reactivity in air (Skei et al. 2019).

Chapter 4: Method and materials

4.1 Sample collection

4.1.1 Sampling area

All samples were collected in the areas surrounding the closed mines at Storwartz and Løkken. The Storwartz mining field and Løkken are located approximately 110 kilometers apart, south of Trondheim (fig. 3.1) in Trøndelag county. Both areas are potentially capable of widespread contamination through streams running from and through the once active mining areas, ultimately running into larger rivers. Just north of the mining field at Storwartz lies Aursunden (fig. 4.1), a large lake often considered the headwaters of Norway's longest river system – Glomma (also Glåma) (*Aursunden* 2019). In Løkken, the river Orkla lies in close proximity west of the mining area (fig. 4.2). Orkla is considered one of the best rivers for salmon and sea trout fishing in Norway (Heggstad and Toldnæs 2020). The climate of both Løkken and Røros is classified as continental subarctic by the Köppen-Geiger-Pohl climate classification (*Köppen climate classification* 2020; *Continental subarctic climate* 2016). The climate is dominated by a winter season that is long, cold and relatively dry (*Continental subarctic climate* 2016).

4.1.2 Sampling strategy

The sampling was performed in early June 2019 and was mainly focused on aqueous samples surrounding the areas that were suspected to be contaminated by previous mining activity, as well as some locations not expected to be affected in the same degree. Also, solid samples of background rock, ore rock, waste rock and sediments were sampled. In order to get an indication of Cu concentration in the collected samples, a portable YSI photometer was used to estimate Cu in the aqueous samples. The photometer was helpful in determining where more sampling would be of interest. In total, 43 aqueous samples and 14 solid samples were collected between the two areas. Water sample locations are displayed in figure 4.1-4.2. Water samples were collected in pairs, where one sample was put in a 60 ml acid-washed bottle and the other one in a 50 ml Falcon tube. The samples in the acid-washed bottles were immediately acidified using 1.35 ml of concentrated nitric acid (HNO_3) to avoid any precipitation or adsorption to the bottle. If precipitation should occur,

the empty bottles were previously weighed so it would be possible to recalculate accurate concentrations if needed. The samples in the Falcon tubes were used for pH measurements and in-field Cu concentration analysis. Further, solid samples were collected in labelled sample bags. The goal of the sampling of solids was to get a representative set of data from ore rock, background rock, waste rock and sediments in close proximity to the aqueous samples. All sample locations were GPS plotted and is displayed in table 4.1 below.

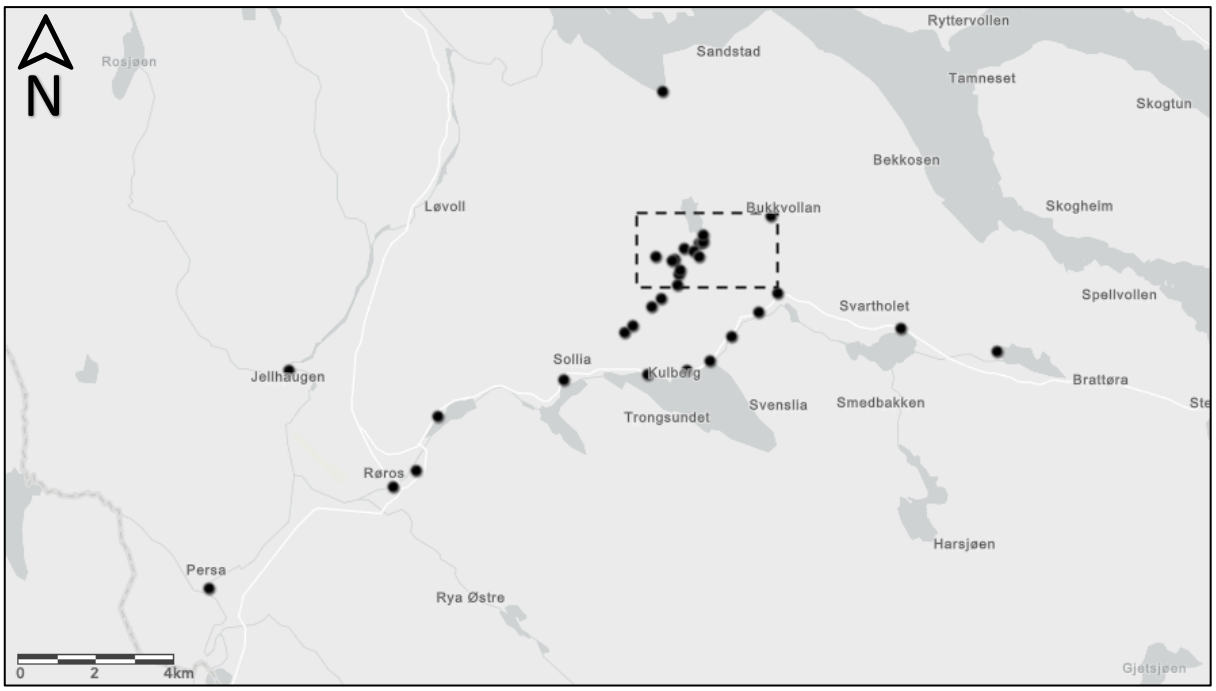

Figure 4.1: Location of all surface water samples collected in the Røros area. All mines in the Storwartz mining field is located within the dashed line box. Aursunden lies to the northeast, Hitterdalsvassdraget lies south of Storwartz. Made with ArcGIS Online (Map layers by Esri, HERE, Garmin, INCREMENT P, METI/NASA, USGS).

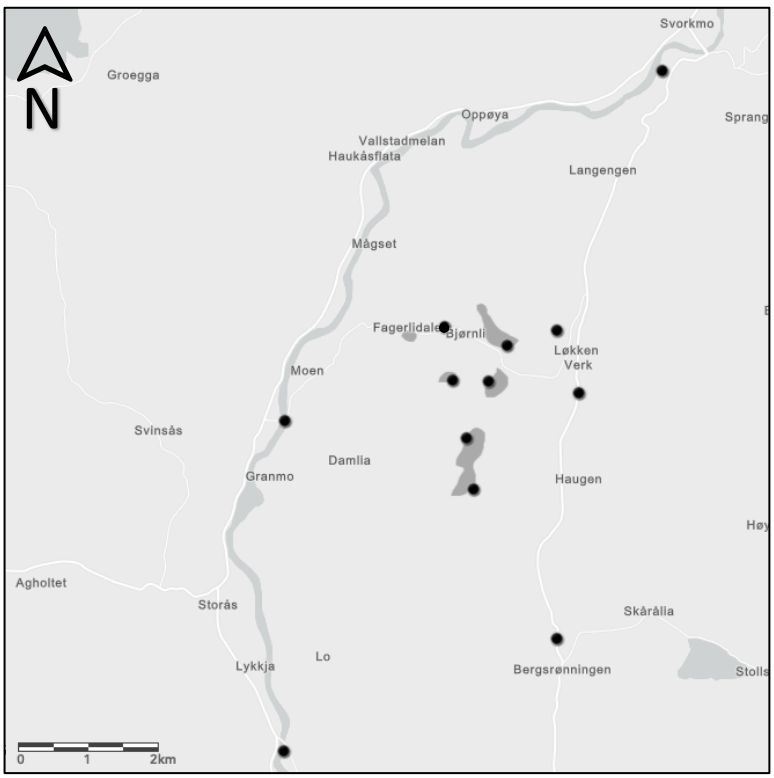

Figure 4.2: Location of all water samples from Løkken. River Orkla lies west of Løkken, Raubekken runs approximately north-south through Løkken. Made with ArcGIS Online (Map layers by Esri, HERE, Garmin, INCREMENT P, METI/NASA, USGS).

Table 4.1: All collected samples with their sample ID, type of sample, location and sampling date.

Sample ID	Sample type	Location	Date (dd.mm.yy)
19-RØR-1	Background rock	Olavsgruva	05.06.19
19-RØR-2	Ore rock	Bought in souvenir shop	05.06.19
19-RØR-3	Lake	62 35 20 N 11 24 21 E	06.06.19
19-RØR-4	Lake	62 35 50 N 11 28 09 E	06.06.19
19-RØR-5	Lake	62 35 56 N 11 30 44 E	06.06.19
19-RØR-6	Stream	62 36 27 N 11 33 17 E	06.06.19
19-RØR-7	Stream	62 36 48 N 11 34 07 E	06.06.19
19-RØR-8	Stream	62 37 04 N 11 34 40 E	06.06.19
19-RØR-9	Lake	62 36 34 N 11 38 25 E	06.06.19
19-RØR-10	Lake	62 36 15 N 11 41 20 E	06.06.19
19-RØR-11	Stream	62 36 31 N 11 30 01 E	06.06.19
19-RØR-12	Stream	62 36 36 N 11 30 16 E	06.06.19
19-RØR-13	Stream	62 36 52 N 11 30 50 E	06.06.19
19-RØR-14	Stream	62 36 59 N 11 31 09 E	06.06.19
19-RØR-15	Pond	62 37 11 N 11 31 38 E	06.06.19
19-RØR-16	Sediment		06.06.19
19-RØR-17	Stream	62 37 20 N 11 31 40 E	06.06.19
19-RØR-18	Sediment		06.06.19
19-RØR-19	Pond	62 37 23 N 11 31 43 E	06.06.19
19-RØR-20	Pond	62 37 45 N 11 32 17 E	06.06.19
19-RØR-21	Sediment		06.06.19
19-RØR-22	Sediment/ Plant		06.06.19
19-RØR-23	Stream	62 37 47 N 11 32 22 E	06.06.19
19-RØR-24	Sediment		06.06.19
19-RØR-25	Waste rock	62 37 47 N 11 32 25 E	06.06.19
19-RØR-26	Waste sediment		06.06.19
19-RØR-27	Lake	62 37 53 N 11 32 24 E	06.06.19
19-RØR-28	Pond	62 37 35 N 11 30 58 E	06.06.19
19-RØR-29	Stream	62 37 41 N 11 31 50 E	06.06.19
19-RØR-30	Stream	62 37 32 N 11 31 32 E	06.06.19
19-RØR-31	Stream	62 37 31 N 11 31 27 E	06.06.19
19-RØR-32	Stream	62 37 39 N 11 32 07 E	06.06.19
19-RØR-33	Stream	62 37 34 N 11 32 17 E	06.06.19
19-RØR-34	Stream	62 38 08 N 11 34 27 E	06.06.19
19-RØR-35	Lake	62 39 53 N 11 31 09 E	06.06.19
19-RØR-36	Stream	62 35 58 N 11 32 37 E	07.06.19
19-RØR-37	Stream	62 36 07 N 11 32 37 E	07.06.19
19-RØR-38	Slag rock	62 34 34 N 11 23 40 E	07.06.19
19-RØR-39	Slag sed.		07.06.19
19-RØR-40	Stream	62 34 21 N 11 22 59 E	07.06.19
19-RØR-41	Stream	62 32 55 N 11 17 23 E	07.06.19
19-RØR-42	Stream	62 35 59 N 11 19 49 E	07.06.19
19-LØK-1	Waste sediment	63 07 17 N 09 42 05 E	08.06.19
19-LØK-2	Waste rock		08.06.19
19-LØK-3	Stream	63 07 49 N 09 41 54 E	08.06.19
19-LØK-4	Lake	63 07 25 N 09 40 41 E	08.06.19
19-LØK-5	'Vasskis'	Bought in museum	08.06.19
19-LØK-6	Lake	63 07 25 N 09 40 04 E	08.06.19
19-LØK-7	Lake	63 06 33 N 09 40 25 E	08.06.19
19-LØK-8	Stream	63 06 57 N 09 40 18 E	08.06.19
19-LØK-9	Lake	63 07 42 N 09 41 01 E	08.06.19
19-LØK-10	Lake	63 07 51 N 09 39 55 E	08.06.19
19-LØK-11	Stream	63 07 06 N 09 37 04 E	08.06.19
19-LØK-12	Stream	63 04 28 N 09 37 01 E	08.06.19
19-LØK-13	Stream	63 05 21 N 09 41 54 E	08.06.19
19-LØK-14	Stream	63 07 19 N 09 42 18 E	08.06.19
19-LØK-15	Stream	63 09 54 N 09 43 47 E	08.06.19

RØR – Røros, *LØK* – Løkken, *Vasskis* – fine grained pyrite in dark matrix of hornfels

4.2 Concentration analyses

4.2.2 Field Cu analysis

An YSI 9500 photometer was used for in-field analysis of Cu concentration. The photometer is used for an optical analysis of the free and total concentration of Cu in an aqueous sample using the Cu reagent starter kit.

4.2.3 pH

pH was measured in all aqueous samples. The measurements were performed within a week after the sampling, using a Metrohm 827 pH-meter.

4.2.4 Major and trace elements (ICP-OES)

All samples, both aqueous and digested solids, were analysed by inductively coupled plasma optical emission spectrometry (ICP-OES) for major and trace element composition. The analysis was performed by University of Bergen *Chief Technician* Hildegunn Almelid. The ICP-OES at the University of Begren is a Thermo Scientific iCap 7600 model.

4.3 Isotope analysis

4.3.1 Sample preparation

Before the isotope analysis, the Cu needed to be dissolved in 2% HNO_3 as well as having all matrix elements removed. Preparation of all samples was performed at the Department of Earth Science at the University of Bergen during fall 2019 and spring 2020. Sediment samples were transferred into disposable trays, dried in an oven and finally placed in labelled glass sample vials. Rock samples were crushed to a fine powder using a *Retsch* BB 250 jaw crusher and *Retsch* PM 200 agate ball mill. The jaw crusher breaks the rock sample into 2 mm fragments and does not contain any heavy metals that can contaminate the samples. The agate ball mill consists of pure SiO_2 and is used to crush the samples into a very fine powder. After crushing, the solid samples were handed over to University of Bergen *Staff Engineer* Yuval Ronen for hydrofluoric (HF) acid digestion. Thereafter, the dissolved solid samples were transferred to University of Bergen *Chief Research Technician*

Hildegunn Almelid for inductively coupled plasma - optical emission spectrometry (ICP-OES). All water samples were also analyzed by Hildegunn Almelid for major element composition using ICP-OES. To avoid contamination of the samples, further preparation was performed in a clean lab. The clean lab at the University of Bergen is a Class 1000 (ISO 6) air filtered room with laminar flow hoods for sample preparation.

The ideal concentration for isotope analysis is 50 ppb Cu in one ml of sample. In order to secure enough material for a few analyses, 3 ml of sample ready for analysis is desired. Further, 3 ml of 50 ppb corresponds to 150 ng of Cu. The amount of sample required to get 150 ng was calculated for each sample, based on the results from the ICP-OES analysis. Some samples with low Cu concentrations would require volumes of sample larger than the size of available Savillex beakers (25 ml) to give 150 ng Cu. Therefore, they had to be prepared with less than 150 ng Cu and could only be run once or twice on the mass spectrometer. The amount of sample needed varied between 0.5 and 25 ml, which was put in individual Savillex beakers. Further, the samples were completely evaporated on a hot plate. Then, 1 ml 10 M HCl was added to the evaporated samples and left for approximately 24 hours on a 130^{o}C hot plate to completely dissolve. After being dissolved in HCl, the samples were ready for ion exchange chromatography to separate Cu from the matrix elements.

4.3.2 Ion exchange chromatography

Ion exchange chromatography was performed in the clean lab, under a laminar flow hood, using narrow columns made of Teflon tubing and 1 ml of anion exchange resin. The resin used for separation was 100-200 mesh AG MP-1. All acids used were ultrapure concentrated nitric (HNO_3) or hydrochloric acids (HCl), diluted with 18.2 MΩ·cm ultrapure H_2O when needed. The ion exchange chromatography method for separating Cu from the matrix was tested by Matthew Walsh (University of Liverpool), in July 2019 at the University of Bergen. Using an artificial rock standard, acid mine drainage, a copper ore standard (CCU-1d), a zinc standard (CZN-4) and an artificial chalcopyrite, the quality of separation was tested on a pipette column versus a Teflon column. The tests showed that the Teflon columns gave a good separation for Cu. A Cu standard was also run over the column and analyzed for isotopes to verify that there was no significant fractionation of Cu during separation.

The first step in the ion exchange chromatography was cleaning of the columns. Columns were cleaned using 5 ml 6 M HCl, 3 ml 1 M HNO_3 and 3 ml milli-Q (18.2 MΩ·cm ultrapure H_2O). Next, the column was conditioned with 3 ml 10 M HCl, 3 ml milli-Q and 4 ml 10 M HCl. The samples were loaded onto the column in 1 ml 10 M HCl. Matrix elements were washed off using a total of 4 ml (1 + 1 + 2 ml) 10 M HCl for water samples and 2 + 1 ml 10 M HCl for dissolved solid samples. In the meantime, the sample beakers were cleaned using ultrapure water and 5 M HCl on the hot plate before the Cu was eluted using 1 + 1 + 1 + 3 ml of 5 M HCl for water samples. For solid samples, Cu was eluted using 1 ml 10 M HCl and 1 + 1 + 2 ml 5 M HCl. The eluted Cu fraction was collected in the same Savillex beakers as before, after they were cleaned. Finally, the HCl was evaporated from the eluted fraction and then re-dissolved in 1 ml 2 % HNO_3. The method is summarized in figure 4.3.

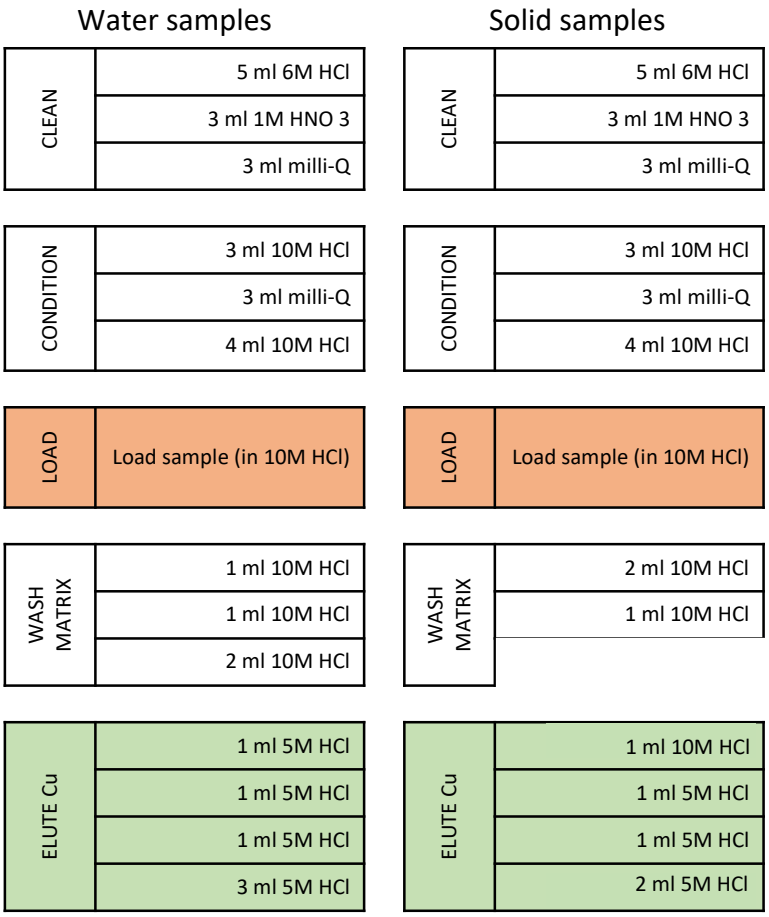

Figure 4.3: Ion exchange chromatography method for separating Cu from matrix elements in water samples and solid samples

4.3.3 Dilution and Ni-doping

For isotope analysis, the analyte should be a 1 ml solution containing 50 ppb Cu from the sample, 50 ppb from a nickel (Ni) dopant and the rest 2% HNO_3. The concentration of Cu and Ni need to be at 50 ppb because the method is checked by analyzing known standards with a Cu/Ni ratio of approximately 1 (50 ppb/50 ppb). The samples of interest are therefore only measured accurately if they have the same Cu/Ni ratio as the standards. The main reason for this is that the mass bias of the instrument is dependent on concentrations. Varying concentrations would affect the efficiency in the plasma, changing the mass bias and making it impossible to correct for. The total beam strengths of Cu and Ni should therefore be less than 10% different from each other and the bracketing standard used (50 ppb Cu). If the total beam strengths were less than 10% deviant, the Ni dopant and bracketing standards could accurately be used for mass bias correction of the Cu results.

Firstly, for the sample preparation, 1 ml vials were labelled with the sample names and the 2% HNO_3 and Ni dopant were prepared. A 500 ppb Ni dopant solution was used to give 50 ppb Ni in the final solution by adding 0.1 ml of the dopant. The Ni dopant was prepared from a 10 μg/ml standard of Ni, called “Bergen Ni”. The standard was diluted 20 times, to 500 ppb, with pure 2% HNO_3 by adding 150 μl Ni standard and 2850 μl HNO_3 (= 3 ml dopant in total) and was prepared recently before each run of analyses. The amount of Cu in each sample beaker after the ion exchange chromatography method depend on how much initial sample was dried down as well as the concentration of the original sample. Using the samples’ concentrations obtained from ICP-OES, the amount of sample stock corresponding to 50 ppb Cu was calculated. To finalize the samples for analysis, the calculated amount of sample stock, plus 0.1 ml of the 500 ppb Ni dopant, and the rest (to give 1 ml total) 2% HNO_3, were pipetted into their respective labelled vials. All samples were shaken and vortexed for a minimum of 15 seconds. The final analyte solutions prepared for MC-ICP-MS analysis were thus 1 ml of 50 ppb Cu (from sample) and 50 ppb Ni (from dopant) dissolved in 2% HNO_3.

For the first analysis run, dilutions were based on the concentration results obtained from ICP-OES analysis as described above. However, total beam strengths during isotope analysis indicated that this dilution yielded signals that were more than 10% off from the standards. To correct for this difference, the dilutions for the first batch of analyses were recalculated using the deviation between the samples’ Cu-beam strength and the average

Cu-beam intensity of the two corresponding bracketing standards (ERM AE647), before being analyzed again with corrected dilutions. The subsequent batches of samples were first measured for concentration on the MC-ICP-MS during a quick concentration check. For the concentration check, three standards with concentrations of 10 ppb, 20 ppb and 50 ppb Cu were made from a single element Cu standard, and together with an acid blank (0 ppb Cu) used to construct a four-point calibration curve. From the calibration curve, the accurate concentrations, and thus appropriate dilution to achieve 50 ppb Cu from each sample, were found. Figure 4.4 illustrates the four-point calibration curve used to correct the Cu concentration of the samples to achieve the correct final dilution prior to the isotope analysis.

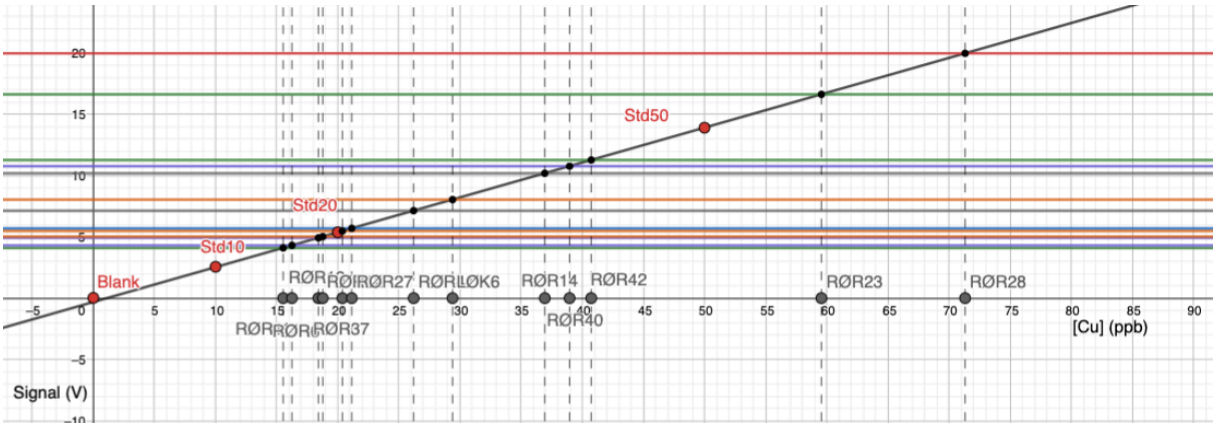

Figure 4.4: Illustration of four-point calibration curve used for concentration correction of samples. Made with GeoGebra.

4.3.2 Isotope analysis (MC-ICP-MS)

Isotope signature was measured on an upgraded Nu Instruments Plasma II mass spectrometer. This is a multi-collector, inductively coupled plasma mass spectrometer (MC-ICP-MS) equipped with 18 faraday cups and 5 ion-counting detectors for high precision and accurate isotope analysis. Samples were placed in an ASX-112FR AutoSampler and sucked into a CETAC Aridus II Desolvating Nebulizer System. The Aridus nebulizes the liquid sample into a perfluoralkoxy (PFA) spray chamber with an argon (Ar) nebulizer gas. An ICP torch generates the argon plasma that dries the sample aerosol, dissociates the molecules and removes one electron to form singly charged ions. Further, the ions are accelerated by a high voltage and four quad lenses reshapes the plasma ion beam. An electrostatic analyzer

(ESA) deflects the ions; Separated by their mass to charge (m/z) ratio, the beams are collected in separate, adjustable faraday cups (table 4.2).

Before analyses, the mass spectrometer and Aridus were tuned so that optimal sensitivity was obtained, typically 10-14 V on ^{63}Cu for a 50 ppb solution. The peak shapes and peak coincidence were subsequently optimized using the Quad lenses, aiming at flat-topped peaks with steep edges that sufficiently overlapped for simultaneous measurement of all isotopes at one magnet set point. For Cu isotope analysis with Ni doping, the 'Cu Static' method was used, with ^{60}Ni measured in Faraday cup L5, ^{61}Ni in L2, ^{62}Ni in H1, ^{63}Cu in H4, ^{64}Ni in H7, ^{65}Cu in H9 and ^{66}Zn in H10 (table 4.2). Each analysis consisted of two blocks with 20 cycles and 8 seconds integration time. No detectable blanks were measured by on-peak zeroing, so blanks were measured by ESA deflection for 30 seconds before each block. Peak centering was performed on ^{63}Cu before each analysis.

Table 4.2: Faraday cups and corresponding isotopes used for analysis with 'Cu static' method

Faraday cup	L5	L2	H1	H4	H7	H9	H10
Isotope measured	^{60}Ni	^{61}Ni	^{62}Ni	^{63}Cu	^{64}Ni	^{65}Cu	^{66}Zn

During analysis, a sample bracketing standard (ERM AE647) was run before and after all samples. In addition, the "Bergen Cu" standard was analyzed after every four samples to ensure the mass spectrometer was stable during analysis and to confirm the accuracy of the analyses. Between all individual analyses of each standard or sample, the sampling probe was washed 20 seconds in the autosampler wash station and 80 seconds in a pure 2% HNO_3 solution. The transfer time was set to 60 seconds on the mass spectrometer. Results were processed in Microsoft Excel after Baxter et al. (2006). The isotope ratios measured by the mass spectrometer are $^{65}Cu/^{63}Cu$, $^{61}Ni/^{60}Ni$, $^{62}Ni/^{60}Ni$ and $^{64}Ni/^{60}Ni$. Instrumental mass bias is calculated based on the $^{62}Ni/^{60}Ni$ ratios for a number of repeated standards and then applied to the $^{65}Cu/^{63}Cu$ results. Standard sample bracketing (SSB) is implemented on the corrected isotope ratios and calculates the delta values relative to the average measured ratio of the standards. A combination of Ni doping and SSB were used for mass bias correction for most samples, but for some samples with no or bad signal on bracketing standards only Ni doping was used.

Chapter 5: Results

5.1 In-field Cu concentration and pH

Table 5.1 shows the Cu concentration results from in-field analysis by photometry together with the pH of all water samples. Sample pH varies between 3.26-7.90. The most acidic samples are from lower Storwartz and downstream of the tailings pond. In Løkken, the two most acidic samples are from the artificial lake used for sulfide disposal. Figure 5.1 shows the total Cu concentration from the photometry and pH together, highlighting the relationship between the two. Many samples cluster around pH= 7, with low Cu concentration. The higher concentrated samples from Røros show an exponential relationship (R^2 = 0.8353) with pH, whereas the Løkken samples appear to have lower Cu concentrations regardless of pH. The photometer results correlate well with the ICP-OES results (fig. 5.2). The near-perfect linear relationship seen in figure 5.2 highlights that the photometer is a great tool for rapid, in-field estimation of Cu concentration. Consequently, ICP-OES results have been used for the remainder of this thesis.

Table 5.1: Free Cu and total Cu concentration from in-field photometer analysis and pH for all water samples.

Sample ID	Free Cu (mg/L)	Total Cu (mg/L)	pH
19-RØR-03	0.1	0.14	7.90
19-RØR-04	0.1	0.14	7.30
19-RØR-05	0.12	0.22	7.32
19-RØR-06	0.14	0.16	7.13
19-RØR-07	0.06	0.2	7.18
19-RØR-08	0.2	0.24	7.14
19-RØR-09	0.18	0.24	7.16
19-RØR-10	0.22	0.24	7.20
19-RØR-11	0.12	0.32	7.33
19-RØR-12	0.12	0.38	7.17
19-RØR-13	0.1	0.16	7.24
19-RØR-14	0.32	0.58	7.29
19-RØR-15	2.1	2.25	3.78
19-RØR-17	2.35	2.45	3.55
19-RØR-19	2.4	2.7	3.43
19-RØR-20	0.8	0.9	4.62
19-RØR-23	0.22	0.28	5.75
19-RØR-27	0.46*	0.38*	6.18
19-RØR-28	0.22	0.4	6.52
19-RØR-29	0.28	0.44	6.90
19-RØR-30	7	7.4	3.54
19-RØR-31	1.85	1.9	4.08
19-RØR-32	3.1	3.1	3.97
19-RØR-33	5.4	5.5	3.26
19-RØR-34	0.04	0.36	6.48
19-RØR-35	0.14	0.3	6.70
19-RØR-36	1.4	1.45	4.09
19-RØR-37	0.16	0.22	6.60
19-RØR-40	0.14	0.22	6.81
19-RØR-41	0.1	0.1	6.88
19-RØR-42	0.04	0.08	6.83
19-LØK-03	0.18	0.22	6.59
19-LØK-04	0.4	0.54	6.62
19-LØK-06	0.22	0.3	6.53
19-LØK-07	0.28	0.34	4.36
19-LØK-08	0.16	0.24	4.29
19-LØK-09	0.3	0.38	6.61
19-LØK-10	0.34	0.42	7.33
19-LØK-11	0.2	0.42	7.43
19-LØK-12	0.16	0.26	7.35
19-LØK-13	0.12	0.16	7.17
19-LØK-14	0.12	0.22	7.19
19-LØK-15	0.06	0.16	7.40

*invalid/uncertain result because free Cu > total Cu

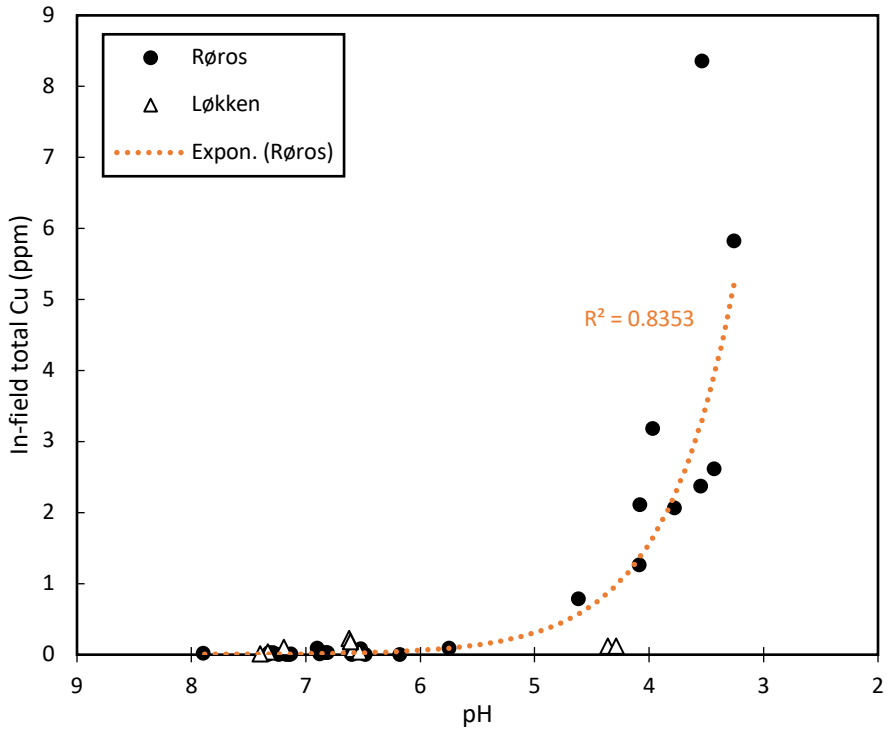

Figure 5.1: Total Cu (from in-field photometer analysis) versus measured pH, displaying exponential (R^2 = 0.8353) relationship between total Cu and pH in Røros samples. Løkken samples show two low-pH samples that do not correlate with elevated Cu concentration.

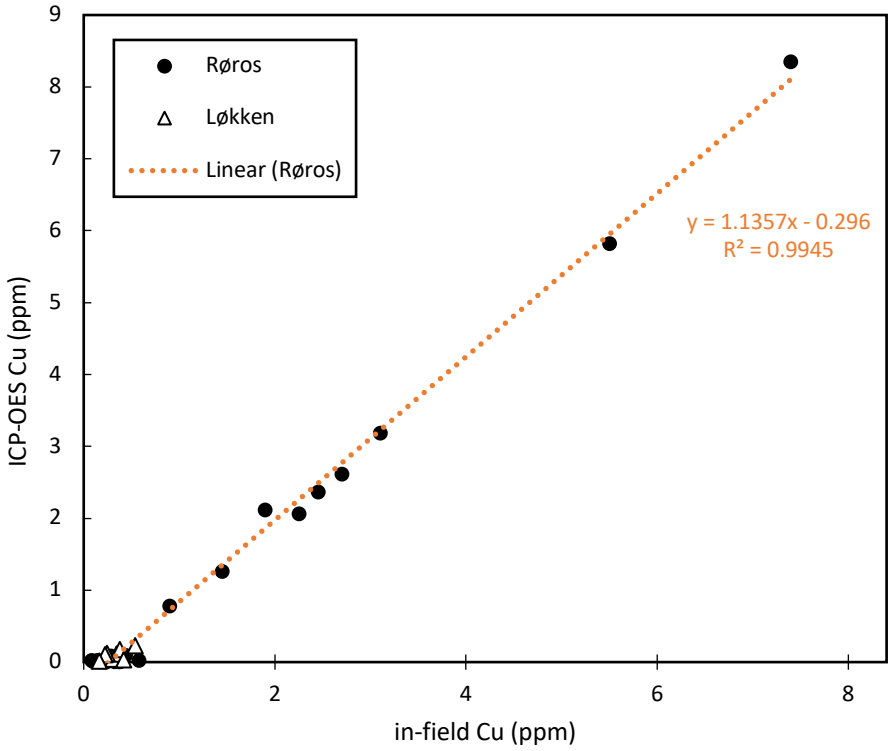

Figure 5.2: ICP-OES Cu versus in-field Cu from photometer analysis, showing near-perfect correlation.

5.2 ICP-OES element concentrations

Samples were analyzed by ICP-OES for elemental concentration for a wide range of cations and anions. For the purpose of this thesis, a selection of the most relevant analysis results is presented in tables 5.2 – 5.4. Table 5.2 shows concentrations of heavy metal pollutants as well as sulphate concentrations for all water samples from Røros and Løkken, as well as the detection limit (DL) for each element. Some samples stand out with high concentrations of several elements. Samples 19-RØR-15, -17, -19, -30, -31, -32, -33 and -36 have the highest Cu concentrations as well as elevated levels of most of the other parameters. They are also the most acidic samples (table 5.1). In the Løkken samples the pattern is less clear; Cu concentrations in Løkken samples are generally low regardless of pH, with 19-LØK-04 being the highest at 0.2297 mg/l. Three Løkken samples show significantly higher sulphate concentration compared to the rest of the water samples, up to 804 mg/l in 19-LØK-04. Figure 5.3 shows plots that illustrates the correlation between Cu concentration and some heavy metals plus sulfate, as well as between sulfate and pH. There appears to be no obvious correlation between Fe and Cu, whereas Cu concentration appears to show some correlation with the other heavy metals (Mg, Zn) and sulfate. Sulfate and pH correlate in a similar matter to Cu and pH (fig. 5.1), with higher sulfate concentration following lower pH. In general, the Løkken samples appears to differ from the Røros samples and the trends described.

Table 5.3 and 5.4 display the concentration of cations in the solid samples analyzed, in ppm and in wt% respectively. The highest concentration of Cu is found in sample 19-RØR-02, which is an ore rock sample that was bought in the museum shop at Olavsgruva (Storwartz, Røros). The ore rock also contains a high concentration of iron (Fe), zinc (Zn) and lead (Pb) in addition to the Cu. The background rock from Røros (metagraywacke/phyllite) contains the lowest amount of Cu out of all the solid samples. Sulfur concentrations indicate which solid samples are metal sulfides, namely 19-RØR-02, -38, -39, 19-LØK-02 and -05. The solid sample dataset is relatively limited and is collected from loose fragments in an open environment, as well as bought from the souvenir shop in Olavsgruva in Røros and at Orkla industrimuseum in Løkken.

Table 5.2: Concentration (in ppm) of heavy metal cations and sulfate from ICP-OES analysis in all water samples.

	Concentration (ppm)										
Sample ID	**Co**	**Cr**	**Cu**	**Fe**	**Li**	**Mg**	**Mn**	**Ni**	**Pb**	**Zn**	**SO_4^{2-}**
19-RØR-03	ND	ND	0.022	0.102	0.010	2.0	ND	ND	ND	0.06	4.4
19-RØR-04	ND	ND	ND	0.048	0.010	1.5	ND	ND	ND	ND	1.4
19-RØR-05	ND	ND	0.031	0.103	0.010	2.2	ND	ND	ND	0.09	5.3
19-RØR-06	ND	ND	0.008	0.171	0.010	2.4	ND	0.0052	ND	0.02	1.6
19-RØR-07	ND	ND	ND	0.080	0.010	0.9	ND	ND	ND	ND	0.9
19-RØR-08	ND	ND	0.002	0.024	0.010	0.9	ND	ND	ND	ND	3.4
19-RØR-09	ND	ND	ND	0.055	0.010	2.4	ND	0.0033	ND	ND	1.4
19-RØR-10	ND	ND	ND	0.084	0.010	3.9	ND	0.0093	ND	ND	1.3
19-RØR-11	ND	ND	0.003	0.016	0.010	0.9	ND	ND	ND	ND	0.8
19-RØR-12	ND	ND	0.004	0.014	0.010	1.0	ND	ND	ND	ND	1.5
19-RØR-13	ND	ND	0.004	0.040	0.010	0.7	ND	ND	ND	0.02	1.0
19-RØR-14	ND	ND	0.025	0.033	0.010	0.9	ND	ND	ND	0.14	2.6
19-RØR-15	0.02	ND	2.063	1.472	0.014	9.3	0.69	0.0168	0.033	6.02	212.2
19-RØR-17	0.03	ND	2.370	0.400	0.014	10.5	0.80	0.0190	0.039	5.10	267.7
19-RØR-19	0.03	0.002	2.615	4.416	0.014	10.6	0.80	0.0184	0.048	5.48	296.0
19-RØR-20	ND	ND	0.785	0.314	0.011	2.1	0.25	0.0040	0.004	1.52	70.1
19-RØR-23	ND	ND	0.089	1.109	0.010	0.4	0.05	ND	ND	0.16	8.1
19-RØR-27	ND	ND	0.005	0.057	0.010	0.6	ND	ND	ND	ND	1.1
19-RØR-28	ND	ND	0.086	0.465	0.010	0.6	ND	ND	0.016	0.14	3.5
19-RØR-29	ND	ND	0.094	0.459	0.014	9.5	0.69	0.0044	ND	1.52	106.8
19-RØR-30	0.07	0.003	8.355	0.937	0.019	9.3	1.16	0.0694	0.097	14.78	286.5
19-RØR-31	0.02	ND	2.114	0.231	0.014	6.9	0.67	0.0192	0.135	11.84	185.0
19-RØR-32	0.02	0.003	3.188	4.850	0.013	4.9	0.37	0.0135	0.0180	3.25	155.3
19-RØR-33	0.06	0.012	5.823	22.733	0.018	10.8	0.88	0.0413	0.173	14.69	354.7
19-RØR-34	ND	ND	0.002	0.141	0.010	1.7	ND	ND	ND	ND	1.4
19-RØR-35	ND	ND	ND	0.046	0.010	0.8	ND	ND	ND	ND	1.3
19-RØR-36	0.02	ND	1.262	0.557	0.013	6.7	0.51	0.0112	0.031	3.09	183.1
19-RØR-37	ND	ND	0.007	ND	0.010	1.1	ND	ND	ND	0.08	7.1
19-RØR-40	ND	ND	0.025	0.077	0.010	1.9	ND	ND	ND	0.06	4.8
19-RØR-41	ND	ND	0.011	0.152	0.010	1.0	ND	ND	ND	0.03	2.0
19-RØR-42	ND	ND	0.028	0.174	0.010	0.9	ND	ND	ND	0.07	3.0

Table 5.2 (cont.): Concentration (in ppm) of heavy metal cations and sulfate from ICP-OES analysis in all water samples.

	Co	Cr	Cu	Fe	Li	Mg	Mn	Ni	Pb	Zn	SO_4^{2-}
19-LØK-03	0.08	ND	0.072	0.113	0.017	26.8	0.60	0.0231	ND	1.81	470.3
19-LØK-04	0.15	ND	0.230	1.355	0.023	50.4	1.11	0.0449	ND	3.85	804.4
19-LØK-06	ND	ND	0.041	0.375	0.010	1.2	ND	ND	ND	0.18	16.7
19-LØK-07	0.01	ND	0.117	0.117	0.010	1.0	0.07	ND	0.003	0.63	46.4
19-LØK-08	0.01	ND	0.119	0.145	0.010	1.0	0.07	ND	0.004	0.64	68.2
19-LØK-09	0.09	ND	0.178	0.175	0.018	29.1	0.68	0.0273	ND	2.39	510.9
19-LØK-10	ND	ND	0.035	0.107	0.010	2.8	0.11	ND	ND	0.16	79.1
19-LØK-11	ND	ND	ND	0.143	0.010	0.5	ND	ND	ND	ND	1.8
19-LØK-12	ND	ND	ND	0.137	0.010	0.6	ND	ND	ND	ND	2.3
19-LØK-13	ND	ND	ND	0.374	0.010	0.9	ND	ND	ND	ND	2.2
19-LØK-14	0.00	ND	0.102	0.385	0.010	1.2	ND	ND	ND	0.14	8.8
19-LØK-15	ND	ND	0.015	0.075	0.010	2.1	ND	ND	ND	0.03	12.5
Detection Limit (DL)	0.01	0.002	0.002	0.002	0.003	0.1	0.05	0.0025	0.0025	0.01	0.5

Color of values indicates dilution used for analysis. Values are calculated back to original concentration for all dilutions. Black values are non-diluted samples. Pink values: 10x diluted, green: 20x diluted, yellow: 50x diluted, blue: 100x diluted. ND: not detected.

Table 5.3: Concentration (in ppm) of selected cations in solid samples from ICP-OES analysis.

		Concentration (ppm)								
Sample ID	**Type**	**Mg**	**Al**	**S**	**K**	**Ca**	**Fe**	**Cu**	**Pb**	**Zn**
19-RØR-01	Background	28232.9	33877.2	ND	ND	ND	64171.4	88.3	ND	151.7
19-RØR-02	Ore rock	ND	9233.9	4640.0	ND	ND	435590.2	67179.8	5545.2	85155.9
19-RØR-16	Sediment	15648.3	60997.5	ND	17809.9	5143.4	139382.3	1864.0	129.6	2075.4
19-RØR-18	Sediment	ND	20112.7	ND	ND	ND	540505.0	1206.7	104.0	338.8
19-RØR-21	Sediment	25263.0	54958.0	ND	7281.1	5054.1	115194.7	403.5	102.0	722.6
19-RØR-22	Sediment	33778.0	71249.9	ND	10088.7	4813.6	147058.0	822.3	151.4	1153.4
19-RØR-24	Sediment	24669.8	52359.0	ND	7090.8	5259.6	112465.8	750.9	146.6	771.8
19-RØR-25	Gangue	27016.0	35268.9	ND	ND	ND	474382.5	5457.5	118.2	12212.0
19-RØR-26	Sediment	23536.5	66042.7	ND	21485.5	3988.9	55447.5	308.9	215.3	1151.0
19-RØR-38	Slag rock	22314.9	37342.8	6904.5	7159.5	9481.8	354275.3	4935.1	270.6	40167.9
19-RØR-39	Slag sed.	23058.4	40718.7	7623.4	7541.2	7954.5	305573.3	4583.8	225.1	28969.8
19-LØK-01	Sediment	14011.9	51496.2	ND	9229.4	20144.0	151631.5	1884.1	4362.5	1273.5
19-LØK-02	Gangue	ND	10360.1	4081.1	ND	21886.9	333153.3	5273.3	635.1	12515.6
19-LØK-05	Vasskis*	17829.9	27271.6	5752.4	12455.6	18933.5	304828.6	343.3	89.2	451.8
Detection limit (DL)		2	0.025	0.5	1	0.5	0.02	0.002	0.005	0.002

*pyrite in dark matrix of hornfels

Black: diluted 5000 times; Pink: diluted 50000 times. Calculated back to non-diluted. ND = not detected

Table 5.4: Element concentrations of solid samples, presented in weight percent (wt%).

		Concentration (wt%)								
Sample ID	**Type**	**Mg**	**Al**	**S**	**K**	**Ca**	**Fe**	**Cu**	**Pb**	**Zn**
19-RØR-01	Background	2.82	3.39	ND	ND	ND	6.42	0.01	ND	0.02
19-RØR-02	Ore rock	ND	0.92	0.46	ND	ND	43.56	6.72	0.55	8.52
19-RØR-16	Sediment	1.56	6.10	ND	1.78	0.51	13.94	0.19	0.01	0.21
19-RØR-18	Sediment	ND	2.01	ND	ND	ND	54.05	0.12	0.01	0.03
19-RØR-21	Sediment	2.53	5.50	ND	0.73	0.51	11.52	0.04	0.01	0.07
19-RØR-22	Sediment	3.38	7.12	ND	1.01	0.48	14.71	0.08	0.02	0.12
19-RØR-24	Sediment	2.47	5.24	ND	0.71	0.53	11.25	0.08	0.01	0.08
19-RØR-25	Gangue	2.70	3.53	ND	ND	ND	47.44	0.55	0.01	1.22
19-RØR-26	Sediment	2.35	6.60	ND	2.15	0.40	5.54	0.03	0.02	0.12
19-RØR-38	Slag rock	2.23	3.73	0.69	0.72	0.95	35.43	0.49	0.03	4.02
19-RØR-39	Slag sed.	2.31	4.07	0.76	0.75	0.80	30.56	0.46	0.02	2.90
19-LØK-01	Sediment	1.40	5.15	ND	0.92	2.01	15.16	0.19	0.44	0.13
19-LØK-02	Gangue	ND	1.04	0.41	ND	2.19	33.32	0.53	0.06	1.25
19-LØK-05	Vasskis*	1.78	2.73	0.58	1.25	1.89	30.48	0.03	0.01	0.05

*pyrite in dark matrix of hornfels

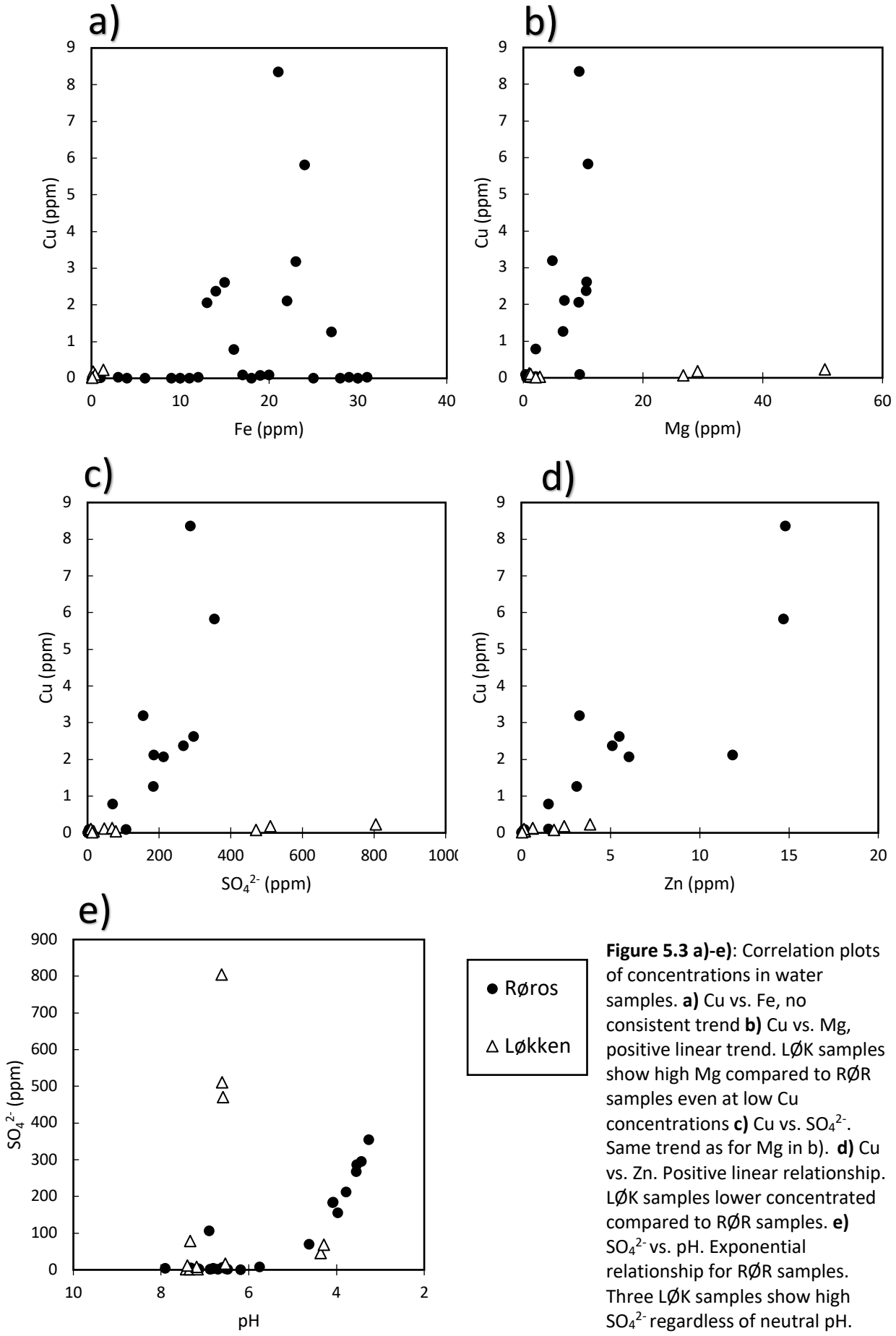

Figure 5.3 a)-e): Correlation plots of concentrations in water samples. **a)** Cu vs. Fe, no consistent trend **b)** Cu vs. Mg, positive linear trend. LØK samples show high Mg compared to RØR samples even at low Cu concentrations **c)** Cu vs. SO_4^{2-}. Same trend as for Mg in b). **d)** Cu vs. Zn. Positive linear relationship. LØK samples lower concentrated compared to RØR samples. **e)** SO_4^{2-} vs. pH. Exponential relationship for RØR samples. Three LØK samples show high SO_4^{2-} regardless of neutral pH.

5.3 Copper isotope results

The processing of isotope data was done after Baxter et al.'s (2006) method, and the samples were normalized to a $^{65}Cu/^{63}Cu$ value of 0.445600 for ERM AE647. Mass bias correction was done using a combination of Ni doping and standard sample bracketing (SSB), except for analyses with no or poor results for bracketing standards (i.e. high uncertainty or calculated $\delta^{65}Cu$ values significantly different from zero). Figure 5.6 shows cross-plots of $\delta^{65}Cu$ values and several concentration parameters. The plots point to a population of datapoints associated with high concentrations and a relatively homogenous isotope composition and is discussed further in chapter 6.

5.3.1 Standards (AE647, Bergen Cu and fractionation check)

Three different standards were measured during isotope analysis on the MC-ICP-MS. Firstly, ERM AE647 to be used as the reference material throughout the analyses. Secondly, 'Bergen Cu' was analyzed in-between every four samples to check stability and accuracy of measurements, and finally, a single element 50 ppb Cu standard was analyzed after and without ion exchange chromatography to confirm that no fractionation occurred on the column. The weighted average of ERM AE647 is 0.01 ± 0.02‰ (95% confidence interval, n= 104) using only Ni doping for mass bias correction. Because all the results are normalized against the ERM AE647 standard during analysis, the value is desired to be at 0.0‰. The weighted average with 95% confidence interval falls within the desired range. Further, the weighted average of the Bergen Cu standard is -0.30 ± 0.11‰ (95% confidence interval, n= 33) using Ni doping and SSB for mass bias correction. From literature, the 'Bergen Cu' standard should be $\delta^{65}Cu$ = -0.27 ± 0.06‰ (Moeller et al. 2012) relative to the AE647 reference, which our results fall within. Finally, the two fractionation-check standards fall within the same range, using one standard deviation (σ), $\delta^{65}Cu$ = 0.22 ± 0.23‰ for the standard that was run over a column, and the standard without column work $\delta^{65}Cu$ = 0.07 ± 0.16‰. These values are reported relative to ERM AE647, using only Ni doping for mass bias correction and with 1σ uncertainty. In addition, the value is as expected, close to zero. This standard is unlikely to be significantly fractionated compared to ERM AE647 as it represents the natural abundance of the Cu isotopes.

5.3.2 Røros samples

Table 5.5 presents the isotope data for all analyzed Røros samples. All water samples with detectable Cu were analyzed, but only a limited selection of solid samples were analyzed. The results have been corrected for mass bias using Ni doping and SSB for most samples. Some samples are corrected by only Ni doping because no or poor bracketing standard results (marked with * in table 5.5). The isotope results obtained from analysis ($\delta^{65}Cu_{AE647}$) were transformed to $\delta^{65}Cu_{SRM976}$ by adding +0.21‰, after Moeller et al.'s (2012) study. The isotope ratio can thus be compared with literature data where NIST SRM976 is most commonly referred to standard. Figure 5.4 displays the isotopes of both solids and water samples as a frequency histogram. The results span a wide range from $\delta^{65}Cu_{SRM976}$ = -0.24‰ to +6.90‰, with the background rock and a sediment sample representing the lowest $\delta^{65}Cu$ values. The other solid samples of gangue material and ore rock have in comparison significantly higher isotope values. Water samples span the entire range from ~0‰ to +7‰, most frequently falling within the 1-2‰ range. Only two samples fall within 2-3‰ range, whereas the 3-7‰ range displays a decreasing number of samples with increasing isotope value.

Table 5.5: Isotope results for all Røros samples. δ^{65}Cu is transformed from relative to AE647 reference material to SRM976 by adding 0.21‰. Lake = relatively large body of water (Klettjønna and the lakes in Hitterdalsvassdraget), pond = relatively small body of water (i.e. Slamdammen).

Sample ID	Sample type	$\delta^{65}Cu_{AE647}$ (‰)	1σ	$\delta^{65}Cu_{SRM976}$ (‰)	Date analyzed
19-RØR-01*	Background rock	-0.40	0.08	**-0.19**	06/May/2020
19-RØR-02	Ore rock	2.74	0.50	**2.95**	13/May/2020
19-RØR-03*	Lake	-0.11	0.09	**0.10**	12/May/2020
19-RØR-05	Lake	1.70	0.09	**1.91**	30/Jan/2020
19-RØR-06	Stream	4.12	0.19	**4.33**	04/Feb/2020
19-RØR-08	Stream	3.62	0.18	**3.83**	05/Feb/2020
19-RØR-11	Stream	6.68	0.61	**6.89**	04/Feb/2020
19-RØR-12	Stream	5.42	0.45	**5.63**	04/Feb/2020
19-RØR-13	Stream	4.74	0.43	**4.95**	04/Feb/2020
19-RØR-14	Stream	5.51	0.37	**5.72**	04/Feb/2020
19-RØR-15	Pond	-0.07	0.14	**0.14**	06/May/2020
19-RØR-16*	Sediment	-0.45	0.07	**-0.24**	12/May/2020
19-RØR-17	Stream	1.01	0.11	**1.22**	30/Jan/2020
19-RØR-19	Pond	0.89	0.10	**1.10**	30/Jan/2020
19-RØR-20	Pond	1.44	0.19	**1.65**	13/May/2020
19-RØR-23	Stream	2.99	0.22	**3.20**	04/Feb/2020
19-RØR-25	Waste rock	1.45	0.12	**1.66**	12/May/2020
19-RØR-27	Lake	3.90	0.21	**4.11**	04/Feb/2020
19-RØR-28	Pond	4.57	0.32	**4.78**	04/Feb/2020
19-RØR-29	Stream	1.97	0.13	**2.18**	30/Jan/2020
19-RØR-30	Stream	1.36	0.10	**1.57**	30/Jan/2020
19-RØR-31	Stream	3.53	0.17	**3.74**	13/May/2020
19-RØR-32	Stream	1.10	0.19	**1.31**	30/Jan/2020
19-RØR-33	Stream	0.88	0.11	**1.09**	30/Jan/2020
19-RØR-34	Stream	2.03	0.12	**2.24**	05/Feb/2020
19-RØR-36	Stream	1.75	0.23	**1.96**	30/Jan/2020
19-RØR-37	Stream	3.27	0.18	**3.48**	04/Feb/2020
19-RØR-38	Slag rock	0.85	0.08	**1.06**	12/May/2020
19-RØR-40	Stream	3.20	0.16	**3.41**	04/Feb/2020
19-RØR-41	Stream	0.03	0.08	**0.24**	06/May/2020
19-RØR-42	Stream	1.60	0.11	**1.81**	05/Feb/2020

*Only Ni doping used for mass bias correction due to no or poor bracketing standard

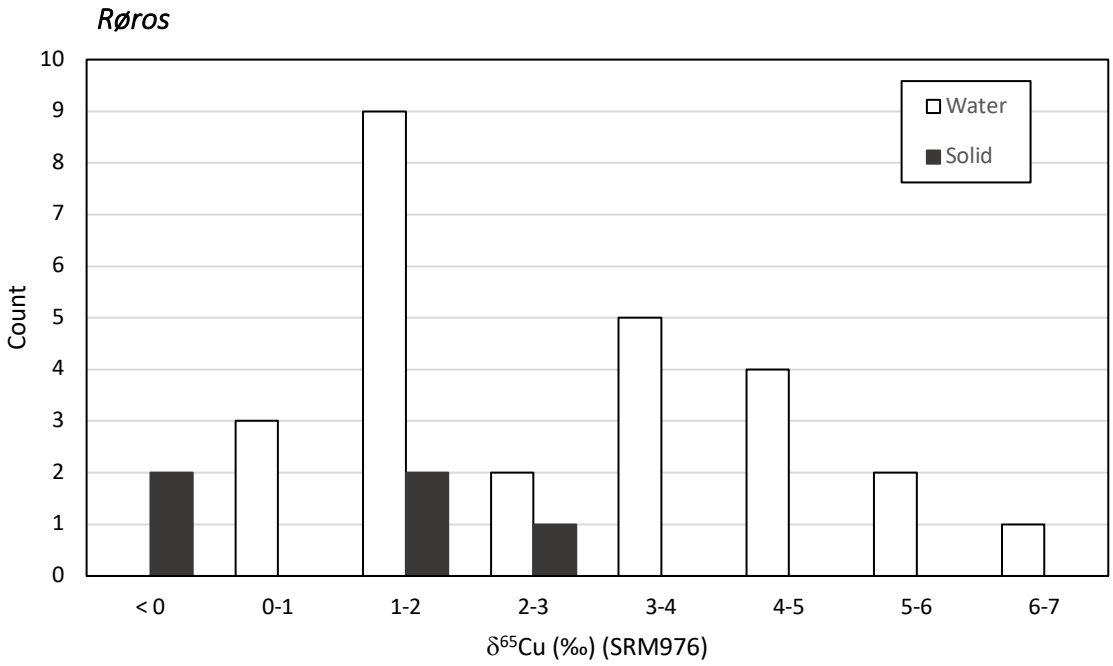

Figure 5.4: Frequency histogram for all analyzed Røros samples, separated by sample type and divided into eight separate bins from < 0 to 7‰. Bimodal skewed right distribution.

5.3.3 Løkken samples

Table 5.6 lists isotope results from the Løkken samples. $\delta^{65}Cu_{AE647}$ results are transformed to $\delta^{65}Cu_{SRM976}$ after Moeller et al. (2012) by adding +0.21‰. Figure 5.5 displays the isotope results in a frequency histogram. The two solid samples represent the lowest values around zero, and the water samples range $\delta^{65}Cu_{SRM976}$ = +1.72‰ to +5.53‰.

Table 5.6: Isotope results for all analyzed Løkken samples. $\delta^{65}Cu$ is transformed from reference material AE647 from MC-ICP-MS output data to SRM976.

Sample ID	Sample type	$\delta^{65}Cu_{AE647}$ (‰)	1σ	$\delta^{65}Cu_{SRM976}$ (‰)	Date analyzed
19-LØK-02	Waste rock	-0.50	0.09	**-0.29**	12/May/2020
19-LØK-03	Stream	2.67	0.19	**2.88**	04/Feb/2020
19-LØK-04	Lake	2.79	0.18	**3.00**	04/Feb/2020
19-LØK-05	Vasskis*	0.35	0.11	**0.56**	12/May/2020
19-LØK-06	Lake	1.52	0.14	**1.73**	05/Feb/2020
19-LØK-07	Lake	4.90	0.25	**5.11**	13/May/2020
19-LØK-08	Stream	4.53	0.20	**4.74**	04/Feb/2020
19-LØK-09	Lake	5.33	0.21	**5.54**	04/Feb/2020
19-LØK-10	Lake	4.15	0.16	**4.36**	04/Feb/2020
19-LØK-14	Stream	4.35	0.19	**4.56**	04/Feb/2020
19-LØK-15	Stream	4.54	0.20	**4.75**	04/Feb/2020

*Fine grained pyrite in dark matrix of hornfels

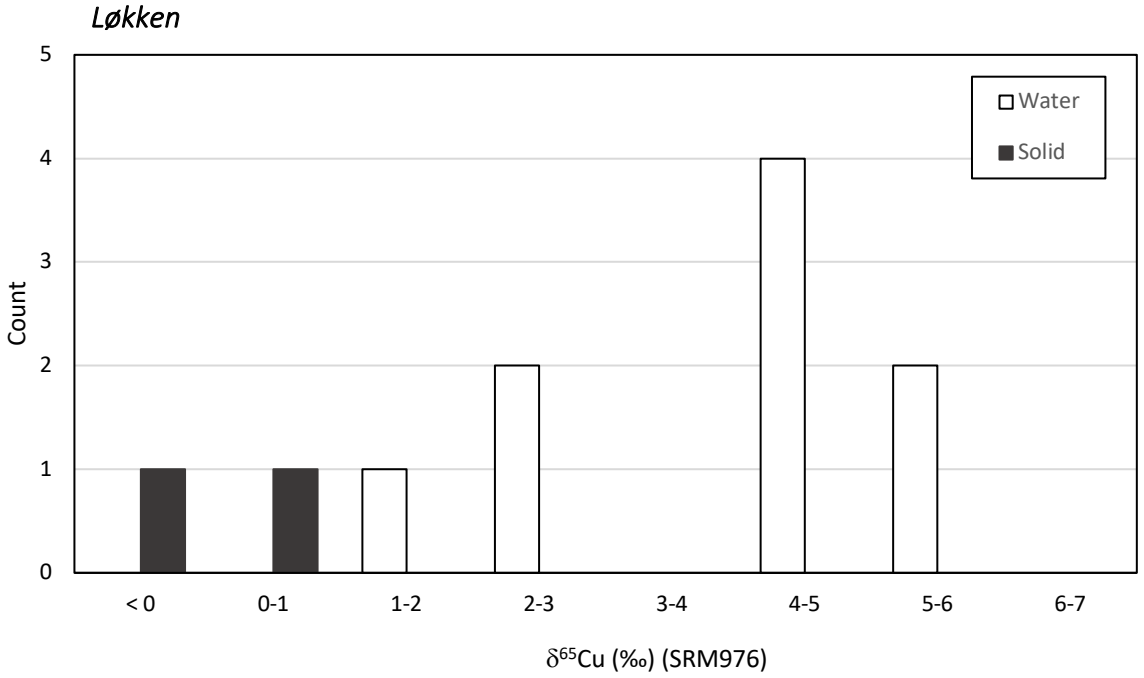

Figure 5.5: Frequency histogram displaying Løkken isotope results for solid and water samples. Solid samples represent the lowest $\delta^{65}Cu$ values up to 1‰. Water samples separated into two main $\delta^{65}Cu$ bins: 1-3‰ and 4-6‰, where the latter bin is the most common.

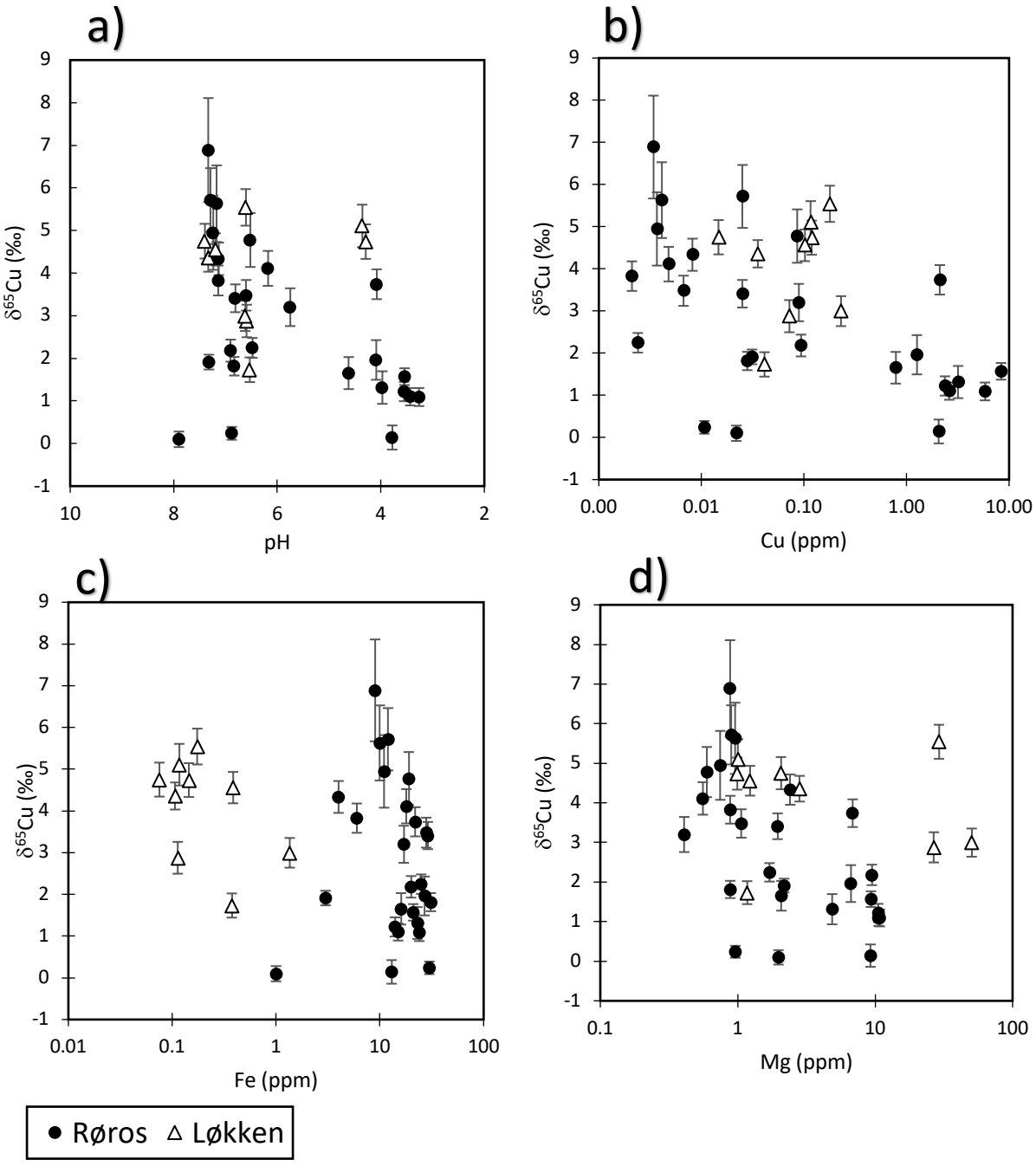

Figure 5.6 a)-d): Cross-plots of δ^{65}Cu values (SRM976) versus concentration parameters in water samples from Røros and Løkken. Error bars represents 2σ **a)** δ^{65}Cu and pH relationship. Low pH samples from Røros clusters around low isotope values (< 2‰). **b)** δ^{65}Cu and [Cu] relationship. High [Cu] correlates with low δ^{65}Cu-values. **c)** δ^{65}Cu – [Fe] relationship. Separation between RØR and LØK samples, with RØR samples having consistently higher Fe concentration, but no particular connection between [Fe] and δ^{65}Cu. **d)** δ^{65}Cu versus [Mg]. Appears to show a negative linear trend.

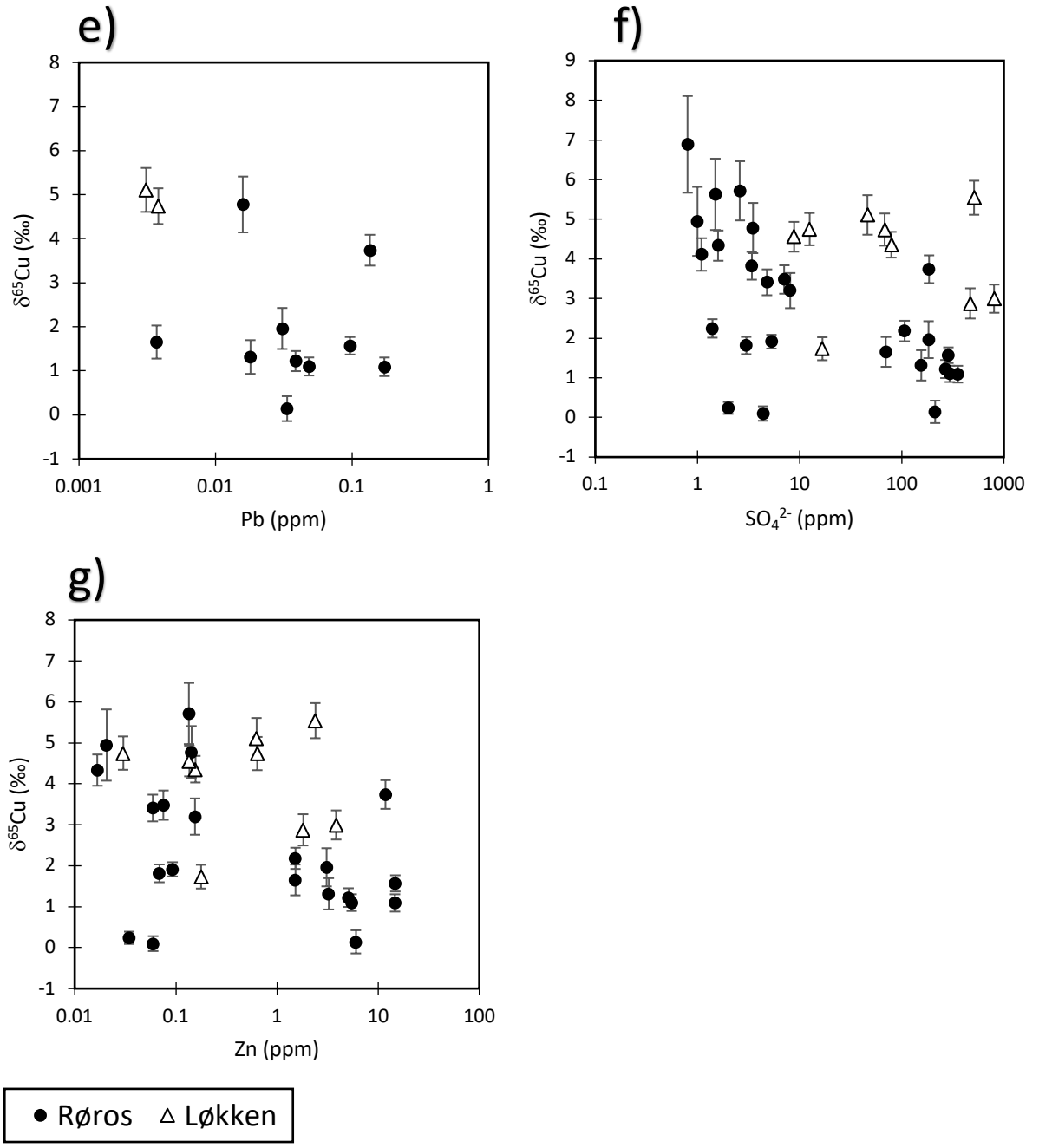

Figure 5.6 e)-g) (cont.): Cross-plots of δ^{65}Cu values versus concentration parameters in water samples from Røros and Løkken. Error bars represents 2σ **e)** δ^{65}Cu versus [Pb]. No visible correlation. **f)** δ^{65}Cu versus sulfate (SO_4^{2-}) concentration. LØK samples appear random. RØR samples divided into two sets of data points: one set with low sulfate concentrations and varied δ^{65}Cu, the other with high sulfate concentration associated with low δ^{65}Cu. **g)** δ^{65}Cu versus [Zn]. Same trend as seen in f) for sulfate. High Zn concentration appears to correlate with low δ^{65}Cu values.

Chapter 6: Discussion

The aim of this discussion is to assess whether Cu isotopes can be used to trace the source of contamination from two closed Cu-sulfide mines in Norway. The main focus of the discussion is the Storwartz mining field in Røros, as we have the most representative dataset from there and no remediation measures have been implemented. The dataset from Løkken is mainly used to consider the effects of remediation. First, we assess the isotopic composition of the potential sources. Secondly, we discuss the chemistry of, and Cu isotopic variations in the sampled surface water, and evaluate the remediation effects in Løkken. Furthermore, the spatial distribution of isotopic values and contamination is investigated with the aim of applying the Cu isotope system as a tracer. Finally, implications and limitations are presented, and future research is discussed.

6.1 Assessing potential sources of copper

Three main sources of released Cu are considered around the closed mines; Either the Cu is released from weathering of the ore minerals or bedrock found naturally in the area (natural sources), or it originates from mining related waste including tailings, gangue and slags (anthropogenic). The high Cu concentrations and low pH values found in surface waters, and also the general appearance of the nature surrounding the closed mines suggests that the anthropogenic mining activity must be at least partially responsible for the condition of the environment (fig. 6.1). The contamination appears to be more prominent at Storwartz compared to Løkken, with overall higher heavy metal concentrations, lower pH and generally more widespread visible clues like rust colored streambeds and solid materials (table 5.1-5.2, fig. 6.1).

Figure 6.1: Example of the difference in nature and visible environmental effects at Løkken and Storwartz. **Left**: *Bjørndalstjørna* tailings pond at Løkken. Sample 19-LØK-07 was collected here. **Right**: *Slamdammen*, the tailings pond at lower Storwartz in the background. Sample 19-RØR-31 sampled from stream in the foreground of the picture.

6.1.1 Storwartz, Røros

The isotope distribution of the Røros samples (fig. 5.4) shows that solid samples generally display lower δ^{65}Cu-values compared to water samples, and that they are separated into three groups in the histogram (fig. 5.4). The solid samples are divided into groups with δ^{65}Cu values below 0‰, between 1-2‰ and between 2-3‰. This gives three isotope reservoirs represented in our solid sample dataset. The lowest isotopic composition is the background rock (19-RØR-01), δ^{65}Cu = -0.19 $\pm$ 0.16‰ (table 5.5). Our background rock sample contains mostly Fe, Al and Mg, with only small amounts of Cu and Zn (table 5.3-5.4). Sample 19-RØR-02 is the only solid sample representing the Storwartz ore rock and belongs to the highest group of δ^{65}Cu. The isotope value of the ore rock is determined to be δ^{65}Cu = +2.95 $\pm$ 1.0‰ (table 5.5) and has high concentrations of Zn, Fe and Cu as well as smaller amounts of Al, Pb and S (Fe >> Zn > Cu >> Al > Pb > S) (table 5.3). The isotopic composition of the sampled gangue rock (19-RØR-25) is δ^{65}Cu = +1.66 ± 0.24‰ (table 5.5). Gangue is material that was rejected for extraction of resources because of low contents of extractable minerals, and ICP-OES analysis (table 5.3) shows that the sample contains for

the most part Fe, Mg, Al and Zn, and only small amounts of Cu. The slag heap rock sample's isotope value (19-RØR-38) is δ^{65}Cu = +1.06 ± 0.16‰ (table 5.5) and has a geochemical composition dominated by Fe, Mg and Al and a relatively low Cu concentration (table 5.3-5.4). A sediment sample collected just south of the main tailings dam (19-RØR-16), in the lower tailings pond, has a similar isotopic value to the background rock, δ^{65}Cu = -0.24 ± 0.14‰, but differs from the background rock in composition; The sediment sample has significantly higher concentrations of heavy metals like Cu, Fe, Zn and Pb (table 5.3) related to the metal sulfide minerals, and most likely represents a tailings sample or a combination of background and tailings material.

The geochemistry of the solids is consistent with what is expected for each different sample type. The background rock contains small amounts of Cu, Pb and Zn, whereas the ore rock contains a lot of Cu, Fe, Pb and Zn related to the most common sulfide minerals in the area (ch. 3.1.2). The gangue sample, tailings sample and slag also appear to be consistent with what is expected for the respective samples.

The geology of Røros is dominated by metasedimentary phyllites and greywackes (ch. 3.1.2; fig. 3.4), and the near-zero Cu isotopic composition of 19-RØR-01 agrees well with literature suggesting that Cu bound to silicates has an isotopic composition of δ^{65}Cu = 0 ± 1‰ (Chapman et al. 2006; Pokrovsky et al. 2008; Li et al. 2009; Bigalke et al. 2010; Song et al. 2016). The most important minerals in the Storwartz deposit are metal sulfide minerals, and the geochemistry of our ore rock sample (19-RØR-02) indicates that the ore is a combination of different types of metal sulfides; High Zn, Fe, Cu and some Pb are all present in the ore rock as well as in the common sulfide minerals sphalerite (ZnS), pyrite (FeS_2), pyrrhotite ($Fe_{1-x}S$), chalcopyrite ($CuFeS_2$) and galena (PbS). There is also Al in the sample which suggests that there is some siliciclastic rock present in the ore as well (table 5.3). The relatively high Zn content suggests the ore rock sample is from the western part of the deposit (Gamle and Nye Storwartz mine) (ch. 3.1.2). The isotope value of our ore rock sample is slightly higher than what is reported from other VMS chalcopyrites in the literature; Rouxel et al. (2004) found δ^{65}Cu = -1.30‰ to +2.91‰ in various oceanic hydrothermal systems (fig. 2.5). However, our value (+2.95‰) has a relatively large uncertainty (2σ = 1.0‰) which means that with 2 standard deviations considered, the value falls within the range determined by Rouxel et al. (2004).

Our gangue rock sample (19-RØR-25) represents material that was rejected for Cu extraction. The sample contains about 5000 ppm Cu, which is only 0.08 times the concentration of the ore rock sample (table 5.3-5.4). The sample is very Zn-rich (12 212 ppm), but Zn was not always extracted from the ore because it was harder to separate using flotation and less profitable compared to the Cu-extraction. The isotopic signature of the gangue rock is lower than the ore rock (+1.66‰ vs. +2.95‰). The difference might be a result of oxidative weathering of the gangue after being disposed of at the surface, where oxidative weathering preferentially leaches the heavy ^{65}Cu from sulfide minerals, leaving the gangue minerals lower in δ^{65}Cu (Mathur et al. 2009; Mirnejad et al. 2010). The δ^{65}Cu signature of the gangue rock may also have been originally different than our Cu-rich ore rock sample before being mined out, due to variations within the deposit.

Slag material (19-RØR-38) is the residue left after smelting of the sulfide ore and consists of mainly iron-oxides. Klein and Rose (2020) experimentally found that under controlled conditions, Cu should not fractionate significantly during the process from metallic ore to produced metal. This implies that the isotopic composition of the slag rock should be within a similar range of the primary sulfide mineral it originated from. In our results, slag rock and ore rock samples are not within the same range (+1.06‰ vs. +2.95‰). The difference observed between the ore and slag could be the result of an isotopically heterogeneous ore deposit with varying δ^{65}Cu values, and that the slag sample originally came from an ore rock with an analogous δ^{65}Cu, as predicted by Klein and Rose (2020). The δ^{65}Cu of the slag falls within the range for VMS chalcopyrites found by Rouxel et al. (2004) (δ^{65}Cu = -1.30‰ to +2.91‰). It is also possible that fractionation occurs during ore processing if conditions are uncontrolled and oxidizing; However, this should lead to a ^{65}Cu enriched slag phase (Klein and Rose 2020), opposite to our result. Also, the observed difference might result from a chemical reaction, like oxidative weathering, occurring after the slag was disposed of in the slag heaps.

The tailings sample (19-RØR-16) contains the common metal sulfide components Cu, Fe, Zn and Pb, and also Mg, Al, K and Ca (table 5.3-5.4). The low δ^{65}Cu of sample 19-RØR-16 overlaps with the background δ^{65}Cu, but the geochemical composition implies this is not simply a background sample (table 5.3). The relatively high concentrations of Cu, Fe, Zn and Pb indicates that it likely represents a tailings sample. Other studies have found that isotopic

compositions of tailings-related Cu vary significantly. For example, Song et al. (2016) found Cu in pyrite tailings to display the largest range of isotopic values in the study area, from -4‰ to +11.9‰. Because we only have one isotope result from the tailings, we can only speculate that the isotopic composition of the tailings at Storwartz possibly show a similarly wide range of tailings-δ^{65}Cu.

6.1.2 Løkken Verk

From Løkken, two solid samples were analyzed for isotopes by MC-ICP-MS. They are one gangue rock sample (19-LØK-02) and one "vasskis". The "vasskis" is a fine-grained pyrite ore in a dark matrix of hornfels bought in Orkla Industrimuseum (19-LØK-05) and is one of two mineral types in the Løkken deposit (ch. 3.2.2). The geochemical compositions are shown in table 5.3-5.4. In the isotope histogram (fig. 5.5), the solids represent the two lowest isotope values of all samples. The "vasskis" (19-LØK-05) has an isotope value of δ^{65}Cu = +0.56 $\pm$ 0.22‰ and the value of the gangue rock (19-LØK-02) is δ^{65}Cu = -0.29 $\pm$ 0.18‰ (table 5.6). The δ^{65}Cu value and geochemistry (table 5.3-5.4) of the "vasskis" is consistent with what is expected for this pyrite mineral type, and because the "vasskis" is syngenetic with the surrounding greenschist bedrock (ch. 3.2.2), the δ^{65}Cu should likely represent a similar isotopic value to the bedrock. The near-zero value agrees well with literature; As described in chapter 2.2.1, igneous rocks are expected to show δ^{65}Cu clustered around 0 $\pm$ 1‰ (i.e. Albarède 2004; Li et al. 2014; Liu et al. 2015). In addition, Mirnejad et al. (2010) found hypogene primary chalcopyrite-pyrite deposits to display δ^{65}Cu = +0.4 ± 0.14‰.

Unfortunately, we do not have a sample of the Cu-rich ore rock from Løkken. The Løkken deposit is an ophiolite hosted, Cyprus-type, VMS deposit (ch. 3.2.2) and chalcopyrite from Løkken is believed to have been formed in an oceanic seafloor black smoker system. Primary chalcopyrite from modern black smoker systems appear to represent an isotopic composition of approximately 0.0‰ to 0.5‰ (Berkenbosch et al. 2015). Zhu et al. (2000) reports δ^{65}Cu values between -0.37‰ and +0.76‰ from various black smoker sulfide deposits. With this data, we can assume the δ^{65}Cu of the Løkken deposit to be approximately δ^{65}Cu = +0.25 $\pm$ 0.50‰. As tailings material is covered for remediation purposes, we do not have a tailings sample isotope signature either.

6.2 Assessing chemical and isotopic variations in surface water samples

The Cu isotope dataset from surface water samples spans a wide range from +0.10‰ to +6.89‰ in Røros samples (table 5.5, fig. 5.4) and +1.73‰ to +5.54‰ in Løkken samples (table 5.6, fig. 5.5). Cu concentrations range from below detection limit (0.002 ppm) to over 8 ppm, with overall higher concentrations found in the Røros samples (table 5.2). The following subchapters discuss the variations in chemistry and δ^{65}Cu values of the surface water related to Cu sulfide mining in Røros and Løkken.

6.2.1 Storwartz, Røros

The chemical and isotopic composition of our surface water samples varies significantly across the sampled area. Cross-plots of the relationships between Cu concentration and some heavy metals plus sulfate, as well as between sulfate concentration and pH are displayed in figure 5.3. In the Røros samples, there is an observable correlation between elevated levels of Cu with sulfate, Zn and also with low pH. In figure 5.6 the correlation between δ^{65}Cu and metal concentrations, sulfate and pH is presented. For the four parameters that appear to be the most related (Cu, Zn, sulfate, pH), a cluster of datapoints falls within a small range of δ^{65}Cu values.

To investigate the isotopic variations across the sampled surface waters in Røros it is essential to look at the chemistry (or contamination) of the water samples together with the δ^{65}Cu values of the dissolved Cu. From the ICP-OES results (table 5.2) it is evident that there are eight Røros samples that show higher concentrations of Cu, sulfate (SO_4^{2-}) and several other heavy metal contaminants like Co, Cr, Fe, Li, Mg, Mn, Ni, Pb and Zn, compared to the rest. These samples are all associated with acidic pH between 3.2 and 4.1, and are samples 19-RØR-15, -17, -19, -30, -31, -32, -33 and -36 (table 5.1-5.2). 19-RØR-20 also has slightly elevated Cu and sulfate concentration, and pH 4.6. The relationship between Cu concentrations and Cu isotope composition in Røros water samples is displayed in figure 6.2. In general, low Cu concentrations correlate with near-neutral pH (table 5.1, fig. 5.1). Samples with low Cu concentration display δ^{65}Cu values ranging from the lowest values found (+0.10‰) to the highest values found (+6.89‰) in the Røros samples (table 5.5). As revealed in figure 6.2, the water samples with elevated Cu concentrations represents a narrow range of δ^{65}Cu values. Apart from the two outliers (19-RØR-15 and 19-RØR-31), all

samples with [Cu] > 0.1 ppm fall between δ^{65}Cu = +1.10‰ and δ^{65}Cu = +1.96‰ (19-RØR-19 and 19-RØR-36, table 5.5, fig. 6.2). The figure highlights that most of the samples with high Cu concentration likely come from the same source because of their similar isotopic signature. The outliers, sample 19-RØR-15 and 19-RØR-31, also show a relatively high Cu concentration but do not fall within the same narrow δ^{65}Cu-range as the previously mentioned samples. 19-RØR-15 represents a low isotope value of δ^{65}Cu = +0.14 ±0.28‰, whereas 19-RØR-31 has a quite high δ^{65}Cu-value at +3.74 ± 0.34‰. Figure 5.6 shows similar plots of Cu isotopic composition (δ^{65}Cu) and various concentration parameters together. Because they are closely related, we can see a similar trend where low pH/high sulfate concentration/high Zn concentration correlates with the same narrow cluster of isotope values between +1‰ to +2‰ (fig. 5.6).

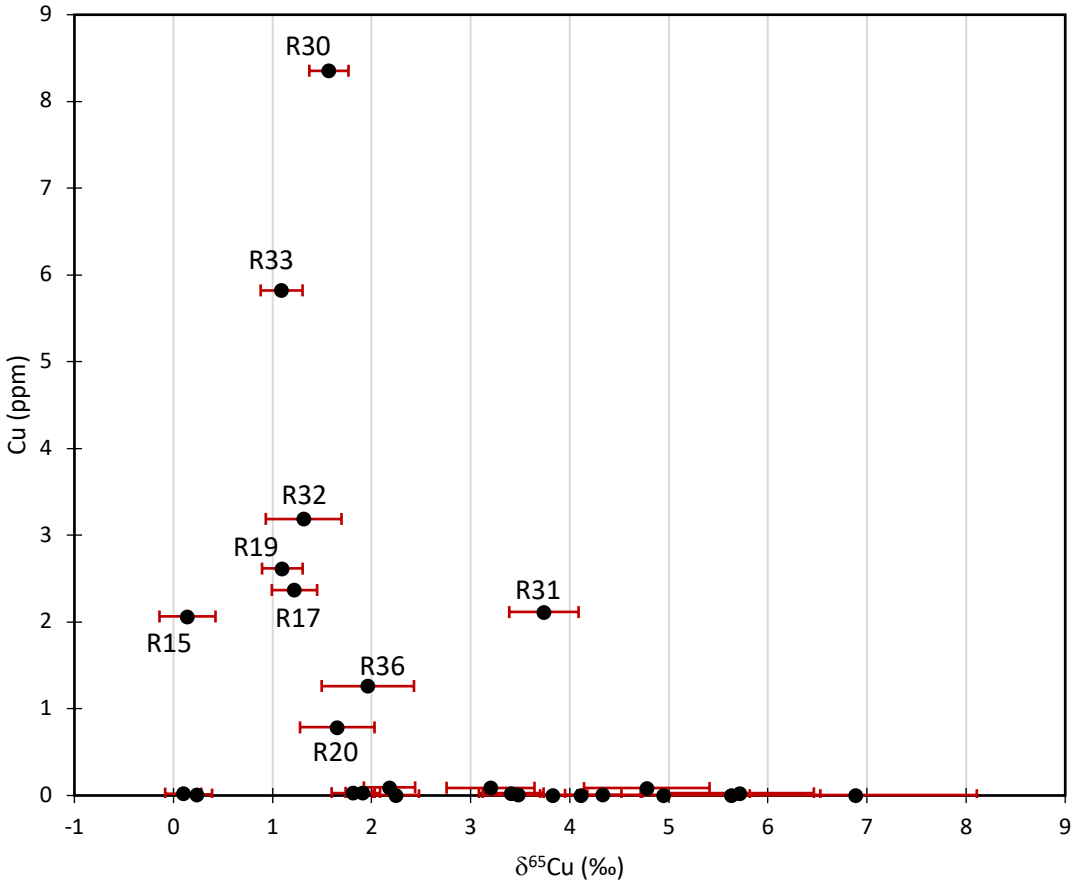

Figure 6.2: Concentration of Cu in ppm versus Cu isotopic composition (δ^{65}Cu in ‰) in Røros water samples. Elevated levels of concentration fall within a narrow isotopic range between approximately +1‰ and +2‰. R15 and R31 are considered outliers. Concentrations are found in table 5.2 and isotope values in table 5.5 Note: Sample names are abbreviated: "R15" = 19-RØR-15 etc. Error bars represent 2σ

The isotopic composition of surface waters is dependent on the source of the Cu and any reactions that cause fractionation of Cu isotopes (ch. 2; fig. 6.3). Different natural processes fractionate stable Cu isotopes in varying degree and also in opposite directions. Figure 6.3 summarizes the natural processes fractionating Cu in natural water systems discussed in this thesis. Oxidative weathering leads to a significantly heavier isotopic signature of Cu in solution (ch. 2.3.2); Inorganic adsorption processes (ch. 2.3.2) preferentially adsorb heavy ^{65}Cu from the solution, resulting in a lower δ^{65}Cu signature of the solution; Most biological processes preferentially incorporate the light ^{63}Cu, leaving the solution enriched in the heavy isotope (higher δ^{65}Cu in solution); The acidophilic bacteria *T. Ferrooxidans* fractionates Cu isotopes in the opposite direction, by preferentially taking up the heavy isotope, resulting in a lighter δ^{65}Cu of solution (ch. 2.3.4). To understand each sample's unique δ^{65}Cu, several possible reactions causing fractionation need to be considered. The largest fractionations occur from oxidative weathering of Cu(I)sulfides. Up to $\Delta^{65}Cu_{Cu(II)\text{-}Cu(I)}$ = +20‰ separation between Cu(II) and Cu(I) has been observed for environmental samples that has undergone one or more redox cycles (Moynier et al. 2017; ch. 2.3.2). Inorganic adsorption is less significant, but fractionates Cu in the magnitude of $\Delta^{65}Cu_{sol.\text{-}solid}$= -0.73‰ (Balistrieri et al. 2008). Organic complexation causes a similar separation of $\Delta^{65}Cu_{free\text{-}complexed}$ = -0.84‰ to -0.14‰ (Ryan et al. 2014; Wang et al. 2017). Biological processes can fractionate Cu quite significantly, in the opposite direction of inorganic adsorption and organic complexation; $\Delta^{65}Cu_{sol.\text{-}bacteria}$ = +0.20‰ to +4.4‰ (Navarrete et al. 2011). The different fractionation separations are presented in figure 6.3, where the Δ^{65}Cu reported is the highest δ^{65}Cu separation for each process discussed in this thesis.

Weathering of the metasedimentary bedrock in Røros should result in a δ^{65}Cu approximately +0.22‰ heavier than the background rock δ^{65}Cu, inferred after Wang et al.'s (2017) findings on the relationship between bedrock and sediment to dissolved Cu. Also, weathering of Cu bound to silicates does not include a change in oxidation state of the Cu as it is bound to silicates as Cu^{2+} and released as Cu^{2+} (Albarède 2004). This means that samples with Cu derived from our background sample (19-RØR-01) should have an isotopic composition of ~0‰. In addition, the samples associated with background Cu values are not expected to have significantly elevated levels of Cu, other heavy metals or acidic pH, as they

emanate from areas without sulfide weathering. These conditions are found in samples 19-RØR-03 and 19-RØR-41 (table 5.5). 19-RØR-15 has a similar low δ^{65}Cu but displays a much higher level of contamination (high heavy metal and sulfate concentration and also low pH). The low δ^{65}Cu of 19-RØR-15 is therefore more likely a result of some other fractionation processes.

The oxidative weathering of chalcopyrite should lead to a +1.2‰ to 2‰ heavier dissolved Cu signature (Mathur et al. 2005; Fernandez and Borrok 2009, Kimball et al. 2009), and weathering of other Cu sulfide minerals is found to result in δ^{65}Cu to be +1‰ to +3.5‰ heavier in solution compared to the primary mineral (Song et al. 2016). The Cu released into the surface waters is mainly controlled by the δ^{65}Cu of the sulfide mineral (both ore rock and mining waste) and isotope fractionation. The fractionation is also dependent on the amount of Cu leached as described by Fernandez and Borrok (2009). With an increased fraction of Cu leached, the δ^{65}Cu value of the Cu in solution converges toward the starting material itself (Fernandez and Borrok). Our ore rock sample at δ^{65}Cu = +2.95‰ should release Cu into solution with approximately δ^{65}Cu = +4.5‰ assuming chalcopyrite is the dominant Cu-sulfide mineral. The most contaminated samples are for the most part associated with δ^{65}Cu around +1‰ to +1.6‰ and is more likely derived from the tailings rather than the ore rock. This is also more likely as there is no exposed ore rock surrounding the most contaminated samples. The rest of the δ^{65}Cu values are for the most part higher, and consistent with either weathering of the ore rock, or from tailings where biological uptake might have resulted in an increased δ^{65}Cu. Overall, nearly all sampled water show δ^{65}Cu values above what is expected for uncontaminated water. Only samples 19-RØR-03 and 19-RØR-41 have isotopic and heavy metal concentrations related to background silicate-bound Cu. The average isotopic composition of rivers and the ocean is +0.53‰ and +0.70‰, respectively (Wang et al. 2017). Our results are generally significantly higher and thus consistent with the findings of several other studies that have found that high δ^{65}Cu values in natural surface waters are related to areas of Cu-sulfide weathering compared to areas without sulfide weathering (i.e. Kimball et al. 2009; Song et al. 2016). Sulfide minerals are unstable at atmospheric conditions and readily oxidize, releasing heavy metals and acidity, in the form of sulfuric acid (H_2SO_4). Table 6.1 lists the main sulfide minerals found in the ore deposit at Storwartz and their reaction when exposed to atmospheric O_2 (and

water). All of the minerals release heavy metals (Fe, Cu, Zn, Pb), and from the reactions it is evident that weathering of pyrite, pyrrhotite and chalcopyrite release acidity, while weathering of sphalerite and galena does not (table 6.1). Pyrite weathering contributes the most to acid formation, with 4 moles H^+ released per mole of FeS_2 (table 6.1). Cu is mainly released from the weathering of chalcopyrite but can also be found in smaller amounts in the other minerals. In addition, acid formation increases the metal sulfide solubility and thus the amount of released metals increases with decreasing pH (fig. 5.1; Seewald and Seyfried 1990).

Table 6.1: Typical sulfide minerals in the Storwartz deposit with mineral names, abbreviations of name, chemical formula and their reactions when exposed to atmospheric O_2 (and water). Pyrrhotite reaction from Oliveira (2014).

Mineral name	Abbrev.	Chemical formula	Reaction with atmospheric O_2
Pyrite	py	FeS_2	$4\ FeS_2 + 15\ O_2 + 14\ H_2O = 4\ Fe(OH)_3 + 8\ SO_4^{2-} + 16\ H^+$
Pyrrhotite	po	$Fe_{1-x}S$	$Fe_{1-x}S + O_2 + H_2O = Fe(OH)_3 + SO_4^{2-} + H^+$
Chalcopyrite	cpy	$CuFeS_2$	$CuFeS_2 + 4\ O_2 + 3\ H_2O = Cu^{2+} + Fe(OH)_3 + 2\ SO_4^{2-} + 2\ H^+$
Sphalerite	sp	ZnS	$ZnS + 2\ O_2 = Zn^{2+} + SO_4^{2-}$
Galena	gn	PbS	$PbS + 2\ O_2 = Pb^{2+} + SO_4^{2-}$

6.2.2 Løkken Verk

The Løkken water samples show a bimodal distribution in their isotopic compositions (fig. 5.5), where the majority of the samples have high $\delta^{65}Cu$ >4‰. A few samples have Cu isotopic compositions between 1‰ and 3‰ (table 5.6, fig. 5.5). As seen in figure 5.1, the Løkken samples show less correlation between Cu concentration and pH. All Løkken samples have relatively low Cu concentrations - including the two samples that are more acidic (pH ~4.3, table 5.1). Figure 5.3a)-d) also shows that the Cu concentration generally does not show any systematic correlation with other elements because the Cu concentration is quite low even at elevated concentrations of other elements. The low Cu concentrations could be a result of the remediation strategies implemented at Løkken to limit the contamination of the environment (ch. 3.3). Figure 5.3e) also shows that sulfate concentrations in three samples are very high, regardless of a near neutral pH ~6.6. The high sulfate concentrations indicate that sulfide weathering-release of SO_4^{2-} (table 6.1) into the environment have had a

strong impact on the aquatic environment, but pH is remediated to near-neutral. Acid mine drainage from Løkken is pumped from the mines into Fagerlivatnet and treated with chalk ($CaCO_3$) to neutralize acidity (Direktoratet for mineralforvaltning 2019). In figure 5.6, the Løkken samples show no clear connection between isotopic composition and concentration of Cu, Fe, Pb, Mg, Zn or sulfate; The pH (fig. 5.6a)) separates the samples into two groups: neutral samples with pH ~7 and acidic samples with pH ~4. The samples with near neutral pH range have no systematic correlation with δ^{65}Cu, but the two low-pH samples have the same δ^{65}Cu ~5‰. It is important to note that the two similar samples (19-LØK-07 and 19-LØK-08) are taken from a lake and the stream that drains the same lake. The lack of correlation between the analyzed chemical parameters indicates that the remediation measures might have affected the condition of the surface water at Løkken. Cu is removed from solution by natural chemical and biological processes (Orkla industrimuseum 2019c). The fractionation of Cu that follows the remediation is not known. It appears to involve preferential removal of the light isotope, according to the high δ^{65}Cu values found in every surface water sample from Løkken (fig. 6.5). Processes that preferentially utilize ^{63}Cu are for example secondary mineralization of Cu sulfides or biological uptake (ch. 2.3). However, opposite fractionations might also occur because of inorganic adsorption, T.Ferrooxidans uptake or organic complexation (fig. 6.3).

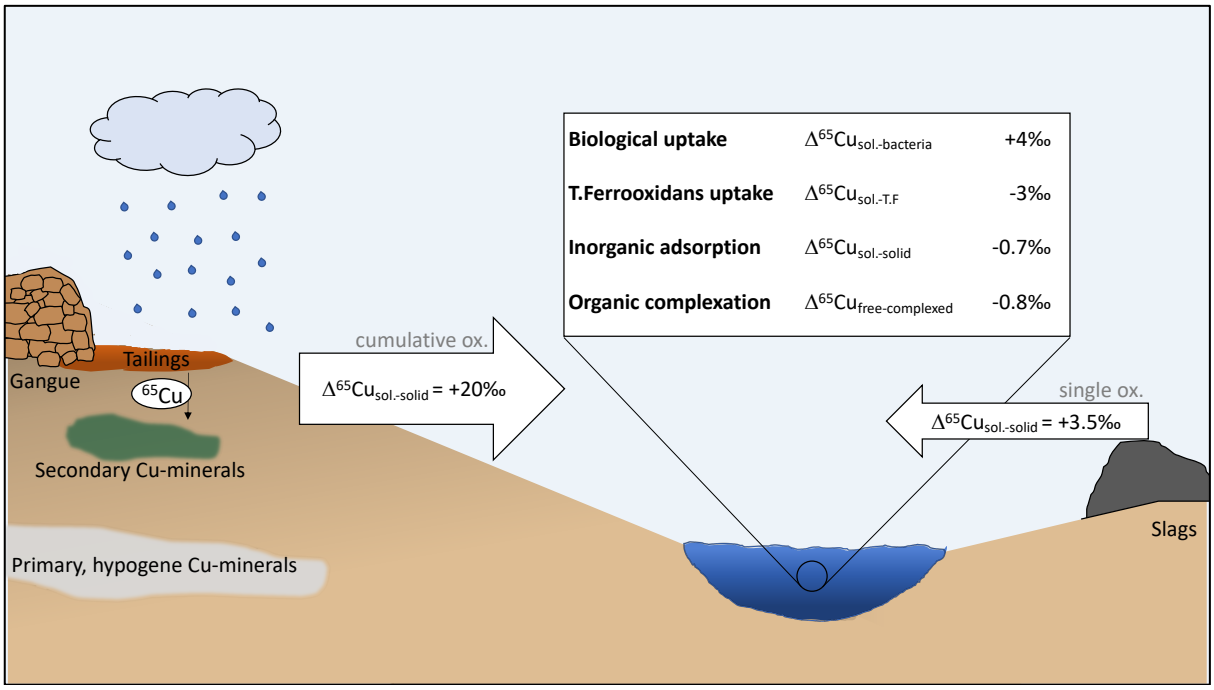

Figure 6.3: Conceptual model of stable Cu isotope fractionation processes important for natural surface water $\delta^{65}Cu$. $\Delta^{65}Cu_{A-B} = \delta^{65}Cu_A - \delta^{65}Cu_B$. $\Delta^{65}Cu$ reported represents the high-end of separation observed from literature (Mathur et al. 2005; Balistrieri et al. 2008; Kimball et al. 2009; Navarrete et al. 2011; Ryan et al. 2014; Song et al. 2016; Moynier et al. 2017; Wang et al. 2017). Oxidative weathering release of Cu cause the most significant fractionations (up to 20‰ separation cumulatively or 3.5‰ separation for a single oxidation). Oxidative weathering of Cu-sulfides is also the main source of Cu release into the environment. Fractionation of natural processes that may occur in a hypothetical natural surface water reservoir is presented in the box, where the $\Delta^{65}Cu$ reported represents the high-end of separation. Biological uptake results in a heavier isotopic signature; Uptake by *T.Ferrooxidans*, inorganic adsorption and organic complexation results in a lighter isotopic signature.

6.3 Stable copper isotopes as an environmental tracer

By assessing the spatial distribution of our water samples, we attempt to establish an understanding of the isotopic variations around the closed Cu-sulfide mines and the use of the stable Cu isotope system as an environmental tracer. Figure 6.4 displays the sample locations and isotopic values of the water samples in the Røros district. Figure 6.5 shows the isotopic variations in Løkken.

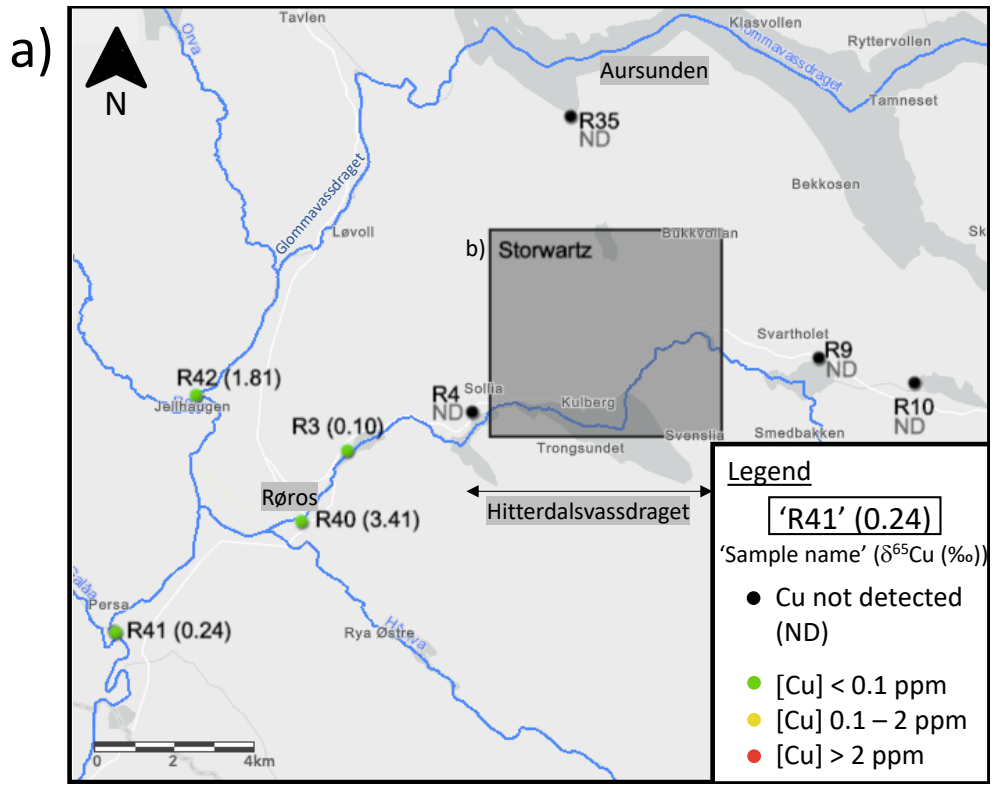

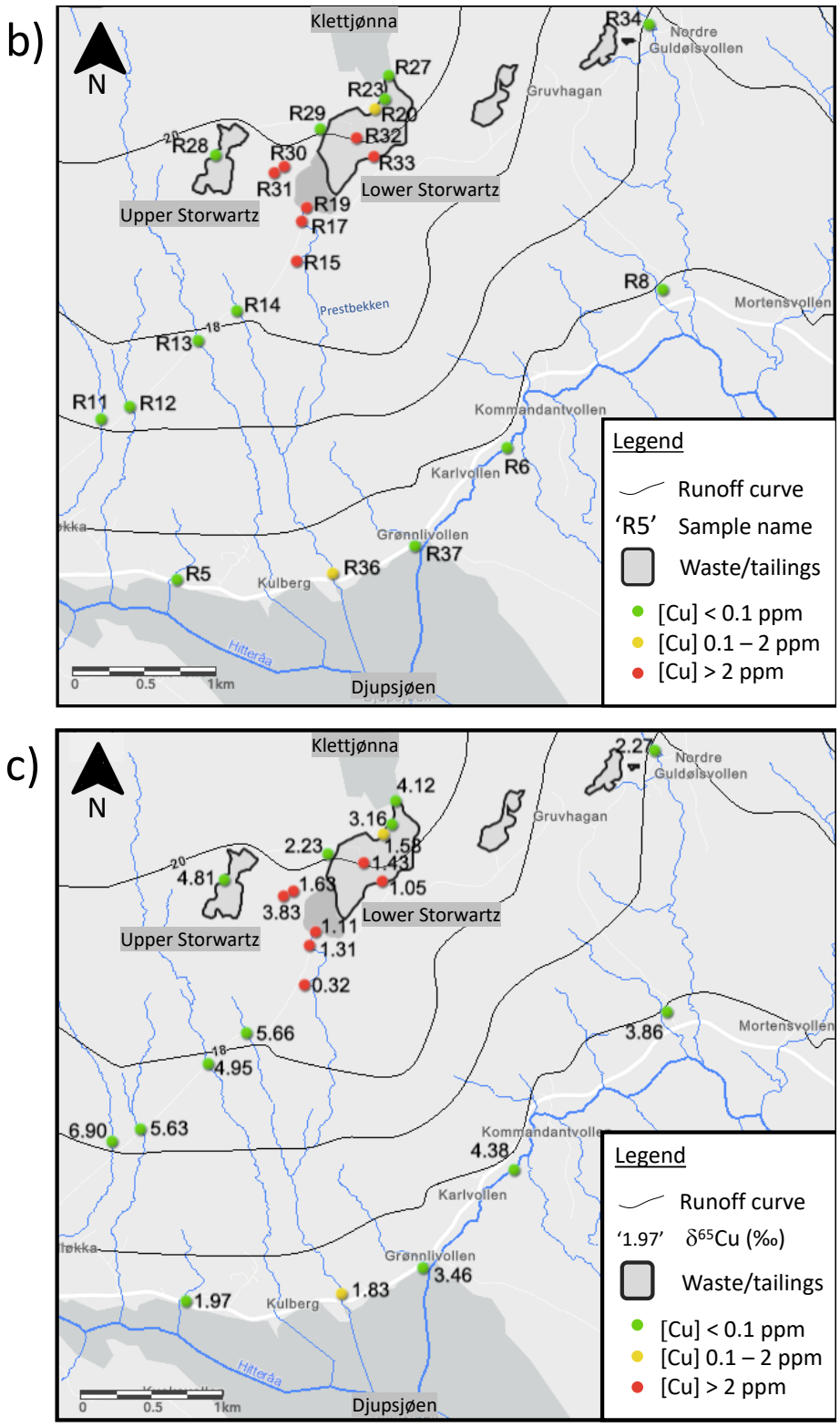

Figure 6.4a)-c): Spatial distribution of water samples in Røros. Sample names are abbreviated like: R3 = 19-RØR-03 etc. Isotope values with error can be found in table 5.5 (SRM976). **a)** Water samples outside of Storwartz mining field with corresponding names and δ^{65}Cu values in brackets. Storwartz mining field lies within the square marked 'b)'. **b)** Water samples with corresponding sample names. Contour lines represent runoff lines to illustrate the drainage direction. Major waste deposits marked with black contours **c)** Same map as in b), but sample names are substituted with isotope values. Made with ArcGIS Online (Map layers by Esri, HERE, Garmin, INCREMENT P, METI/NASA, USGS).

Figure 6.4a) shows that four samples located away from the Storwartz mining area could not be analyzed by MC-ICP-MS because ICP-OES analysis found no detectable Cu in the samples (DL: 0.002 ppm for Cu on ICP-OES). It also shows that the four samples that are analyzed near Røros display significantly different δ^{65}Cu values. As described in chapter 6.2, surface waters with Cu from the background rock in Røros should have δ^{65}Cu near 0‰, low concentrations of Cu and neutral pH. Near-zero δ^{65}Cu values are found in samples 19-RØR-03, 19-RØR-15 and 19-RØR-41 (table 5.5). These values give an initial indication that the Cu might be derived from background rock. However, 19-RØR-15 has a high concentration of Cu and other contaminants (table 5.2), and also acidic pH (table 5.1) which makes it unlikely that the Cu is leached from the background rock. Sample 19-RØR-15 is collected together with the sediment sample earlier described as a tailings sample (19-RØR-16) (ch. 6.1.1). Its location, directly downstream from the tailings pond at lower Storwartz also points to the signature likely representing the tailings, even though it lies outside of what is defined as waste deposits by available maps (fig. 6.4). The small pond in which the 19-RØR-15 sample is collected has several stream inputs that could mean the isotope value is a result of several competing isotopic signatures. δ^{65}Cu might also be lower than expected because of natural processes preferentially removing the heavy isotope. For example, uptake by *T.Ferrooxidans* bacteria is found to adsorb ^{65}Cu resulting in a separation of -3‰, where the surface water δ^{65}Cu is decreased (ch. 2.3.3). Inorganic adsorption and organic complexation also preferentially remove the heavy isotope giving a lower δ^{65}Cu than expected from purely oxidation of sulfides.

In most water samples from lower Storwartz, the δ^{65}Cu values are similar to each other and also noticeably lower than most surrounding samples. Six samples at lower Storwartz have isotopic compositions between +1.09‰ (19-RØR-19) and +1.65‰ (19-RØR-20), located across the tailings and flotation plant. All other samples around the Storwartz field (fig. 6.4b)-c)), except 19-RØR-05, have higher isotope values. The samples at lower Storwartz with similar δ^{65}Cu are amongst the most contaminated in Cu, sulfate and other heavy metals, as discussed in chapter 6.2. Taking into consideration the high concentrations, the location of the samples relative to the tailings and the isotope values of the samples, the source of Cu for these samples are likely the tailings at lower Storwartz. The high concentrations of Cu and several other heavy metals, sulfate and the low pH are related to

oxidative weathering of metal sulfides that have been exposed to atmospheric O_2 due to the mining activity. The single tailings isotope value determined in this study is δ^{65}Cu= -0.24 ± 0.14‰, and the dissolved Cu isotope values are thus consistent with oxidative weathering of tailings sulfides (ch. 2.3.2). In addition, this range of isotopic compositions is found exclusively in waters closely related to known tailings deposits (fig 6.4). This also tells us that the most contamination comes from the tailings at Storwartz.

The four highest δ^{65}Cu-values are located in four separate streams emanating from an area west of the waste deposits at upper Storwartz (fig 6.4). The Cu concentrations of these samples are relatively low, but the high isotope values and their location excludes the background rock as the Cu source. The high isotope values should not result from the bedrock of the area, as it is determined to be much lower in Cu isotopic composition. The Cu from background rock to dissolved Cu should not result in large enough fractionation to give δ^{65}Cu values any higher than approximately +0.5‰ (ch. 2.3.2). The streams appear to lie outside of where mining waste has been disposed, which means the Cu might originate from an occurrence of the ore mineralization located in the general area to the west. However, the runoff curves (fig. 6.4) show that there might be some drainage leading from waste piles at upper Storwartz into these streams. And, if we compare the isotope values with other isotope results around Storwartz, we find similarly high values in a variety of locations; One sample taken at upper Storwartz (19-RØR-28) and a small stream going from upper Storwartz down to Slamdammen (19-RØR-31) also displays a similar high δ^{65}Cu (fig. 6.4). Samples from Klettjønna north of the mines, and some samples from smaller streams near Hitterdalsvassdraget to the south also display high δ^{65}Cu values (fig. 6.4). Furthermore, most of the high δ^{65}Cu samples have one important thing in common – they have relatively low concentrations of Cu (<0.1 ppm, except 19-RØR-31). Because the low concentrations appear to correlate with higher δ^{65}Cu values, it is plausible that there are processes that removes Cu from solution while also fractionating to a heavier solution-δ^{65}Cu affecting the surface waters located further away from the most contaminated area at lower Storwartz (fig. 6.4). As previously discussed, most biological processes preferentially incorporate ^{63}Cu, and can fractionate Cu up to $\Delta^{65}Cu_{sol.-bacteria}$ = +4‰ (ch. 2.3.3, fig. 6.3) and consequently the δ^{65}Cu of surface waters increases.

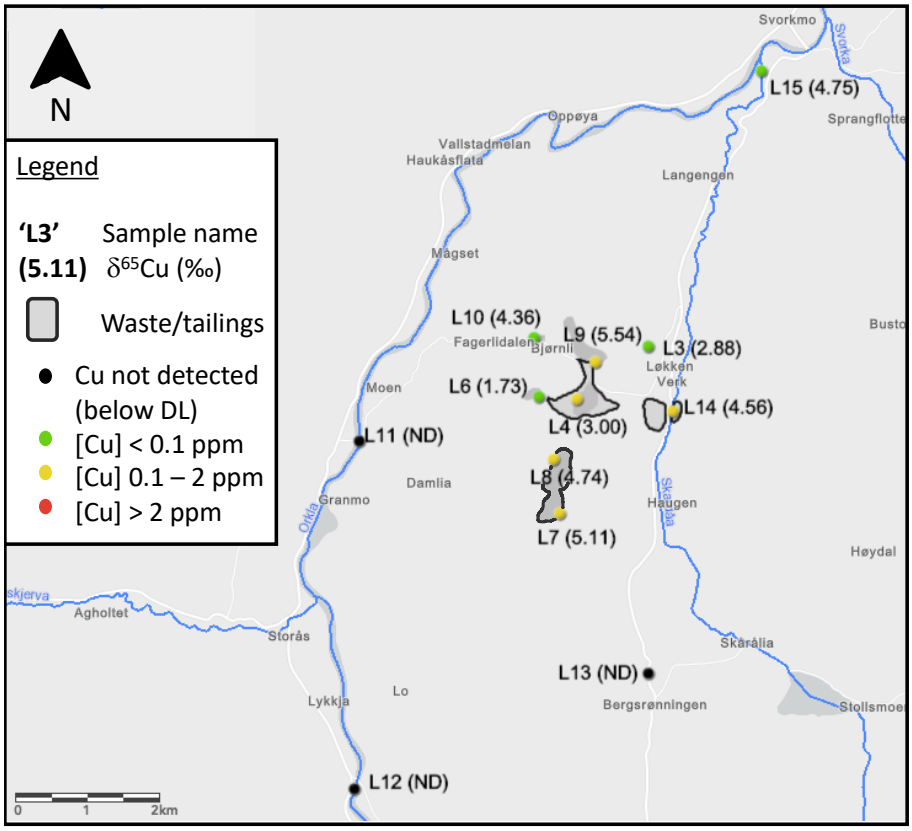

Figure 6.5: Isotope map of Løkken samples. Isotope results with errors can be found in table 5.6 (SRM976). Made with ArcGIS Online (Map layers by Esri, HERE, Garmin, INCREMENT P, METI/NASA, USGS).

All Løkken surface water isotope results have significantly higher δ^{65}Cu than the sampled solids (table 5.6). No sampled surface water has Cu concentrations above 2 ppm (fig. 6.4c)). The two lowest δ^{65}Cu values also are among the lowest concentrated in Cu. Further, the high δ^{65}Cu makes it unlikely the Cu present in solution comes from the background rock that is around 0‰, represented by the "vasskis" (19-LØK-05 δ^{65}Cu = 0.56 ± 0.22‰). Gangue rock δ^{65}Cu is also low. The important difference between Løkken and Røros is the much lower Cu concentrations and for the most part neutral pH found in Løkken. It appears that the remediation measures (ch. 3.3.3) has had an effect on heavy metal release and pH. The δ^{65}Cu of surface waters appear to be relatively high compared to our solid samples and also assumptions made for the ore rock. The high δ^{65}Cu might be a consequence of the remediation measures employed at Løkken. Most surface runoff is directed into the mine, where the heavy metals are removed by natural chemical and biological processes. The acidic mine drainage is pumped into Fagerlivatnet and treated with

chalk to neutralize acidity. With increasing pH, the solubility of Cu decreases and Cu precipitates from solution. The apparent shift toward heavier $\delta^{65}Cu$ indicates that ^{63}Cu is preferentially precipitated, as seen with both secondary mineralization and adsorption onto for example iron oxyhydroxides (ch. 2.3).

6.4 Implications, limitations and future research

Our study includes Cu isotope analysis and concentration analysis of both water samples and solid samples. By discussing our results together with what is known about the history and geology of the area as well as knowledge acquired from literature research, the method appears to be promising but not comprehensive enough to certainly explain all isotopic variations. Nearly all sampled water with detectable Cu (> 2 ppb) shows Cu isotope values above what is expected for the natural background rocks of the area. This tells us that the Cu sulfide mining has had, and still has an impact on the surrounding environments. Even where Cu concentration is low, $\delta^{65}Cu$ displays heavy signatures indicative of oxidative weathering of metal sulfides. Our results show that for the most part, the $\delta^{65}Cu$ of surface waters and solid sources gave an indication on how Cu sulfide mining has affected local streams and lakes. In Røros, the highest contaminated samples show a similar range of isotope signatures. Samples that are less contaminated show for the most part significantly heavier isotopic signatures, except a few samples that are interpreted to represent background Cu. The high $\delta^{65}Cu$ in low contaminated waters indicates that there are natural processes that preferentially removes Cu as the light isotope, ^{63}Cu, from solution resulting in higher $\delta^{65}Cu$ values. Most biological processes, including plant uptake and bacterial incorporation and adsorption, preferentially adsorb ^{63}Cu causing separations up to $\Delta^{65}Cu_{sol.-bacteria}$= +4‰ (Navarrete et al. 2011).

The main limitation of our method is the difficulty in constraining fractionation processes and the limited dataset on the possible sources of Cu. As previously discussed, the $\delta^{65}Cu$ values of surface waters are dependent on the isotopic composition of the Cu source as well as natural processes causing fractionation of Cu, and that the $\delta^{65}Cu$ values of a natural surface water system is quite complex. Sillerová et al. (2017) attempted to use the stable Cu isotope system to trace the source of contamination and concludes that the

method requires a complex analytical approach because of the complex nature of the biogeochemical system in natural surface waters. Isotopic composition of Cu in surface waters can be affected by many other processes besides the more obvious oxidative sulfide weathering. As discussed in chapter 2, inorganic adsorption, biological processes and organic complexation are examples of processes that fractionates Cu significantly, in particular biological processes. There is a high likelihood that some, or all, of these processes have affected our isotope values, resulting in higher (biological uptake) or lower (inorganic adsorption, organic complexation) δ^{65}Cu than expected. These fractionation processes are not possible to constrain any further based on the analyses we have performed and can only be qualitatively considered here.

Further, the number of solid samples analyzed is very limited. Also, the isotope result for the single ore rock sample from Røros (19-RØR-02) has a relatively large uncertainty at 2σ = 1.0‰ and it would have been beneficial to analyze this sample again on the MC-ICP-MS to achieve a better value. In addition, it would have been valuable to further constrain the isotopic composition, and any variations, across the ore deposit by collecting and analyzing more ore rock samples. The ore rock sample is bought in a souvenir shop, making it hard to determine from where in the deposit it is taken from. Ideally, samples from drill cores could have limited the uncertainties of the ore rock source composition, but this is not feasible to achieve in the Storwartz mining field as it is protected from such invasive sampling. In addition, we do not have a sample of the Cu-rich ore rock at Løkken and can only assume its isotopic composition. The waste material dataset initially was more extensive, but we did not get to analyze all our solid samples on the MC-ICP-MS due to the outbreak of COVID-19. This means that it is impossible to decide the range of isotopic values in the tailings, where Song et al. (2016) found significant variations.

When comparing our results to our baseline study by Song et al. (2016), it is important to take into consideration that the Dexing mine is an active, open-pit porphyry copper mine whereas Løkken and Røros are closed, underground mines of VMS deposits. Løkken and Røros also differs between them in VMS type (Cyprus-type vs. Besshi-type) and host rocks (igneous vs. metasedimentary) (ch. 3). From Song et al.'s (2016) paper, it also appears that the Dexing deposit is more homogenous in comparison to our study areas, where pure chalcopyrite is considered as the only hypogene primary mineralization. Song et al. (2016) use pyrites as exclusively tailings related, while in our two deposit types pyrite is

one of the sulfide minerals that exists in the deposit as a hypogene mineral. In general, most isotope work is done on pure chalcopyrites, whereas the deposits in our study areas have more complex mineralogy.

Future research should in general further attempt to understand and constrain all reaction mechanisms involving Cu in natural surface water systems. Research on the method sometimes give varied results between studies, so I would argue that any research on Cu isotope behavior, especially less researched topics like fractionation of Cu in more complex sulfide mineral weathering systems, would be a welcome contribution. It would be interesting to eventually attempt to make a complex model explaining Cu isotope variations in Cu-sulfide systems. This would most likely require an advanced multidisciplinary approach to understand and constrain all parameters of the Cu isotope behavior in a natural system. It would require an extensive amount of data on the mineralogy and formation of ore rocks, background rocks and waste materials as well as different analyses of surface water to understand all processes causing fractionation. To produce an accurate and precise model, one would also need to include variables like climate, relief, vegetation, redox conditions, time, transport and much more.

Chapter 7: Conclusion

This thesis tested the stable copper isotope system as a tracer for copper in contaminated waters around two historical copper-sulfide mines in Røros and at Løkken Verk in Trøndelag, Norway. Based on geochemical and Cu isotope analysis of surface waters and potential copper sources (ore rock, background rocks, mining waste), we conclude the following:

- Sulfide weathering is responsible for elevated Cu concentrations (and other heavy metals like Fe, Zn, Pb) and acidic pH.
- Because of our limited solid sample dataset, separating waste derived and ore derived Cu is difficult based on isotope values only.
- Background Cu is identified by near-zero δ^{65}Cu values, in addition to low concentrations of Cu and neutral pH.
- The highest contaminated samples show a relatively small range of δ^{65}Cu values (+1.05‰ to +1.63‰) consistent with oxidative weathering of tailings and gangue.
- Most samples with low concentrations of Cu display high δ^{65}Cu values (>+3‰) consistent with sulfide weathering and most likely affected by preferential removal of ^{63}Cu by biological processes.
- The most important source of contamination is the oxidation of sulfide minerals exposed at the surface, and the most important remediation method to reduce further contamination would be to make sure the non-oxidized material is not exposed to weathering.
- Because we have no means of quantifying biological processes it is difficult to determine whether aqueous copper is derived from tailings, gangue, slag or ore rock, as all these sources give δ^{65}Cu values in surface waters overlapping due to the effects of sulfide weathering and other natural processes.
- Løkken remediation appears to have been successful and resulted in removal of Cu from solution, neutralized acid mine drainage and relatively high δ^{65}Cu values possibly due to the preferential removal of ^{63}Cu during remediation.

Overall, we conclude that stable Cu isotope system has the potential to be used for tracing sources of copper contamination in surface waters and is able to identify waters affected by sulfide weathering. However, compared to heavily polluted mining areas (Cu > 100 ppm), in areas with moderate degrees of contamination (< 10 ppm Cu) the original isotopic compositions of contaminated waters may be overprinted by isotopic fractionation during biological processes, organic and inorganic complexation reactions, potentially compromising the interpretation of Cu isotope values.

Bibliography

Albarède, F. (2004). The Stable Isotope Geochemistry of Copper and Zinc. *Reviews in Mineralogy and Geochemistry*, *55*, 409–427.

Balistrieri, L. S., Borrok, D. M., Wanty, R. B., & Ridley, W. I. (2008). Fractionation of Cu and Zn isotopes during adsorption onto amorphous Fe (III) oxyhydroxide : Experimental mixing of acid rock drainage and ambient river water. *Geochimica et Cosmochimica Acta*, *72*, 311–328. https://doi.org/10.1016/j.gca.2007.11.013

Balistrieri, L. S., Seal, R. R., Piatak, N. M., & Paul, B. (2007). Assessing the concentration , speciation , and toxicity of dissolved metals during mixing of acid-mine drainage and ambient river water downstream of the Elizabeth Copper Mine, Vermont, USA, *22*, 930–952. https://doi.org/10.1016/j.apgeochem.2007.02.005

Barrie, C. D., Cook, N. J., & Boyle, A. P. (2010). Textural variation in the pyrite-rich ore deposits of the Røros district , Trondheim Region , Norway : implications for pyrite deformation mechanisms. *Mineralium Deposita*, (45), 51–68. https://doi.org/10.1007/s00126-009-0261-3

Baxter, D. C., Rodushkin, I., Engstrom, E., & Malinovsky, D. (2006). Revised exponential model for mass bias correction using an internal standard for isotope abundance ratio measurements by multi-collector inductively coupled plasma mass spectrometry. https://doi.org/10.1039/b517457k

Berkenbosch, H. A., Ronde, C. E. J. De, Paul, B. T., & Gemmell, J. B. (2015). Characteristics of Cu isotopes from chalcopyrite-rich black smoker chimneys at Brothers volcano , Kermadec arc , and Niuatahi volcano , Lau basin. *Miner Deposita*, *50*, 811–824. https://doi.org/10.1007/s00126-014-0571-y

Blundy, J., Mavrogenes, J., Tattitch, B., Sparks, S., & Gilmer, A. (2015). Generation of porphyry copper deposits by gas–brine reaction in volcanic arcs. *Nature Geoscience*, *8*(March), 235–240. https://doi.org/10.1038/NGEO2351

Bigalke, M., Weyer, S., Kobza, J. & Wilcke, W. (2010). Stable Cu and Zn isotope ratios as tracers of sources and transport of Cu and Zn in contaminated soil. *Geochimica et Cosmochimica Acta* 74 (23), 6801–6813.

Chapman, J. B., Mason, T. F. D., Weiss, D. J., Coles, B. J. & Wilkinson, J. J (2006). Chemical separation and isotopic variations of Cu and Zn from five geological reference materials. *Geostandards and Geoanalytical Research* 30 (1), 5–16.

Chi Fru, E., Rodríguez, N. P., Partin, C. A., Lalonde, S. V, Andersson, P. & Weiss, D. J. (2016). Cu isotopes in marine black shales record the Great Oxidation Event. *PNAS*. https://doi.org/10.1073/pnas.1523544113

De Laeter, J. R., Böhlke, J. K., Hidaka, H., Peiser, H. S., Rosman, K. J. R., & Taylor, P. D. P. (2003). Atomic weights of the elements: Review 2000, *75*(6), 683–800.

Drever, J. I. (1997). *The Geochemistry of Natural Waters. Surface and Groundwater Environments* (3rd ed.). Upper Saddle River, New Jersey: Prentice-Hall, Inc.

Ehrlich, S., Butler, I. B., Halicz, L., Rickard, D., Oldroyd, A., & Matthews, A. (2004). Experimental study of the copper isotope fractionation between aqueous Cu (II) and covellite , CuS. *Chemical Geology*, *209*, 259–269. https://doi.org/10.1016/j.chemgeo.2004.06.010

El Azzi, D., Viers, J., Guiresse, M., Probst, A., Aubert, D., Caparros, J., Charles, F., Guizien, K. & Probst, J. L. (2013). Origin and fate of copper in a small Mediterranean vineyard

catchment : New insights from combined chemical extraction and δ 65 Cu isotopic composition. *Science of the Total Environment, The*, *463–464*, 91–101. https://doi.org/10.1016/j.scitotenv.2013.05.058

Fekiacova, Z., Cornu, S., & Pichat, S. (2015). Tracing contamination sources in soils with Cu and Zn isotopic ratios. *Science of the Total Environment*, *517*, 96–105. https://doi.org/10.1016/j.scitotenv.2015.02.046

Fernandez, A., & Borrok, D. M. (2009). Fractionation of Cu , Fe , and Zn isotopes during the oxidative weathering of sulfide-rich rocks. *Chemical Geology*, *264*(1–4), 1–12. https://doi.org/10.1016/j.chemgeo.2009.01.024

Graham, S., Pearson, N. J., Jackson, S. E., Griffin, W., & Reilly, S. Y. O. (2004). Tracing Cu and Fe from source to porphyry : in situ determination of Cu and Fe isotope ratios in sulfides from the Grasberg Cu – Au deposit. *Chemical Geology*, *207*, 147–169. https://doi.org/10.1016/j.chemgeo.2004.02.009

Grammeltvedt, G. (2004). Geologisk berggrunnskart LØKKEN 1521 3, M 1:50 000 Norges geologiske undersøkelse

Gregory, M., & Mathur, R. (2017). Understanding Copper Isotope Behavior in the High Temperature Magmatic-Hydrothermal Porphyry Environment. *Geochemistry, Geophysics, Geosystems*, 4000–4015. https://doi.org/10.1002/2017GC007026

Iversen, E. R. (2010). *Kontroll av massebalanse i Løkken gruveområde, Meldal kommune. Undersøkelser i perioden 1.9.2009 - 31.2.2010.*(NIVA rapport O-29386). Retrieved from: http://www.vannportalen.no/globalassets/vannregioner/trondelag/trondelag---dokumenter/rapporter/kontroll-av-massebalanse-ved-lokken-gruveomrade-meldal-kommune.pdf

Kimball, B. E., Mathur, R., Dohnalkova, A. C., Wall, A. J., Runkel, R. L., & Brantley, S. L. (2009). Copper isotope fractionation in acid mine drainage. *Geochimica et Cosmochimica Acta*, *73*(5), 1247–1263. https://doi.org/10.1016/j.gca.2008.11.035

Klein, S., & Rose, T. (2020). Evaluation copper isotope fractionation in the metallurgical operational chain: An experimental approach, (March), 1–22. https://doi.org/10.1111/arcm.12564

Larson, P. B., Maher, K. C., Ramos, F. C., Chang, Z., Gaspar, M., & Meinert, L. D. (2003). Copper isotope ratios in magmatic and hydrothermal ore-forming environments. *Chemical Geology*, *201*, 337–350. https://doi.org/10.1016/j.chemgeo.2003.08.006

Li, W., Jackson, S.E., Pearson, N.J., Alard, O., Chappell, B.W., (2009). The Cu isotopic signature of granites from the Lachlan Fold Belt, SE Australia. *Chem. Geol*. 258 (1–2), 38–49.

Li, D., Li, S., & Teng, F. (2014). High-precision copper and iron isotope analysis of igneous rock standards by MC-ICP-MS. *The Royal Society of Chemistry*, *29*, 122–133. https://doi.org/10.1039/c3ja50232e

Li, W., Jackson, S. E., Pearson, N. J., & Graham, S. (2010). Copper isotopic zonation in the Northparkes porphyry Cu – Au deposit , SE Australia. *Geochimica et Cosmochimica Acta*, *74*(14), 4078–4096. https://doi.org/10.1016/j.gca.2010.04.003

Little, S. H., Vance, D., Walker-Brown, C. & Landing, W. M. (2014). The oceanic mass balance of copper and zinc isotopes , investigated by analysis of their inputs , and outputs to ferromanganese oxide sediments. *Geochimica et Cosmochimica Acta*, *125*, 673–693. https://doi.org/10.1016/j.gca.2013.07.046

Little, S. H., Vance, D., Mcmanus, J., Severmann, S. & Lyons, T. W. (2017). Copper isotope signatures in modern marine sediments. *Geochimica et Cosmochimica Acta*, *212*, 253–

273. https://doi.org/10.1016/j.gca.2017.06.019

Liu, S., Huang, J., Liu, J., Wörner, G., Yang, W., Tang, Y., Chen, Y., Tang, L., Zheng, J. & Li, S. (2015). Copper isotopic composition of the silicate Earth. *Earth and Planetary Science Letters*, *427*, 95–103. https://doi.org/10.1016/j.epsl.2015.06.061

Lydon, J. W. (1984). Ore deposit models - 8. Volcanogenic massive sulphide deposits Part:I A descriptive model. *Geoscience Canada*, *11*(4).

Løkken Verk: En norsk grube gjennom 300 år (1954). Trondheim: F. Bruns bokhandels forlag. Retrieved from https://urn.nb.no/URN:NBN:no-nb_digibok_2011011003045

Maher, K. C., Jackson, S. E., & Mountain, B. W. (2011). Experimental evaluation of the fluid – mineral fractionation of Cu isotopes at 250°C and 300°C. *Chemical Geology*, *286*(3–4), 229–239. https://doi.org/10.1016/j.chemgeo.2011.05.008

Mathur, R., Falck, H., Belogub, E., Milton, J., Wilson, M., Rose, A., & Powell, W. (2018). Origins of Chalcocite Defined by Copper Isotope Values. *Geofluids*, *2018*, 9. https://doi.org/10.1155/2018/5854829

Mathur, R., Ruiz, J., Titley, S., Liermann, L., Buss, H., & Brantley, S. L. (2005). Cu isotopic fractionation in the supergene environment with and without bacteria. *Geochimica et Cosmochimica Acta*, *69*(22), 5233–5246. https://doi.org/10.1016/j.gca.2005.06.022

Mathur, R., Titley, S., Barra, F., Brantley, S. L., Wilson, M., Phillips, A., Munizaga, F., Maksaev, V., Vervoort, J. & Hart, G. (2009). Exploration potential of Cu isotope fractionation in porphyry copper deposits. *Journal of Geochemical Exploration*, *102*(1), 1–6. https://doi.org/10.1016/j.gexplo.2008.09.004

McClenaghan, M. B., & Peter, J. M. (2016). Thematic set : Till geochemical signatures of volcanogenic massive sulphide deposits : an overview of Canadian examples. *Geochemistry: Exploration, Environment, Analysis*, *16*(Boivin 2007), 27–47. https://doi.org/10.1144/geochem2014-315

Mirnejad, H., Mathur, R., Einali, M., Dendas, M., & Alirezaei, S. (2010). A comparative copper isotope study of porphyry copper deposits in Iran. *Geochemistry: Exploration, Environment, Analysis*, *10*, 413–418. https://doi.org/10.1144/1467-7873/09-229

Moeller, K., Schoenberg, R., Pedersen, R.-B., Weiss, D. J., & Dong, S. (2012). Calibration of the New Certified Reference Materials ERM-AE633 and ERM-AE647 for Copper and IRMM-3702 for Zinc Isotope Amount Ratio Determinations. *Geostandards and Geoanalytical Research*, *36*(2), 177–199. https://doi.org/10.1111/j.1751-908X.2011.00153.x

Moynier, F., Vance, D., Fuji, T., & Savage, P. (2017). The Isotope Geochemistry of Zinc and Copper. *Reviews in Mineralogy and Geochemistry*, *82*(1), 543–600. https://doi.org/10.2138/rmg.2017.82.13

Navarrete, J. U., Borrok, D. M., Viveros, M., & Ellzey, J. T. (2011). Copper isotope fractionation during surface adsorption and intracellular incorporation by bacteria. *Geochimica et Cosmochimica Acta*, *75*(3), 784–799. https://doi.org/10.1016/j.gca.2010.11.011

Nissen, G. B. (1976). *Røros kobberverk 1644-1974*. Trondheim. Retrieved from https://urn.nb.no/URN:NBN:no-nb_digibok_2016020907561

Oliveira, I., Cavalaro, S.H.P. & Aguado, A. (2014) Evolution of pyrrhotite oxidation in aggregates for concrete. *Materiales de Construcción* 64 [316], e038 http://dx.doi.org/10.3989/mc.2014.08413

Orkla industrimuseum (2019a) *Løkkenforekomsten* [Museum plaque]

Orkla industrimuseum (2019b) *Kis fra Løkken Verk* [Museum plaque]

Orkla industrimuseum (2019c) *Tiltak mot gruveforurensing* [Museum plaque]

Petit, J. C. J., Schäfer, J., Coynel, A., Blanc, G., Deycard, V. N., Derriennic, H., Lanceleur, L., Dutruch, L., Bossy, C. & Mattielli, N. (2013). Anthropogenic sources and biogeochemical reactivity of particulate and dissolved Cu isotopes in the turbidity gradient of the Garonne River (France). Chemical Geology, 359, 125–135. https://doi.org/10.1016/j.chemgeo.2013.09.019

Pokrovsky, O.S., Viers, J., Emnova, E.E., Kompantseva, E.I. & Freydier, R., (2008). Copper isotope fractionation during its interaction with soil and aquatic microorganisms and metal oxy(hydr)oxides: possible structural control. *Geochimica et Cosmochimica Acta* 72 (7), 1742–1757.

Rouxel, O., Fouquet, Y., & Ludden, J. N. (2004). Copper Isotope Systematics of the Lucky Strike , Rainbow , and Logatchev Sea-Floor Hydrothermal Fields on the Mid-Atlantic Ridge. *Economic Geology*, *99*, 585–600.

Rui, I. J. (1981). Røros, berggrunnsgeologisk kart 1720 III, M 1:50 000 Norges geologiske undersøkelse.

Ryan, B. M., Kirby, J. K., Degryse, F., Scheiderich, K., & Mclaughlin, M. J. (2014). Copper Isotope Fractionation during Equilibration with Natural and Synthetic Ligands. Environmental Science and Technology, 48, 8620–8626. https://doi.org/10.1021/es500764x

Rosholt, B. & Wilberg, R. (2001). *Exploration in Storwartz Ore Field, Røros, Norway* (Bergvesenet rapport 4805). Retrieved from https://dirmin.no/sites/default/files/bibliotek/BV4805.pdf

Savage, P., Moynier, F., & Chen, H. (2015). Copper isotope evidence for large-scale sulphide fractionation during Earth ' s differentiation, 53–64. https://doi.org/10.7185/geochemlet.1506

Seewald, J. S., & Seyfried, W. E. J. (1990). The effect of temperature on metal mobility in subseafloor hydrothermal systems " constraints from basalt alteration experiments. *Earth and Planetary Science Letters*, *101*, 388–403.

Sillerová, H., Chrastný, V., Vítkov, M., Francov, A., Jehli, J., Aspholm, P. E., Nilsson, L. O., Gutsch, M. R., Kocourkov, J., Berglen, T. F., Jensen, H. K. B. & Kom, M. (2017). Stable isotope tracing of Ni and Cu pollution in North-East Norway : Potentials and drawbacks, *Environmental Pollution, 228*. https://doi.org/10.1016/j.envpol.2017.05.030

Skei, J., Sørby, H., Storbråten, G., Braastad, G., Løkeland, M., Dalen, M., Thornhill, M., Bøe, R., Rye, H., Fosså, J. H., Dekko, T. & Jensen, T. (2019). *Mining industry and tailings disposal*. *Status, environmental challenges and gaps of knowledge* (Norwegian Environment Agency Report M-1335). Retrieved from: https://www.miljodirektoratet.no/globalassets/publikasjoner/m1335/m1335.pdf

Song, S., Mathur, R., Ruiz, J., Chen, D., Allin, N., Guo, K., & Kang, W. (2016). Fingerprinting two metal contaminants in streams with Cu isotopes near the Dexing Mine, China. *Science of the Total Environment*, *544*, 677–685. https://doi.org/10.1016/j.scitotenv.2015.11.101

Sun, W., Wang, J., Zhang, L., Zhang, C., Li, H., Ling, M., Ding, X., Li, C. & Liang, H. (2016). The formation of porphyry copper deposits. *Acta Geochemica*, (36). https://doi.org/10.1007/s11631-016-0132-4

Takano, S., Tanimizu, M., Hirata, T., & Sohrin, Y. (2014). Isotopic constraints on biogeochemical cycling of copper in the ocean. *Nature Communications*, 1–7. https://doi.org/10.1038/ncomms6663

Taylor, C. D., Zierenberg, R. A., Goldfarb, R. J., Kilburn, J. E., Seal II, R. R. & Kleinkopf, M. D. (1995). Volcanic associated massive sulfide deposits. Retrieved from: https://pubs.usgs.gov/of/1995/ofr-95-0831/CHAP16.pdf

Wang, Z., Chen, J., & Zhang, T. (2017). Cu Isotopic Composition in Surface Environments and in Biological Systems : A Critical Review. *International Journal of Environmental Research and Public Health*, *14*(538). https://doi.org/10.3390/ijerph14050538

World Health Organization (2004). *Copper in Drinking-water* (03.04/88). Retrieved from: https://www.who.int/water_sanitation_health/dwq/chemicals/copper.pdf

Zhu, X. K., O'Nions, R. K., Guo, Y., Belshaw, N. S., & Rickard, D. (2000). Determination of natural Cu-isotope variation by plasma-source mass spectrometry : implications for use as geochemical tracers. *Chemical Geology*, *163*, 139–149. https://doi.org/10.1016/S0009-2541(99)00076-5

Internet resources

Aursunden (2019). In *Store norske leksikon*. Retrieved March 6. 2020 from https://snl.no/Aursunden

Bjerkgård, T. (2015). Kismalmer og norske kisforekomster. [Published presentation]. Retrieved from: https://norsk-bergverksmuseum.no/wp-content/uploads/sites/10/2015/10/Terje-Bjerkg%C3%A5rd-Kismalmer.pdf

Continental subarctic climate (2016). In *Encyclopedia Britannica.* Retrieved March 6. 2020 from: https://www.britannica.com/science/continental-subarctic-climate

Direktoratet for mineralforvaltning (2019). Løkken. Retrieved June 14. 2020 from: https://dirmin.no/lokken

Forskrift om fredning av statens kulturhistoriske eiendommer. (2015). FOR-2015-08-14-962 Retrieved from: https://lovdata.no/forskrift/2011-11-09-1088

Geithe, L. (2013a, 27. October). Hestkletten. Retrieved March 6. 2020 from: http://www.bergstaden.org/no/kobberverket/gruvedrifta-pa-roros/hestkletten

Geithe, L. (2013b, 27. August). Storwartzfeltet. Retrieved March 6. 2020 from: http://www.bergstaden.org/no/kobberverket/gruvedrifta-pa-roros/storwartzfeltet

Geithe, L. (2014, 5. April). Hans Olsen Aasen. Retrieved March 6. 2020 from: http://www.bergstaden.org/no/personer/hans-olsen-aasen

Heggstad, R. & Toldnæs, J. P. (2020). Orkla. In *Store norske leksikon.* Retrieved March 6. 2020 from: https://snl.no/Orkla

Köppen climate classification (2020). In *Encyclopedia Britannica.* Retrieved March 6. 2020 from: https://www.britannica.com/science/Koppen-climate-classification

Lenntech (n.d.) WHO EU water standards. Retrieved March 6. 2020 from: https://www.lenntech.com/who-eu-water-standards.htm

Orkla industrimuseum (n.d.). I Løkkengrubens ganger. Retrieved April 27. 2020 from: https://oi.no/besok/gammelgruva/historie

Rio Tinto (n.d.) About the project. Retrieved June 14. 2020 from: http://www.holdenminecleanup.com/about-the-project

Rygg, T. (n.d.). Gruvene i Storwartz-feltet. Retrieved April 27. 2020 from: https://verdensarvenroros.no/gruvene-i-storwartzfeltet#899

Voller, L. & Andersen, M. (2016). Broken promises. *Danwatch.* Retrieved April 27. 2020 from: https://old.danwatch.dk/undersogelse/broken-promises/?chapter=3

Online map services etc.

NGU (2020). Nasjonal berggrunnsdatabase. *Norges geologiske undersøkelse*. Retrieved from: http://geo.ngu.no/kart/berggrunn/

Norge i bilder (2020). *Statens vegvesen, Norsk institutt for Bioøkonomi (NIBIO) & Statens kartverk*. Retrieved from: https://www.norgeibilder.no/

ArcGIS online (2020). *Environmental Systems Research Institute.* Retrieved from: https://www.arcgis.com/